NASA CONTRACTOR REPORT

NASA CR-2433

NASA CR-2433

DIGITAL FLIGHT CONTROL RESEARCH

by J. E. Potter, R. G. Stern, T. B. Smith, and P. Sinha

Prepared by
MEASUREMENT SYSTEMS LABORATORY
MASSACHUSETTS INSTITUTE OF TECHNOLOGY
Cambridge, Mass. 02139
for Langley Research Center

NATIONAL AERONAUTICS AND SPACE ADMINISTRATION • WASHINGTON, D. C. • AUGUST 1974

1. Report No.	2. Government Accession No.	3. Recipient's Catalog No.
NASA CR-2433		

4. Title and Subtitle	5. Report Date
Digital Flight Control Research	August 1974
	6. Performing Organization Code

7. Author(s)	8. Performing Organization Report No.
J. E. Potter, R. G. Stern, T. B. Smith, and P. Sinha	

9. Performing Organization Name and Address	10. Work Unit No.
Measurement Systems Laboratory Massachusetts Institute of Technology Cambridge, Mass. 02139	501-26-05-01
	11. Contract or Grant No.
	NAS1-10677
	13. Type of Report and Period Covered
	Contractor Report

12. Sponsoring Agency Name and Address	14. Sponsoring Agency Code
National Aeronautics and Space Administration Washington, DC 20546	

15. Supplementary Notes

Final report.

16. Abstract

This report represents the results of studies which were undertaken to contribute to the design of digital flight control systems, particularly for transport aircraft. In addition to the overall design considerations for a digital flight control system, the following topics are discussed in detail: aircraft attitude reference system design, the digital computer configuration, the design of a typical digital autopilot for transport aircraft, and a hybrid flight simulator.

17. Key Words (Suggested by Author(s))	18. Distribution Statement
Digital Flight Control System Attitude Reference Digital Autopilot Flight Simulation	Unclassified - Unlimited STAR Category 02

19. Security Classif. (of this report)	20. Security Classif. (of this page)	21. No. of Pages	22. Price*
Unclassified	Unclassified	214	$5.75

* For sale by the National Technical Information Service, Springfield, Virginia 22151

CHAPTER I

INTRODUCTION

1.1 Summary

This report represents the results of studies at the MIT Measurement Systems Laboratory which were undertaken to contribute to the design of digital flight control systems, particularly for transport aircraft. In this chapter the overall design considerations for a digital flight control system are discussed. The design areas chosen for study are presented and the contents of the succeeding chapters are outlined.

1.2 Design Considerations for a Digital Flight Control System

The basic function of a flight control computer is to stabilize and control the attitude and flight path of an aircraft by processing sensor data to generate commands for control surface actuators and throttles. In addition, the computer must perform several supervisory functions. First, it must adjust the stabilization and control data processing algorithm to fit existing flight conditions and the flight control task being executed. Second, it must monitor flight control system performance and switch from primary to backup modes of operation in case of subsystem failures. Finally, the computer must interact with the pilot through suitable switches and displays in order to communicate to him the flight control system status and

allow him to select the mode of operation which he desires.

For the basic stabilization and control data processing task, the bandwidth easily obtained with digital computation is narrower than the bandwidth easily obtained with analog computation. The bandwidth of a digital computer is limited by the times it requires to carry out additions and multiplications and reducing these times usually incurs relatively large penalties in weight, power consumption and dollar cost. Since a digital computer samples its inputs periodically rather than reading them continuously, digital control is subject to the phenomena of aliasing in which signals whose frequencies are near a multiple of the sampling frequency are indistinguishable from low frequency signals. Limited bandwidth and aliasing are relatively minor problems since the bandwidths of modern flight rated digital computers are adequate for most aircraft stabilization and control tasks and the effects of aliasing can usually be eliminated by passing the sensor signals through low pass filters before sending them to the computer. The major advantage of digital over analog computation for the stabilization and control task is the ease with which the computational algorithm can be altered to meet changing requirements during a flight.

It is in the performance of supervisory functions that digital computation is most advantageous. The extreme flexibility of a general purpose digital computer in performing supervisory tasks makes it much better suited to these tasks than the special purpose switching

circuits employed in conjunction with analog computation.

Certain factors have tended to limit the use of digital flight control systems. Present day flight rated computers are quite complex and provide more computational power than is required in simple flight control systems. Since increased complexity brings with it higher cost and lower reliability, digital computation is not economical for flight control systems below a certain level of sophistication. Furthermore, although digital computers themselves are highly developed, the interface between the digital computer and the sensors and actuators and the aircraft electrical environment has not received nearly as much design attention and its design involves some risk.

Uniform standards for signal formats within flight control systems have not yet been achieved. As an example, the F-106 airborne digital computer communicates with other avionics system components via signals in the following formats:

High Voltage A-C Analog

High Voltage D-C Analog

Low Voltage D-C Analog

Time Duration Between Pulses

Thirteen Bit Parallel Digital

Discrete (on-off)

Somewhere in the flight control system, the signals external to the computer must be converted to the parallel digital format employed in

the computer and these external signals must be accessed by the parallel digital input-output addresses employed in the computer. Signal transmission external to the computer must be carried out in the relatively noisy electrical environment of the aircraft with its poorly regulated power line voltages, high potential for ground loops and high radiation intensity from vhf communication and radar equipment. Although many signals could remain in digital form throughout the flight control system, if for example digital encoders were employed as the mechanical to electrical conversion elements in sensors and stepper motors were used to drive control surface actuators, some signal formating electronics will be required in any digital flight control system.

Several hardware configurations have been proposed for handling the interface between the digital computer and the remainder of the flight control system. One method is to employ a centralized interface unit which converts all signals external to the computer to and from a parallel digital format and exchanges these signals with the computer via parallel digital data and address lines. Another approach is to employ a minimal interface unit at the computer and extend the computer input-output data and address lines throughout the aircraft. Although the data and address signals might be changed from parallel to serial digital formats as they leave the computer, they would receive a minimum amount of processing at this point and each subsystem communicating with the computer would have its own interface

unit at its own location. These interface units would include address circuitry to determine which unit was being called by the computer and whatever signal formating electronics is required by the subsystem being served by a particular unit. A third alternative is to employ a multiplexing system to transmit most or all of the flight control system signals over a common wire in a format designed for noise tolerance and tolerance of aircraft wiring failures. Since this signal format would not necessarily be compatible with the signals employed inside the computer and the other flight control subsystems, interface units would be required both at the computer and at the locations of the other subsystems (i.e., sensors and actuators).

The choice between the first and second alternatives is not clear cut since similar interface circuits are employed in both cases, the primary difference being their location in the system. Some capability for expansion should be provided and this depends on providing spare input-output addresses in the computer and, in the centralized interface alternative, on leaving space for more circuit cards in the interface unit and installing spare wires in the aircraft. In the second alternative, in which the digital data and address lines are extended throughout the aircraft, information is transmitted as short duration pulses and electrical problems can arise because of reflections at discontinuities in the lines and susceptibility to noise. However, whenever a large volume of data is

to be transmitted over a few wires, wide bandwidth circuits are required and reflections and noise may be problems. Therefore these problems are not limited to this particular system configuration.

In determining the digital computer configuration to be employed in a flight control system, two alternatives are possible - federated and integrated systems. In a federated system, two or more separate digital computers with different primary tasks are employed, while in an integrated system one central computation unit performs all computational tasks. In a federated digital flight control system, air data computation might be performed by a separate small digital computer, a separate computer might be used for pilot display generation while a third computer executes the stabilization and control and supervisory functions. The use of more than one digital computer is costly in weight, power and dollars and is difficult to justify unless the data processing or reliability requirements are beyond the capability of a single computer. Even in this case, a multiprocessor in which several central processors (arithmetic units) address the same memory or a central computer complex containing several computers provides a more flexible system.

Considering the entire aircraft avionics system, rather than just the flight control subsystem, the choice between a federated or an integrated system takes on a new aspect. Other avionics system tasks which might involve digital computation include navigation and system status and maintenance checks. The use of a

federated system, in which one computer is dedicated to the flight control task and a second computer performs the other tasks, protects the flight control subsystem from interference by other subsystems both at the programming and operating levels. Since in a federated system, the other computations would not have direct access to the memory of the computer performing flight control computations, it would be difficult for the other computations to insert bad data into the flight control computations or to trap the central processor used for flight control computations and prevent it from executing the flight control program. During computer program preparartion, the limited possibilities of interaction between the flight control program and other programs with a federated system would make program checkout and verification easier and would ease the problem of delegating programming responsibility. On the other hand, if the flight control computer has excess capacity, it is economically attractive to employ the integrated system concept and have the flight control computer perform other functions.

The large data processing capability available with a digital flight control computer allows the use of simpler flight control sensors. Thus, the mechanical computational elements in the air data computer may be eliminated and body mounted rather than gimballed gyros may be employed to sense aircraft attitude.

For automatic landing of transport aircraft, analog autopilots employ redundant autopilot computers as well as redundant sensors and actuators to meet reliability requirements. With present digital

equipment reliability, it is clear that a digital autopilot must also employ redundant computers in the autoland application. The ability of the general purpose digital computer to reorganize its computations to meet the requirements of changing system status should be most useful in this area.

1.3 Design Areas Chosen for Study

In this report the results of studies leading to the design of a digital flight control system are presented. From the aspects of digital flight control system design outlined above, certain areas were selected for study. It was hoped that these areas would be of pivotal importance and would be relatively invariant from one flight control application to another. These areas were the feasibility of performing the basic attitude and flight path stabilization and control function with a digital computer, how the presence of a digital computer would affect the choice of flight control system sensors and the structuring of the digital computer system to provide tolerance to computer failures.

To study digital stabilization and control, an extensive flight simulation was set up on a hybrid computer and digital flight control simulation results were obtained for a KC-135 aircraft. The question of the impact of digital computation on flight control sensors was attacked by studying the case of attitude sensors in detail.

Since this study was not primarily concerned with the electronic

design of a digital flight control system, some of the important design areas mentioned above such as the interface between the digital computer and the rest of the flight control system were not considered in detail.

1.4 Outline of Following Chapters

Chapter 2 treats the problem of sensor selection for a digital flight control system by considering the case of the aircraft attitude sensors. Along with the air data sensors, the attitude sensors provide an area in which flight control system complexity and cost can be reduced by eliminating mechanical computational elements and routing the signals from the basic sensors directly to the main flight control computer. The basic quantity measured by all gyro attitude instruments is angular velocity. In conventional flight control systems, some gyros are employed to stabilize gimballed platforms from which the attitude (Euler angles) of the aircraft is determined by measuring shaft angles. In a digital flight control system, the computational capability is available to carry out the computation relating angular velocity to Euler angles numerically allowing all the gyros to be mounted directly on the airframe and eliminating the gimballed platforms. Mounting the gyros directly on the aircraft body also simplifies the problem of providing redundant attitude information to enhance reliability for critical flight control tasks such as automatic landing. The problem of detecting

and identifying failed instruments within a set of body mounted gyros or accelerometers is investigated and a configuration of instruments which facilitates failure detection and identification is proposed. The interaction between the aircraft attitude computations and the stabilization and control function of a flight control system is also discussed. This interaction occurs because the longitudinal and lateral acceleration sensors employed to provide long term attitude information provide an unwanted feedback path around the autopilot. Finally, several attitude sensor configurations for a digital flight control system are suggested.

Chapter 3 investigates the design of the digital computer system for a digital autopilot where very high reliability is required. Very high reliability is required for automatic landing and in other transport operations to the extent that safety of flight depends on the operation of the automatic flight control system. For flight control system applications requiring more reliability than is provided by a single computer operating without backup, various multiple computer configurations are examined, and a three computer configuration providing fail-operational/fail-passive operation is recommended.

Chapter 4 is concerned with the design of data processing algorithms for aircraft attitude and flight path stabilization and control. Algorithms for control of a KC-135 aircraft for several cruise flight conditions are obtained. The autopilot modes imple-

mented are altitude hold, heading hold and control wheel steering. The control algorithms were found by root locus techniques assuming that autopilot operation was continuous rather than sampled. The continuous control algorithms were then converted to sampled data algorithms with the same frequency response at low frequencies. The autopilot algorithms were tested with the flight simulation described in Chapter 5 and recordings of the simulated aircraft/autopilot responses are presented. A sampling rate of twenty samples per second was employed with the control algorithms and no adverse effects due to sampling were noted.

The authors wish to acknowledge the support given them by the Charles Stark Draper Laboratory of M.I.T. in providing computer time in the Hybrid Computer Facility and also in providing basic computer programming for the study of the stability of digital feedback systems.

CHAPTER II

DESIGN OF THE AIRCRAFT ATTITUDE REFERENCE SYSTEM

2.1 Introduction

The function of the attitude reference system is to provide the autopilot with the aircraft attitude, that is heading, pitch and roll angles and the aircraft attitude rates, yaw, pitch and roll rate. The autopilot may also require the components of aircraft linear acceleration and, since the attitude reference system contains linear accelerometers which aid it in performing its primary function, the function of determining aircraft linear acceleration will also be assigned to the attitude reference system in this report.

The attitude reference system design for a digital autopilot will differ from the design for a conventional analog autopilot because the large data processing capability of the digital system opens up the possibility of eliminating the normal gimbaled attitude sensors, that is the vertical gyro, directional gyro and/or gyro stabilized platform, with a resulting saving in cost and improvement in reliability. The increased data processing capability also allows the use of more sophisticated techniques for detecting and isolating failed attitude reference sensors.

The attitude reference system contains the following sensors: gyros to provide attitude rate and short-term attitude information,

a fluxgate compass to provide long-term heading information, and accelerometers to sense gravity and thus provide long-term pitch and roll information as well as providing aircraft linear acceleration.

The rate gyros, which provide attitude rate information, must be mounted on the aircraft body; that is, they are not gimbaled. However, there are two alternatives for mounting the gyros which sense aircraft attitude. In the first alternative the attitude gyros are mounted on gimbals, either employing two-degree-of-freedom gimbal systems as in a vertical gyro and a directional gyro, or employing a three-gimbal or four-gimbal stabilized platform. The second alternative consists of integrating the outputs of the body mounted rate gyros in the autopilot digital computer to determine the rotation matrix relating a fixed reference frame to the aircraft body coordinate frame. This rotation matrix contains the same information as would be obtained from the gimbal angles of gimbaled attitude gyros, and the second alternative is thus equivalent to the first from the standpoint of satisfying autopilot attitude information requirements.

Gimbaled attitude gyros simplify the data processing problem since the high-frequency attitude computations are carried out mechanically by the gimbals rather than by the digital computer. The primary factor determining the short-term accuracy of attitude determination is the drift rate of the gyros employed. Drift rate in turn is primarily a function of the cost of the gyros and is not materially affected by whether they are employed

as attitude or rate gyros. However, gimbaled gyros are not subjected to the high aircraft angular velocities which are applied to body-mounted gyros, and thus a given gyro will provide somewhat better performance in the gimbaled mode than in the body-mounted mode of operation.

The advantages of the body-mounted gyro mode of attitude determination are flexibility and simplicity of the sensor system, which in turn facilitates implementation of redundancy for assurance of high reliability. Flexibility is provided by the body-mounted gyro mode of operation in the sense that the basic short-term attitude information provided by any gyro is attitude rate. If this information is provided directly to the computer, it can be processed in any way which is desired for a given autopilot mode, whereas, if gimbals are employed, the rate to attitude computation is done in a fixed way by the gimbals and cannot be changed. If the body-mounted gyro attitude determination mode is employed, the artificial horizon displays must be driven by the autopilot digital computer, placing a safety of flight requirement on the computer.

For subsonic flight the autopilot does not require highly accurate attitude and attitude rate information, accuracies on the order of one half degree for attitude angles and a tenth of a degree per second for attitude rate being acceptable. Thus, for the purpose of providing information for the autopilot, relatively inexpensive low-quality gyros may be employed. On the other hand, the aircraft

avionics system is likely to include a set of high-quality gyros and accelerometers for area navigation or trans-oceanic inertial navigation. To assure high autopilot reliability for automatic landing, it is necessary to duplicate or triplicate the gyros and accelerometers employed to provide autopilot information so that the automatic landing can be completed if one sensor fails during the landing approach. With an integrated system in which the digital computer performs the navigation as well as the autopilot computations, it is possible to employ the navigation gyros to provide attitude information for the autopilot with redundancy provided by less expensive instruments. This approach decreases the total number of gyros and accelerometers required without reducing the performance of the system.

Section 2.2 of this chapter describes the digital computer algorithms required for implementation of the attitude reference system employing body mounted gyros along with a discussion of gyro requirements for this system. Section 2.3 analyzes redundancy configurations to provide failure detection and identification for the body-mounted sensors. Section 2.4 discusses the interaction between longitudinal autopilot modes and the attitude reference system. Section 2.5 describes proposed attitude reference system configurations.

Section 2.2 Implementation of a Gimbal-less Attitude Reference System

The discussion of the gimbal-less attitude reference system will

be taken up in the following order. First the requirements for rate gyros and accelerometers will be determined. Second, the computer integration routine which employs the rate gyro outputs to calculate the rotation matrix relating a set of reference coordinates to aircraft body coordinates will be discussed. Third, the computation of the kinematic correction to account for rotation of the reference coordinate system due to aircraft motion over the earth and earth rotation will be described. Next, the vertical erection computation which employs the direction of gravity sensed by the accelerometers to provide a long-term vertical reference will be discussed. Then the formulas for computing the aircraft heading, pitch, and roll angles from the rotation matrix provided by the integration routine will be given. Finally, the azimuth erection computation which employs the fluxgate compass to provide a long-term heading reference will be described, followed by a summary of the conclusions reached in the section.

2.2.1 Rate Gyro and Accelerometer Requirements

The basic attitude reference system specification which determines the gyro and accelerometer requirements is that the system provide aircraft attitude angles to an accuracy of 0.5 degree (9 milliradians). Accuracy of this order is required for course guidance and attitude stabilization of a subsonic aircraft. Since the accelerometers provide the long-term local vertical reference by sensing the direction of the gravity vector and the direction of the vertical must be determined to within nine milliradians, it follows that the accelerometer errors should

be smaller than 10^{-2}g.

Although rate gyro errors arise from many sources, the errors tend to divide into two classes: (a) drift rate or bias errors which are independent of the magnitude of the angular velocity being sensed and (b) scale factor and linearity errors which depend on the magnitude of the sensed angular velocity. The drift rate specification is determined by two factors. First, since the local vertical rotates at 15 degrees per hour due to earth rotation and the north east and down coordinate system rotates at rates of the same order of magnitude due to motion of the aircraft over the surface of the earth at subsonic speeds, these effects, if uncompensated, will tend to mask gyro drift rates smaller than 15 degrees per hour. Second, during an accelerated maneuver, such as a turn, the flux-gate compass sensor is not level and provides poor heading information due to magnetic dip (the fact that the magnetic lines of force are not horizontal). Also, the accelerometers do not provide good vertical information during an accelerated maneuver since they sense aircraft acceleration as well as gravity. For this reason, during an accelerated maneuver, the attitude reference system must rely on the gyros as the sole source of attitude information. A standard rate (three degrees per second) 180 degree turn lasts for one minute, and it is desired that the attitude indication errors due to gyro drift rate not build up to more than one half degree in this time period. This situation requires a drift rate of less than 0.5 degree per minute, or thirty degrees per hour. Thus it appears that the drift rate requirements for a minimal attitude reference system are in the

vicinity of 15 to 30 degrees per hour. If possible economically, it is desirable to employ gyros with smaller drift rates in order that less reliance need be placed on the flux-gate compass and accelerometers for short-term attitude indication accuracy. Reliance on the latter instruments for short-term accuracy results in relatively large attitude indication errors due to short-term flux-gate compass errors (caused, for example, by the compass transducer swinging on its gimbals and sensing magnetic dip) and errors due to aircraft acceleration sensed by the accelerometers during takeoff and speed changes.

Scale factor and linearity errors are specified as a percentage of the sensed angular velocity and sometimes also as a percentage of full scale angular velocity readings. The following consideration determines the requirements for errors which are a percentage of the sensed angular velocity. The longest continuous turn which will occur frequently is a 180 degree turn. In order that the scale factor/linearity error following the turn be less than one half degree, the outputs of the yaw and pitch gyros must be accurate to $0.5°/180°$ or 3 parts per thousand. The roll gyro does not sense steady angular velocities for long periods of time in maneuvers typical of a transport aircraft, so its accuracy need not be as great. The minimum acceptable full-scale rate gyro outputs for a transport aircraft are on the order of 15 degrees per second for the pitch and yaw gyros and 50 degrees per second for the roll gyro. Angular velocities of this magnitude would not be sustained for any length of time but would occur as peaks during maneuvering and must be correctly sensed by the rate gyros without

saturation if accurate attitude indication is to be obtained. Since an absolute angular velocity accuracy of 30 degrees per hour is desired, the specification of errors which are a percentage of full scale reading is one part in 1800 for the pitch and yaw gyros and one part in 6000 for the roll gyro. The roll gyro requirements could probably be relaxed because the natural constraints on the bank angle reduce the requirements for accurate bank angle information from the roll gyro.

The basic gyro requirements are thus a drift rate of 15 to 30 degrees per hour, scale factor and linearity good to three parts per thousand and full-scale readings of 15 degrees per second for the yaw and pitch gyros and 50 degrees per second for the roll gyro. These specifications are almost impossible to meet with spring-restrained rate gyros of the type normally employed for providing body rates for use in pitch, roll and yaw damping autopilot modes. Good spring-restrained rate gyros sell for about $500 per unit. It is possible to meet these requirements with the least expensive electrically torqued integrating gyros such as the Honeywell GG250, which sells for about $1,500 per unit.

Unfortunately the gyro wheel bearings of these gyros usually have a lifetime on the order of 1000 hours. Hopefully, in the near future gyros of this quality will be introduced which have gas or other longer lived gyro wheel bearings.

2.2.2 Computer Integration Routine

Let R denote the 3-by-3 rotation matrix which transforms vectors

from a fixed reference coordinate system to aircraft body coordinates.

$$R \underline{V}_{ref} = \underline{V}_{body} \qquad (2.2.2\text{-}1)$$

The reference coordinates are normally chosen to be the attitude reference system's approximation to the north, east and down coordinate system. Define the following angular velocity vectors.

$\underline{\omega}_A$ = indicated aircraft angular velocity in body coordinates, that is, rate gyro outputs corrected for known bias and scale factor errors.

$\underline{\omega}_R$ = angular velocity of north, east and down reference coordinate system (caused by earth rotation and motion of aircraft over earth) expressed in the north east and down (reference) coordinate system.

$\underline{\omega}_E$ = erection angular velocity expressed in reference coordinates.

If aircraft latitude is not known, $\underline{\omega}_R$, the angular velocity of the reference coordinate system may be ignored and set to zero. The function of the erection angular velocity, $\underline{\omega}_E$, is to provide an input for correcting attitude indication errors due to inaccuracies in $\underline{\omega}_A$, the rate gyro outputs, and $\underline{\omega}_R$. Applying a $\underline{\omega}_E$ signal causes the indicated north and east and down directions to rotate relative to the aircraft with an

angular velocity $\underline{\omega}_E$. The $\underline{\omega}_E$ vector is analogous to the electrical erection torque inputs of conventional directional and vertical gyros. The differential equation which must be solved by the digital autopilot computer in the gimbal-less attitude reference mode is

$$\frac{dR}{dt} = -[\underline{\omega}_A \times]R + R[\underline{\omega}_R \times] + R[\underline{\omega}_E \times] \qquad (2.2.2\text{-}2)$$

where the symbol $[\underline{\omega} \times]$ denotes the 3-by-3 skew-symmetric matrix

$$[\underline{\omega} \times] = \begin{bmatrix} 0 & -\omega_3 & \omega_2 \\ \omega_3 & 0 & -\omega_1 \\ -\omega_2 & \omega_1 & 0 \end{bmatrix} \qquad (2.2.2\text{-}3)$$

The basic differential equation (2.2.2-2) may be integrated in two ways; it may either be integrated directly as a matrix differential equation, or the rotation matrix R may be expressed in terms of a quaternion, which consists of a scalar and a three-component vector, and the differential equations for these quantities may be solved. These two approaches involve essentially the same computer loading, that is, the same size program and the same computation time, and they yield comparable accuracies. In principle, it would be possible to integrate the yaw, pitch and roll Euler angles to determine the rotation matrix R. However, this approach requires computer evaluation of several sine and

cosine functions which increases computation time without any payoff in accuracy relative to the other methods.

In the quaternion approach, four new variables q_0 and

$$\underline{q} = \begin{bmatrix} q_1 \\ q_2 \\ q_3 \end{bmatrix} \qquad (2.2.2\text{-}4)$$

are introduced. The rotation matrix R is determined from the quaternion q_0, $\underline{q}$ by the formula

$$R = (2q_0^2-1)I + 2\underline{q}\,\underline{q}^T + 2q_0[\underline{q}\times] \qquad (2.2.2\text{-}5)$$

where

I = 3 by 3 identity matrix

$\underline{q}^T$ = $\underline{q}$ transpose

= the row vector $[q_1, q_2, q_3]$

The quaternion components, q_0 and $\underline{q}$ satisfy the differential equations

$$\frac{dq_0}{dt} = \frac{1}{2}(\underline{\omega}_A+\underline{\omega}_R+\underline{\omega}_E)\cdot\underline{q} \qquad (2.2.2\text{-}6)$$

$$\frac{d\underline{q}}{dt} = \frac{1}{2}\{q_0(\underline{\omega}_A-\underline{\omega}_R-\underline{\omega}_E) - (\underline{\omega}_A+\underline{\omega}_R+\underline{\omega}_E)\times\underline{q}\}$$

where (•) denotes the scalar product of two vectors and (×) denotes the vector product of two vectors.

In principle, only three parameters, for example the Euler angles, are required to specify the attitude of the aircraft. When more than three parameters, four in the case of a quaternion and nine in the case of a 3-by-3 rotation matrix, are employed to specify attitude, there must exist constraints among the parameters. In the case of a quaternion, the constraint is that the sum of the squares of the quaternion components is one, i.e.

$$q_0^2 + |\underline{q}|^2 = 1 \qquad (2.2.2\text{-}7)$$

In the case of the rotation matrix, the columns of the matrix must have unit length and be mutually orthogonal, that is

$$R^T R = I \qquad (2.2.2\text{-}8)$$

where the superscript T indicates the matrix transpose. If these constraints were initially satisfied and the differential equations for the quaternion or rotation matrix were solved without error these constraints would be satisfied for all time. However, since the differential equations are solved numerically, round-off errors and errors generated by the integration formula employed will cause the constraints to drift slowly away from their correct values. Since, if the constraints are violated by too wide a margin, the attitude computations become

meaningless, slow numerical feedback loops must be employed to drive the constraints to their correct values. These numerical feedback loops control small errors which have little effect on attitude accuracy as long as the constraints are kept near their correct values, so the primary consideration in specifying them is simplicity. For the case of the quaternion, the constraint may be met by adding the following terms to the right-hand side of the differential equation (2.2.2-6)

$$K(1-q_0^2 - |\underline{q}|^2)q_0$$

$$K(1-q_0^2-|\underline{q}|^2)\,\underline{q} \qquad (2.2.2\text{-}9)$$

Note that these terms would not change the values of dq_0/dt and $d\underline{q}/dt$ if the constraints were satisfied. The correction gain, K, is half the inverse time constant of the correction process and the choice of its value would depend on the magnitude of the numerical integration errors.

In the case where the rotation matrix is integrated directly, let $\underline{r}_1$, $\underline{r}_2$ and $\underline{r}_3$ denote the columns of the rotation matrix R.

$$R = [\underline{r}_1, \underline{r}_2, \underline{r}_3] \qquad (2.2.2\text{-}10)$$

The constraints given in Eq. (2.2.2-8) may be held by adding the expression

$$K(1-\underline{r}_1\cdot\underline{r}_1)\underline{r}_1 \qquad (2.2.2\text{-}11)$$

to the normal expression for the derivative of the first column, $\underline{r}_1$, adding the expression

$$K(1-\underline{r}_2\cdot\underline{r}_2)\underline{r}_2 - K(\underline{r}_1\cdot\underline{r}_2)\underline{r}_1 \qquad (2.2.2\text{-}12)$$

to the normal expression for the derivative of second column, $\underline{r}_2$, and adding the expression

$$K(1-\underline{r}_3\cdot\underline{r}_3)\underline{r}_3 - K(\underline{r}_1\cdot\underline{r}_3)\underline{r}_1 - K(\underline{r}_2\cdot\underline{r}_3)\underline{r}_2 \qquad (2.2.2\text{-}13)$$

to the normal expression for the derivative of the third column, $\underline{r}_3$. Again, K is the correction gain or inverse time constant and is chosen on the basis of the size of the numerical integration errors.

The sampling rate for integrating the differential equations for the rotation matrix or quaternion is determined by two considerations: (a) desired bandwidth of the attitude reference system and (b) errors due to coning motions of the aircraft. Unless unusual precautions are taken in the numerical integration method employed to solve the differential equations, the highest frequency component of attitude motion which will be passed without significant distortion is on the order of one fourth the sampling rate. The desired system bandwidth for a transport aircraft would probably be a few cycles per second. If the attitude of the aircraft is undergoing a coning motion (for example, if the aircraft is pitching and yawing so that the nose travels in

a small circle while the wings remain nearly level), a difficult situation arises. Such a coning motion might be caused by vibration, small autopilot limit cycles or air turbulence. When the aircraft cones, a small steady component of angular velocity is present parallel to the axis of the cone while oscillatory angular velocities appear about axes normal to the cone axis. Over long periods of time the net change of attitude of the aircraft is small since it returns to its original attitude at the end of each coning cycle. If both the steady and oscillatory components of angular velocity are within the passband of the system, they are correctly processed by the numerical integration routine, and correct attitude information indicating a small net attitude change is generated. However, if the coning frequency is high enough, the oscillatory components of angular velocity will be beyond the bandwidth of the system and will be lost while the steady component of angular velocity about the cone axis is retained, giving the false indication that the aircraft is rotating steadily about the cone axis rather than coning and holding essentially constant attitude. Thus, the gyro and computational bandwidths must be high enough to track any coning motion present in the aircraft's motion which would cause too large an indicated attitude drift if they were outside the bandwidth of the system. This coning error is a second-order effect due to the rectification (or lack of rectification) of the oscillatory angular velocity components in the nonlinear

differential equations and thus, fortunately, is not too large. Data on typical motions of the aircraft would be necessary in order to determine the bandwidth needed to meet coning accuracy requirements.

2.2.3 Correction for Angular Velocity of Reference Frame

The formula for $\underline{\omega}_R$, the angular velocity of the north, east and down coordinate frame relative to inertial space expressed in north, east and down coordinates as required in Eq. (2.2.2-2) is

$$\underline{\omega}_R = \begin{bmatrix} \Omega_e \cos L + \frac{U}{R} \sin \psi \\ -\frac{U \cos \psi}{R} \\ -\Omega_e \sin L - \frac{U}{R} \tan L \sin \psi \end{bmatrix} \qquad (2.2.3\text{-}1)$$

where

Ω_e = angular velocity of the earth

ψ = aircraft true (as opposed to magnetic) heading angle

L = latitude of aircraft (positive in northern hemisphere)

U = true airspeed of aircraft

R = radius of the earth

Note that the sine and cosine of the heading angle rather than the heading angle itself are required in this calculation. To gain an

idea of the size of $\underline{\omega}_R$, note that earth rate, Ω_e, is fifteen degree per hour and that for a true airspeed, U, of one thousand miles per hour the quantity (U/R) corresponds to about fifteen degrees per hour.

2.2.4 Vertical Erection Computation

Due to gyro errors and inaccuracies in the compensation for the angular velocity of the reference coordinate frame described above, the integration of rate gyro outputs alone does not provide an adequate long-term attitude reference. The approach normally adopted is to employ the gyros to provide short-term attitude information while accelerometers are employed to sense gravity and provide long-term information on the direction of the local vertical and a magnetic compass is employed to provide long-term heading information. The accelerometers and magnetic compass do not provide good short-term attitude information for the following reasons. Since the accelerometers actually sense aircraft acceleration minus gravity, in the short term the accelerometer outputs are likely to be dominated by signals due to aircraft motion. However, over a one-minute period, if the aircraft is not executing an accelerated maneuver, it is unlikely that the horizontal component of the aircraft velocity will change by more than twenty feet per second, and the average horizontal acceleration over a one minute time period is less than

$$\frac{20}{60} \cdot \frac{G}{32} \simeq \frac{1}{90} G \qquad (2.2.4\text{-}1)$$

Thus, over a one-minute period, the average accelerometer output will be within one percent or one half degree of angle of the gravity vector. The magnetic (flux-gate) compass is mounted on pendulous gimbals so that it remains level and does not sense magnetic dip, which would produce large indicated heading errors. These gimbals are lightly damped in order to prevent aircraft pitch and roll rotation from being transmitted to the suspended compass sensor. Thus, linear accelerations of the aircraft cause the compass sensor to swing like a pendulum and the sensor output signals contain oscillatory error signals due to the vertical component of the magnetic field (dip effect), which is sensed as the compass sensor swings. Since, on the average, the compass sensor is level, these errors will average out to zero.

The long-term attitude information from the accelerometers and compass enters the rotation matrix calculation through the erection angular velocity, $\underline{\omega}_E$. The effect of the $\underline{\omega}_E$ input is to cause the indicated vertical and north directions to rotate relative to the aircraft with an angular velocity $\underline{\omega}_E$. The erection angular velocity $\underline{\omega}_E$ is most conveniently expressed in the reference coordinate system and is made up of two components, $\underline{\omega}_V$, the vertical erection angular velocity and $\underline{\omega}_A$, the azimuth erection angular velocity.

$$\underline{\omega}_E = \underline{\omega}_V + \underline{\omega}_A \qquad (2.2.4\text{-}2)$$

Let $\underline{a}_{body}$ denote the indicated acceleration in aircraft body coordinates, that is, the body-mounted accelerometer outputs corrected

for known scale factor and bias errors. The indicated acceleration in reference coordinates, $\underline{a}_{ref}$, is determined from the equation

$$\underline{a}_{ref} = R^T \underline{a}_{body} \tag{2.2.4-3}$$

If there is an indicated acceleration along the reference coordinate system Y axis (indicated east axis), the reference coordinate frame should be rotated in a positive sense about its X (indicated north) axis in order to force the indicated acceleration to lie entirely along the minus Z reference axis. Similarly, if there is an indicated acceleration along the reference coordinate frame X (indicated north) axis, the reference coordinate frame should be rotated in a negative sense about its Y axis to eliminate this acceleration component. Thus

$$\underline{\omega}_V = K_V \begin{bmatrix} a_{ref,y} \\ -a_{ref,x} \\ 0 \end{bmatrix} \tag{2.2.4-4}$$

where K_V is the vertical erection gain. The quantity $(1/K_V g)$ is the time constant of the vertical erection loop and normally would not be chosen smaller than one minute. The dynamics of the vertical erection loop is discussed in Section 2.4. At this point it may be noted that the vertical erection gain K_V is small, so that the accelerometer outputs have only a long term effect on the indicated attitude.

Provision must be made for erection cutoff during accelerated maneuvers by setting K_V to zero when the bank angle is larger than a preset value and also, if desired, when the longitudinal acceleration exceeds a preset value. It is also desirable to limit the maximum magnitude of the erection angular velocity, $\underline{\omega}_V$, since it is known that the drift rates being corrected by $\underline{\omega}_V$ are relatively small. Provision must also be made for inserting a large vertical erection gain, K_V, for pre-takeoff alignment of the attitude reference system. Initial alignment may also be accomplished by calculating the intial rotation matrix, R, from the accelerometer and compass outputs when the aircraft is stationary before takeoff. However, this method requires a special subroutine for initial alignment and thus increases computer memory requirements.

2.2.5 Calculation of Attitude Angles from Rotation Matrix Elements

The purpose of this section is to give the formulas for extracting the heading angle ψ, the pitch angle θ, and the roll angle ϕ from the elements of the rotation matrix R relating reference to body coordinates. The attitude angles ψ, θ, and ϕ are needed to drive the artificial horizon and compass displays and as autopilot inputs, while the heading angle ψ is also required for the azimuth erection loop described in the next section.

It should be noted that for most, if not all, of these purposes the quantities required are the sine and cosine of the attitude angles

rather than the actual angles themselves. Thus, the displays require synchro or resolver signals which are the sine and cosine of the angle to be displayed. Also, the vehicle motion angular velocity correction, $\underline{\omega}_R$, is computed employing cos ψ and sin ψ but not ψ itself and the formulas for azimuth erection given in the next section require cos ψ and sin ψ rather than ψ. The reason that this fact is important is that it is costly in time to compute trigonometric and inverse trigonometric functions, and the attitude reference computer program must run at a high cyclic rate to provide the necessary bandwidth. Thus, it is desirable to eliminate all unnecessary trigonometric function evaluations.

To obtain the formulas for the cosine and sine of the heading angle, note that the first row of the rotation matrix R is the aircraft X body axis unit vector expressed in reference coordinates.

$$\cos \psi = \frac{R_{11}}{\sqrt{R_{11}^2+R_{12}^2}}$$

$$\sin \psi = \frac{R_{12}}{\sqrt{R_{11}^2+R_{12}^2}} \qquad (2.2.5\text{-}1)$$

Since the denominator in these expressions turns out to be the cosine of the pitch angle, it will not be small for normal transport aircraft attitudes.

Again, using the fact that the first row of the rotation matrix is the body X axis expressed in reference coordinates, it follows that

$$\cos\theta = \sqrt{R_{11}^2 + R_{12}^2}$$

$$\sin\theta = -R_{13} \tag{2.2.5-2}$$

Finally, consider the vertical plane containing the aircraft X axis and let $\underline{e}$ be the unit vector in this plane normal to the aircraft X axis. Then

$$\underline{Z}_{ref} = \underline{e}\cos\theta - \underline{X}_{body}\sin\theta \tag{2.2.5-3}$$

where $\underline{Z}_{ref}$ and $\underline{X}_{body}$ are the reference Z and body X axis unit vectors. Solving Eq. (2.2.5-3) for $\underline{e}$, employing (2.2.5-2) and the fact that the third column of R contains the components of the reference Z axis expressed in body coordinates, it follows that

$$\underline{e}_{body} = \frac{1}{\sqrt{R_{11}^2 + R_{12}^2}} \begin{bmatrix} 0 \\ R_{23} \\ R_{33} \end{bmatrix} \tag{2.2.5-4}$$

and thus

$$\cos \phi = \frac{R_{33}}{\sqrt{R_{11}^2+R_{12}^2}}$$

$$\sin \phi = \frac{R_{23}}{\sqrt{R_{11}^2+R_{12}^2}} \qquad (2.2.5\text{-}5)$$

2.2.6 Azimuth Erection Computation

Let ψ_c denote the magnetic heading indicated by the fluxgate compass sensor. The electrical signals provided by the compass sensor are proportional to the sine and cosine of the magnetic heading of the aircraft rather than to the heading angle itself. Let ψ_v be the magnetic variation, that is, the difference between true heading and magnetic heading at the present location of the aircraft. Since magnetic variation is a slowly varying quantity, the azimuth erection routine would be provided with values of cos ψ_v and sin ψ_v which would be updated occasionally.

Since the function of the azimuth erection routine is to drive the indicated heading angle into agreement with the compass heading corrected for magnetic variation, the azimuth erection angular velocity, $\underline{\omega}_A$, expressed in reference coordinates will be taken to be

$$\underline{\omega}_A = \begin{bmatrix} 0 \\ 0 \\ -K_A \sin (\psi_c+\psi_v-\psi) \end{bmatrix} \qquad (2.2.6\text{-}1)$$

In this case, the erection gain, K_A, is the inverse time constant of the azimuth erection loop.

To avoid evaluation of trigonometric functions in the computer, the following expression would be used to compute the erection signal.

$$\sin(\psi_c+\psi_v-\psi) = (\cos\psi_c\sin\psi_v+\sin\psi_c\cos\psi_v)\cos\psi$$

$$- (\cos\psi_c\cos\psi_v-\sin\psi_c\sin\psi_v)\sin\psi \qquad (2.2.6\text{-}2)$$

It may be desirable to display magnetic rather than true heading. In this case, another correction for magnetic variation may be carried out before displaying the heading angle or the reference coordinate system may be erected to magnetic north rather than true north. In the latter case, the equations for $\underline{\omega}_R$, the angular velocity of the reference coordinate system relative to inertial space must be modified to include magnetic variation and its rate of change.

As with the vertical erection loop, provision must be made to set the azimuth erection gain, K_A, to zero during accelerated maneuvers since the fluxgate compass sensor will not remain level during accelerated flight and will give erroneous readings due to magnetic dip. Provision must also be made to employ a high value of K_A for initial alignment of the attitude reference system before takeoff.

2.2.7 Summary of Implementation of Gimbal-Less Attitude Reference System

Unfortunately, the rate gyros normally employed for autopilot

rate damping modes are not accurate enough to meet attitude indication requirements and the next better grade of single-degree-of-freedom gyros, costing about three times as much, would have to be employed. However, the outputs of these gyros would be used for rate damping as well as attitude indication, resulting in a savings in the total number of gyros required.

The computer algorithm required to process the data is more complex than the average algorithm encountered in autopilot applications. However, it is simple enough to be easily implemented on a mini-computer. The major computational problem is the high cyclic rate at which the algorithm must be operated to provide the necessary bandwidth. A cyclic rate of twenty cycles per second would provide a five cycles per second bandwidth, which should meet normal autopilot requirements. However, the bandwidth required to eliminate significant attitude indication errors due to aircraft coning would depend on the coning behavior of the particular type of aircraft carrying the system and could be higher than five cycles per second.

Long-term attitude indication accuracy would be provided by erection loops employing accelerometers and a fluxgate magnetic compass as in a conventional system.

The gimbal-less implementation has a slight advantage over the conventional directional gyro because the gimbaling of the directional gyro causes a small heading indication error when the aircraft is banked and the heading is not a cardinal direction while the gimbal-less system has no short-term heading sensitivity to roll angle.

2.3 Provision for High Reliability from the Body-Mounted Instruments

A number of the attitude reference system sensors are mounted directly on the airframe rather than being mounted on gimbals. This class of sensors includes the rate gyros employed to provide aircraft body rates for the autopilot rate stabilization modes. These same gyros may also be employed to provide attitude angle information if the gimbal-less attitude reference implementation described in the preceding section is employed. (In this case, all the gyros and accelerometers in the attitude reference system will be body-mounted.) The attitude reference system may also contain body-mounted accelerometers to provide load factor, side force and vertical acceleration (for autoland mode) information for the autopilot.

With gimbaled sensor packages such as a vertical gyro, directional gyro, or stabilized platform, the most practical approach to providing high reliability through redundancy is to install several identical sensor packages which measure the same physical quantities and arrange for voting among their outputs. This is true because the failure of a single component of a sensor package, for example a single gyro on a gimbaled platform, tends to render the entire sensor package inoperative.

The redundancy situation with body-mounted rate gyros and accelerometers is different because these sensors measure a single component of a three-dimensional vector. Thus, if these sensors are mounted

in such a way that each sensor measures the component of the desired angular velocity or acceleration in a different, carefully chosen direction in space, the desired vector can be determined from any three sensor outputs. Employing a redundancy technique in which each sensor measures a different quantity results in a smaller number of sensors being required for a given level of reliability than if several sensors measure the identical quantity. However, when a failure occurs, the task of determining which sensor has failed becomes more difficult when the instruments all measure different quantities.

In this section two redundant configurations of single-degree-of-freedom body-mounted sensors are proposed. The first configuration provides the maximum possible economy of sensors but requires extensive computer processing to identify failed sensors. The second configuration employs more sensors, although still fewer than a pure voting technique would require, and lends itself to relatively simple identification of failed sensors.

The term "body-mounted instruments" refers in this section to the body-mounted single-degree-of-freedom rate gyros and accelerometers. The two major considerations in providing high reliability are (1) detecting and identifying instrument failures and (2) the configuration in which the instruments are mounted.

When an instrument fails, the data processing system must be informed of the failure so that the output of the failed instrument can be removed from the calculations. (This removal may occur

implicitly rather than explicitly if majority voting of instrument outputs is employed.) Two modes of failure detection/identification are possible: self test and functional test. The term "self test" is intended to cover the cases when information from a single instrument is employed to determine whether that instrument has failed, without using signals from other instruments. "Functional test" covers the cases in which the output of an instrument is compared with the outputs of other instruments in the system to determine whether a failure has occurred.

The two modes of self test described below are commonly available in rate gyros, and the second mode is also available in accelerometers. Mode (a): A signal is available which indicates whether or not the gyro wheel is rotating at the proper speed. Since wheel bearing failures occur frequently, this is a useful check and should be employed. Mode (b): a self-test torquer is provided which produces an accurately controllable torque about the same axis that receives gyroscopic torque from sensed angular velocity. In an accelerometer, the self-test torque is applied about the axis which receives torque due to sensed vehicle acceleration. This is a reliable test of the instrument's ability to sense changes of angular velocity or linear acceleration. It has two limitations. First, it does not test for biases; that is, it cannot determine if the instrument output is zero when the angular velocity or linear acceleration is zero. Biases may develop in flight due to mass unbalance in the instruments or due to more subtle causes

such as convection and gas bubbles in the flotation fluid. Thus the self-test torquer provides a complete preflight test, when the aircraft angular velocity and linear acceleration are known and both instrument biases and scale factors can be checked, but it provides an incomplete in-flight test. Second, during flight through turbulent air, it may be difficult to discriminate between instrument outputs caused by aircraft motion and self-test torques. The simplest solution to this problem is to compute the aircraft rate or acceleration which the instrument should sense based on the outputs of the other instruments of a redundant configuration. In this case, any difference between the computed and actual instrument output should be caused by the self-test torque. Using this approach, the test becomes a hybrid one but may be useful in flight to provide identification of failures at a lower failure level than a pure functional test would provide.

In a functional test, the outputs of redundant instruments are available, and the output of any instrument is calculable from the outputs of other instruments. Any difference between the computed and actual output beyond the tolerance due to normal instrument errors indicates that either the original instrument or one of the instruments employed in the calculation of its output has failed. The difficulty in functional testing arises in identifying which instrument has failed. In order to identify a single failure, it is necessary to employ an array of at least five instruments. (That is, a total of at least five rate gyros must be used, not five gyros per body axis.) Thus, if two

failures are to be tolerated, six instruments must be employed, so that, after the first failed instrument is removed from the calculations, five instruments remain, and the second failure can be identified. On the other hand, if functional failure identification were not a consideration, a system consisting of five instruments with their input axes skewed so that no set of three input axes lies in the same plane would be able to tolerate two instrument failures. The computer program required for functional failure identification may consist of several hundred words and must have a high repetition rate so that failures are identified before they do serious harm to the mission. Thus, failure identification has a significant effect on computer loading.

The conclusion reached relative to testing modes is that functional testing for failures must be carried out. If minimizing computer loading is an important factor, a simple voting scheme with a redundant set of instruments mounted on each of three mutually orthogonal body axes may be employed. However, if computer time is available, it will be seen below that a saving in the number of instruments required is possible by employing a non-orthogonal configuration of instruments with more complex failure identification algorithms.

Two redundant instrument configurations are described below. The instrument configuration is the arrangement of the instrument input axis directions relative to the body axes of the aircraft. The configurations are designed to tolerate two instrument failures and provide for identification of the failed instruments by functional testing, that is, by comparison of instrument outputs.

It is assumed that the two instrument failures to be tolerated occur as sequential single failures with enough time between failures to allow the first failure to be identified before the second failure occurs. This is a valid assumption if the failures occur randomly with a constant failure rate. Multiple simultaneous failures are difficult to identify because the failures may tend to mask each other. As a somewhat oversimplified example of how double failures may mask each other, consider the case of four instruments measuring the same quantity whose correct value is one, and assume that two instruments have failed to zero output. Then the four instrument outputs are zero, zero, one and one, and it is difficult to determine whether zero or one is the correct answer. On the other hand, if the failures had occurred sequentially, the outputs after the first failure would have been zero, one, one, one, and the decision would have been made to ignore the output of the first instrument from then on. The output after the second failure, ignoring the first instrument would be zero, one, one, and it would be clear that one is correct. In the case of measuring angular velocity or linear acceleration, a configuration consisting of at least seven instruments is required to guarantee functional identification of all large simultaneous double failures. Note that this figure compares with a minimum of six instruments required to identify two sequential single failures. Furthermore, if the possibility of double simultaneous failures is allowed, the size of the smallest single failure which will be identified increases. This is undesirable because of errors produced while employing the output of the failed instrument before it is identified.

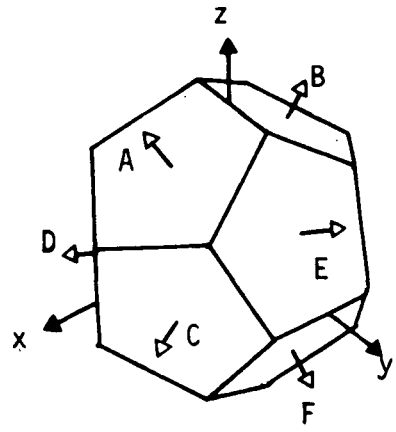

Figure 2.1a Six-instrument system

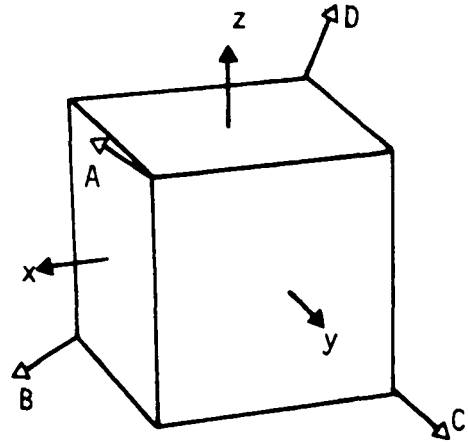

Figure 2.1b Eight-instrument system

The first suggested instrument configuration employs six instruments and therefore provides the best possible economy of instruments. If it is desired to reduce the amount of computation required for failure identification, a second configuration employing eight instruments is suggested. Failure identification with the eight-instrument configuration is almost as simple as majority voting and can be accomplished with either analog or digital signals. The voting approach would require four instruments for each aircraft body axis, a total of twelve instruments. Therefore, the eight-instrument configuration is recommended rather than voting with twelve instruments if computational simplicity is desired.

If the minimum possible number of instruments is to be employed, it is important to distribute their input axes in space as widely as possible. For this reason, the instruments of the six instrument system are configured so that their input axes are normal to the faces of a regular dodecahedron as shown in Figure 2.1a. This configuration is described in Reference [1], and optimum failure detection and identification algorithms and an error analysis are contained in Reference [2]. Since this configuration is documented elsewhere, it will not be discussed further.

In the eight-instrument configuration, direct comparison between outputs of instruments with parallel input axes is employed to simplify the failure identification logic. Therefore, the instruments are mounted in pairs with two instrument input axes normal to each face of a regular tetrahedron as shown in Figure 2.1b. In the discussion of this configuration,

the instruments will be assumed to be rate gyros and the measured vector will be assumed to be aircraft angular velocity, although the results apply equally well to acceleration measurement.

The problem of calculating aircraft angular velocity along body axes from gyro information along axes that are skewed to the body will be discussed first. Since there is a high degree of redundancy in the measurement of angular velocity with zero or one failure (for example, with no failures, from three to eight gyro outputs may be employed in this calculation), the alternative methods of computation will be pointed out, but the relatively arbitrary choice of which is most desirable with a given number of failures will not be made. The four axes $\underline{a}$, $\underline{b}$, $\underline{c}$ and $\underline{d}$ along which the input axes of pairs of instruments are aligned are given by

$$\begin{aligned}
\underline{a} &= \frac{1}{\sqrt{3}} (\underline{i} + \underline{j} + \underline{k}) \\
\underline{b} &= \frac{1}{\sqrt{3}} (\underline{i} - \underline{j} - \underline{k}) \\
\underline{c} &= \frac{1}{\sqrt{3}} (-\underline{i} + \underline{j} - \underline{k}) \\
\underline{d} &= \frac{1}{\sqrt{3}} (-\underline{i} - \underline{j} + \underline{k})
\end{aligned} \tag{2.3-1}$$

where $\underline{i}$, $\underline{j}$ and $\underline{k}$ are unit vectors along the body x, y, and z axes respectively. The $\underline{a}$, $\underline{b}$, $\underline{c}$, and $\underline{d}$ axes will be called "configuration axes". The component of angular velocity along a configuration axis

is obtained by either selecting the output of one of the two instruments whose input axes lie along that configuration axis or averaging the two outputs. Naturally, the outputs would not be averaged if one of the instruments has been identified as failed. Averaging should reduce the effect of normal (unfailed) gyro errors somewhat, giving an improvement by a factor of $(\sqrt{2}/2)$ if the errors are independent random variables. If the angular velocity components, ω_a, ω_b, ω_c, and ω_d along all four configuration axes are available, the least-squares estimate of angular velocity along body axes, ω_x, ω_y, and ω_z, may be employed.

$$\omega_x = \frac{\sqrt{3}}{4}(\omega_a + \omega_b - \omega_c - \omega_d)$$

$$\omega_y = \frac{\sqrt{3}}{4}(\omega_a - \omega_b + \omega_c - \omega_d) \qquad (2.3\text{-}2)$$

$$\omega_z = \frac{\sqrt{3}}{4}(\omega_a - \omega_b - \omega_c + \omega_d)$$

The body axis angular velocity may be computed from the angular velocity components along three configuration axes as follows. With the a, b and c axes:

$$\omega_x = \frac{\sqrt{3}}{2}(\omega_a + \omega_b)$$

$$\omega_y = \frac{\sqrt{3}}{2}(\omega_a + \omega_c)$$

$$\omega_z = \frac{\sqrt{3}}{2}(-\omega_b - \omega_c)$$

With the a, b, and d axes:

$$\omega_x = \frac{\sqrt{3}}{2}(-\omega_c - \omega_d)$$

$$\omega_y = \frac{\sqrt{3}}{2}(\omega_a + \omega_c) \qquad (2.3\text{-}3)$$

$$\omega_z = \frac{\sqrt{3}}{2}(\omega_a + \omega_d)$$

With the b, c and d axes:

$$\omega_x = \frac{\sqrt{3}}{2}(-\omega_c - \omega_d)$$

$$\omega_y = \frac{\sqrt{3}}{2}(-\omega_b - \omega_d)$$

$$\omega_z = \frac{\sqrt{3}}{2}(-\omega_b - \omega_c)$$

If the body-axis angular velocity components are to be computed with analog signals, the fact that the coefficients within each expression above have equal magnitudes is a convenience. Switching from a four configuration-axis to a three configuration-axis computation may be accomplished by switching off two inputs in each expression in Eq. (2.3-2) and multiplying the result by two. Since there are only two possible three-configuration-axis expressions for each body axis component of angular velocity, an alternative mechanization would evaluate both expressions, averaging them for four-axis operation and selecting the

one appropriate single expression for three-axis operation. Finally, the component of angular velocity which should be measured along one of the configuration axes may be calculated from the components along the other configuration axes using the expression

$$\omega_a + \omega_b + \omega_c + \omega_d = 0 \qquad (2.3\text{-}4)$$

The advantage of spreading the configuration axes out in space as widely as possible may be seen at this point. If three instruments with independent random (unfailed) errors of one unit rms magnitude are mounted with one instrument input axis along each of the three mutually mutually orthogonal body axes, the angular velocity uncertainty about any axis in space has an rms magnitude of one unit. On the other hand, if three instruments with the same errors are mounted with one instrument input axis along each of three of the four configuration axes defined above, the largest angular velocity uncertainty occurs about the fourth configuration axis and has an rms magnitude of $\sqrt{3}$ units (1.7 units) while the uncertainties about axes normal to this axis have rms magnitddes of $\sqrt{3}/2$ units (0.9 units). This extra uncertainty is the price paid for the flexibility of being able to employ any three of the of the four configuration axes and results even though the configuration axes are nearly orthogonal, the angle between any two configuration axes being 109.5°.

Failure detection and identification with the eight-instrument configuration are performed as follows. Preceding the first failure,

there are two "good" instruments on each of the four configuration axes. The first instrument failure is detected by noting that the outputs of the two instruments along the configuration axis containing the failed instrument disagree. The problem of identifying the failed instrument reduces to deciding which of the two instruments along the configuration axis with disagreement is the bad one. Eq. (2.3-4) above determines the angular velocity which instruments along this axis should read as a function of the outputs of the instruments along the other axes, which are known to be good. The failed instrument is identified as the instrument whose output disagrees with this computed value, and the output of the failed instrument is removed from use in further computations. In order to handle the case of temporary transient failures, it would be possible to reintroduce the output of a failed instrument into the computations if the output remains correct over a period of time.

After the occurrence of failures, some configuration axes will contain two good instruments, while other configuration axes will contain only one, or zero, good instruments. Configuration axes containing two good instruments will be called "duplex axes", while axes containing only one good instrument will be called "simplex axes". The second failure may occur in two ways. First, the axis mate to the first failed instrument may fail. This failure is detected because equation (2.3-4) is no longer satisfied by the four configuration axis outputs. The second failed instrument is identified as the axis mate of the first failed instrument, because the three remaining duplex axes still display intra-axis agreement. Correct outputs are available along three of the four

configuration axes, and the system remains operable. After this failure, the six remaining instruments are located on three duplex axes, and a third failure will be detected by intra-axis disagreement. This detection capability may be employed to engage mission (landing) abort logic. However, with this type of triple failure, it is impossible to determine, from the instrument angular velocity outputs alone, which instrument on the axis with disagreement has failed, and the system is inoperable unless the failed instrument can be identified by self-test.

The second type of second failure is one in which one of the instruments along one of the three remaining duplex axes fails. This failure is detected by intra-axis disagreement along the failure axis. The failed instrument must be on the duplex axis with disagreement and is identified by computing the correct axis output from Eq.(2.3-4). The output of the failed instrument is removed from the computations, and the system remains operable with two duplex and two simplex axes. If the third failure occurs in an instrument along a duplex axis, the failure is detected by intra-axis disagreement and may be identified by employing Eq. (2.3-4) to determine which instrument on the axis has the correct output, and the system remains operable. Of all triple failures, this type, with failed instruments on three different configuration axes, occurs 4/7 of the time. Thus, there is better than a fifty-percent chance that the third failure can be identified by functional testing. If the third failure occurs in one of the two simplex axes, the failure will be detected because equation (2.3-4) is not satisfied. With this type of triple failure, it is impossible to

determine from the instrument angular velocity outputs alone which instrument has failed, and the system is inoperable unless the failed instrument can be identified by self test.

The failure probabilities for the two instrument configurations may be calculated as follows. The six-instrument configuration is not capable of functionally identifying the third failed instrument. Therefore, its dominant failure mode is a triple failure with the third failure of a type which cannot be identified with self test. Let

Q_g = probability of failure of a single instrument

Q_s = probability that self test will not identify a failed instrument

Q_{system} = system failure probability.

Since there are

$\binom{6}{3}$ = 20 distinct triple failures with six instruments,

$$Q_{system} \approx 20\, Q_s\, Q_g^3 \qquad (2.3.4)$$

The eight-instrument configuration is not capable of functionally identifying the third failure if two failures occur on the same configuration axis. Thus, the dominant failure mode with the eight instrument configuration consists of a triple failure with two failures on the same configuration axis and the third failure of a type which cannot be identified by self test. Since there are 24 distinct triple failures

with two instruments on the same configuration axis,

$$Q_{system} \approx 24\, Q_s\, Q_g^3 \qquad (2.3\text{-}5)$$

The six-instrument configuration has fewer instruments, so failures will occur less often with this configuration. However, the eight-instrument configuration is able to identify functionally some triple failures, and for this reason the failure probabilities for both configurations are about equal.

2.4 Interaction between Longitudinal Autopilot Modes and the Attitude Reference System

Vertical erection loops are usually employed in the aircraft attitude reference system to provide long-term stabilization of the indicated vertical to the true local vertical. The pitch erection loop derives its input from a horizontal accelerometer which senses aircraft speed changes as well as vertical indication errors. When the indicated pitch angle from the attitude reference system is used as an autopilot input, the sensitivity of this signal to aircraft speed changes provides an undesired positive feedback path in longitudinal autopilot modes.

The effects of this feedback path are analyzed in this section. It is found that at subsonic cruising speeds a fairly serious degradation of the pitch hold mode results, while the effect on altitude and Mach hold modes is minor The degradation of the pitch hold mode probably has little operational significance. It could be eliminated in a straightforward way by employing a better than normal grade vertical indicating system with either weak erection loops or Schuler tuning. Other corrective measures include limiting the maximum pitch erection rate, adding a Mach hold loop which controls airspeed by varying power setting or employing an airspeed rate signal derived from a pressure sensor to null out the unwanted component of the pitch erection signal.

2.4.1 Erection Loop Dynamics

The subsystem which provides short-term attitude information in the attitude reference system may be either (a) a vertical gyro - directional gyro combination, (b) a gyro-stabilized platform, or (c) a strapdown system in which signals from body-mounted rate gyros are integrated in a computer to generate the rotation matrix for the transformation from navigation coordinates (north, east, down) to aircraft body coordinates. Over time periods of a few minutes, which are of interest for this discussion, all three subsystems behave in the same way, providing an indicated vertical whose angular velocity relative to inertial space is the sum of a small drift rate and an electrical input signal for providing long-term corrections, the latter called the "torquing signal". For convenience of terminology, this subsystem will be referred to as the "vertical gyro", although it may in actuality be any one of the three subsystems described above.

If the vertical gyro is operated without the correction (torquing) signal, the indicated vertical will not remain parallel to the true local vertical for two reasons. (a) The local vertical rotates relative to inertial space due to the rotation of the earth and the motion of the aircraft around the earth while the indicated vertical stays fixed in inertial space except for gyro drift. Since the local vertical angular velocity component due to aircraft motion over the earth is approximately one earth rate for each 1000 miles per hour of forward speed (the angular velocity of the earth is 15 degrees per hour), the maximum value of local vertical angular velocity which must be corrected in subsonic aircraft is twice earth rate. (b) Gyro drift caused by unwanted torques such as gimbal friction and mass unbalance. Gyro drift depends on the quality of the gyros employed; it varies from one earth rate for a minimal system to much smaller values.

The compensating angular velocity required to eliminate type (a) effects may be calculated if aircraft position and velocity are known. This compensation is an open-loop correction, since the vertical indication error magnitude has no effect on the correction signal. However, even if this compensation is not exact due to uncertainties in aircraft position and velocity and torquing signal scale-factor uncertainty, it will reduce the rate at which the indicated vertical tends to drift away from the true local vertical and thus reduces the requirements imposed on the closed-loop correction system. The only quantity required to calculate this correction which is not normally available in a flight control system is aircraft latitude (longitude is not needed in the calculation). In the design of simple attitude reference systems, the improvement in vertical indication accuracy provided by this correction is often considered to be not worth the com-

plexity of obtaining latitude, and this correction is not carried out.

In order to provide long-term vertical indication accuracy, some signal proportional to vertical indication error must be obtained to eliminate the effect of any kinematic drift (type (a)) which is not completely compensated and gyro drift (type (b)). Since the gravity vector lies along the local vertical, it is natural to employ a pendulum, level, or accelerometer to sense the direction of the local vertical. Each of these instruments senses the same physical quantity, the component along its sensitive axis of the acceleration of its mounting point minus gravity. If an accelerometer (or level) is mounted with its sensitive axis normal to the indicated vertical, that is, on the gimbal which is stabilized to the indicated vertical, and the aircraft is not accelerating, the accelerometer output will be the component of gravity normal to the indicated vertical and thus is proportional to the vertical indication error. Normally, two accelerometers are employed, one to sense vertical indication error about the pitch axis and one for roll axis error. The pitch error accelerometer is nearly parallel to the longitudinal axis of the aircraft and therefore senses rate of change of airspeed as well as gravity. In cruise the average longitudinal acceleration is small, and the low-frequency component of the pitch error accelerometer signal provides a good vertical indication error signal. During the take-off run and speed changes in flight, it is desirable to disable the signal from the pitch error accelerometer. Similarly, during turns, since the roll error accelerometer remains approximately horizontal, it senses the centripetal acceleration of the aircraft, hence does not provide an accurate vertical indication error signal, and must be disabled. The outputs of the accelerometers are scaled and serve as torquing signals for the vertical gyro. These signal paths from the error-sensing accelerometers

to the vertical gyro torquing inputs are called vertical erection loops.

In a strapdown attitude reference system the accelerometers are mounted on the aircraft body rather than on a gimbaled structure stabilized to the indicated vertical. However, the acceleration that would be measured by accelerometers mounted normal to the indicated vertical can be calculated as linear combinations of the body mounted accelerometer outputs using the elements of the rotation matrix for the transformation from navigation to body coordinates. From this point on, the operation of strapdown and conventional systems is the same.

To obtain the transfer function of the vertical gyro with erection, assume that the aircraft is flying with a constant heading. (When the aircraft turns, pitch vertical indication error is rotated into roll vertical indication error and vice-versa. Also the erection loops would probably be disabled during a turn). If ε is the angle measured about the pitch axis from the true local vertical to the indicated vertical, then

$$\frac{d\varepsilon}{dt} = \omega_d - K_e a_i \qquad (2.4\text{-}1)$$

where ω_d is the drift rate of the vertical gyro without erection, K_e is the scale factor or gain relating the torquing signal to the accelerometer output and a_i is the output of the pitch error accelerometer. The quantity

$$T_e = \frac{1}{K_e g} \qquad (2.4\text{-}2)$$

has the dimensions of time and turns out to be the time constant for the decay of vertical indication errors due to erection. To first order (see Figure 2.2)

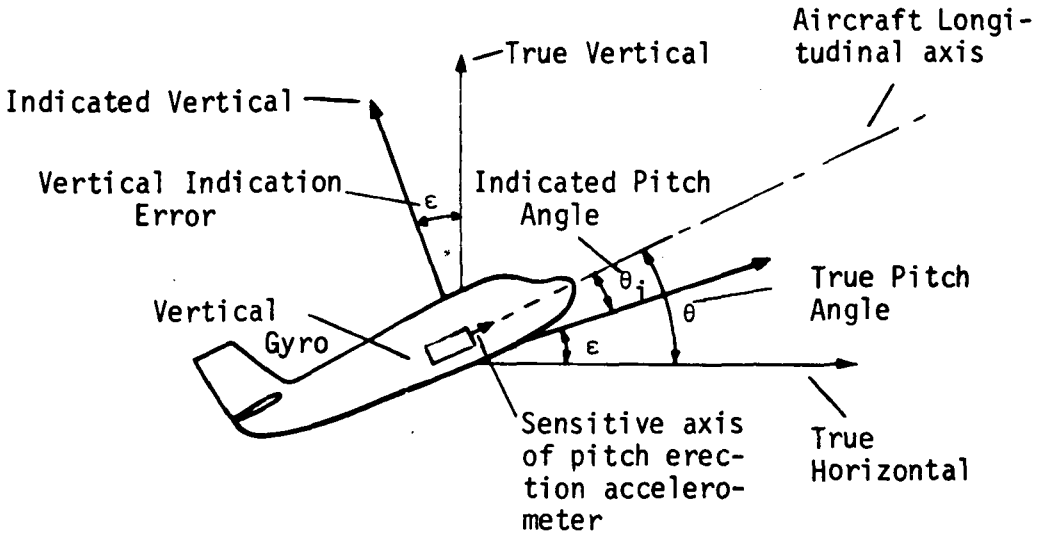

Figure 2.2 Pitch Plane Geometry of Attitude Reference System.

$$a_i = \frac{du}{dt} + g\epsilon \qquad (2.4\text{-}3)$$

where g is the acceleration due to gravity and u is aircraft speed. Combining these equations yields

$$\epsilon = \frac{1}{T_e s+1} \left\{ T_e \omega_d - \frac{s}{g} u \right\} \qquad (2.4\text{-}4)$$

Note that the steady-state vertical indication error due to a constant drift rate is the product of the erection time constant and the drift rate. This fact tends to set the upper limit on the size of the time constant for a given drift rate.

At this point, two variations of the basic erection approach should be mentioned. First, some vertical gyros employ bang-bang torquing in which the erection angular velocity (torquing signal) is always either plus or minus the maximum rate depending on the sign of the accelerometer output except for a dead band with zero erection rate for small accelerometer outputs. The advantage of this design is simplicity of mechanization. It is more difficult to analyze and has no performance advantage over linear torquing except that by its nature the maximum erection rate is limited. It will appear later that limiting the maximum erection rate helps to reduce vertical gyro/autopilot interaction and a linear erection system should also include a limiter.

Secondly, some type of compensation network or filter may be inserted in the erection loop between the accelerometer output and the vertical gyro torquing input. Schuler tuning consists of in-

serting an integrator with the correct scale factor in the erection loop. If high-quality gyros and accelerometers are employed, Schuler tuning provides good performance and eliminates the problem of interaction with autopilot modes. Except with inertial quality gyros and accelerometers, another input signal such as airspeed may be needed to damp the tuned erection loop.

Another filtering approach is to insert a compensation network with a transfer function of the form

$$\frac{(as+b)}{s} \qquad (2.4\text{-}5)$$

in the erection loop. The accelerometer output signals which cause vertical gyro/autopilot interaction have time constants on the order of one or two minutes, while the drift rate which the erection loop is designed to eliminate usually has much slower variations, with time constants on the order of ten or twenty minutes. The filter transfer function of Eq. (2.4-5) has very high gain at low frequencies and yields acceptable vertical indication errors due to slowly varying drift rates while still having a low enough gain at autopilot interaction frequencies to avoid interaction difficulties. When the aircraft executes a 180° turn, the drift rates due to some kinematic effects reverse sign when referred to vertical gyro gimbal axes, while the drift rate due to gyro drift is likely to remain reasonably constant relative to the gimbal axes. Thus the assumption that total drift rate remains relatively constant over times of the order of ten minutes is not

justified if the kinematic drift terms are large.

These alternative approaches will not be pursued further in this section.

Physically, a vertical gyro with erection responds to aircraft motion in the same way as a very heavily damped pendulum whose pivot point is attached to the aircraft. In this analogy, it is assumed that the damping moment on the pendulum is proportional to the angular velocity of the pendulum relative to inertial space. If ε is the angle between the pendulum and the vertical in the pitch plane with a positive value corresponding to a forward swing of the pendulum bob, then

$$\varepsilon = \frac{\omega^2}{s^2+2\xi\omega s+\omega^2}\left(-\frac{s}{g}u\right) \qquad (2.4\text{-}6)$$

where $\omega = \sqrt{g/\ell}$ is the natural frequency of the pendulum and ξ is its damping ratio. Letting

$$\xi = \frac{1}{2}\left(\omega T_e + \frac{1}{\omega T_e}\right)$$

yields

$$\varepsilon = \frac{1}{\left(\frac{s}{\omega^2 T_e} + 1\right)(T_e s+1)}\left(-\frac{s}{g}u\right) \qquad (2.4\text{-}7)$$

This transfer function has an extra pole which the erection loop does

not have. However, with a short pendulum length, the time constant of the extra pole is so short that it has a negligible effect on the pendulum motion. Thus if the pendulum is one foot long and the erection time constant T_e is 60 seconds, then

$$\epsilon = \frac{1}{(0.0005s+1)(60s+1)} \left(-\frac{s}{g} u\right) \qquad (2.4\text{-}8)$$

A heavily damped pendulum cannot actually be used by itself as an aircraft vertical indicator because of the difficulty of damping the pendulum to inertial space rather than to the airframe.

Finally, the aircraft pitch angle θ_i indicated by the vertical gyro is the difference between the true pitch angle of the aircraft, θ, and the pitch plane vertical indication error ϵ, that is

$$\theta_i = \theta - \epsilon \qquad (2.4\text{-}9)$$

2.4.2 Physics of Vertical Gyro-Autopilot Interaction

Consider the action of a pitch hold autopilot mode. Suppose that the aircraft is in straight steady flight when a one degree pitch up command is set into the autopilot. The autopilot will rapidly bring the aircraft nose up one degree and continue to hold the nose up. This causes the aircraft to decelerate slowly towards the lower equilibrium speed with the new pitch angle and the given power setting. The deceleration causes the bottom of the indicated vertical axis of the vertical gyro to swing forward since the indicated vertical acts like a

pendulum. This in turn decreases the indicated pitch angle, and the autopilot calls for more nose-up pitch, and the aircraft decelerates faster. Because of the phase lead caused by the differentiation between aircraft speed and longitudinal acceleration, this positive feedback results in an oscillation in pitch or a pitch overshoot rather than a pitch divergence. The time scale on which the interactive motion takes place is on the order of the erection time constant, that is minutes. Thus, when the relatively fast Mach hold and altitude hold loops are employed as outer loops around the pitch attitude loop, their performance is not significantly degraded by the interaction, just as a pilot can easily control the slow phugoid mode of the aircraft and may not even know that it is present.

2.4.3 Pitch Transfer Function Including Erection

Since the interaction between the vertical gyro and autopilot modes occurs at low frequencies, on the order of one radian per minute, while a digital autopilot would operate with a sampling rate of several samples per second, the autopilot transfer function can be adequately represented for the purposes of this analysis as an equivalent s-plane continuous system transfer function.

It will be assumed that the longitudinal autopilot has an inner pitch damping loop of the form shown in Fig. 2.3.

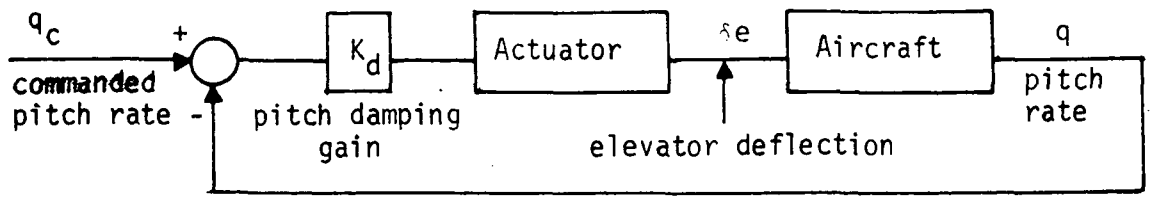

Figure 2.3 Pitch damping loop

If the pitch damping of the bare aircraft meets the requirements of the other autopilot modes, the commanded pitch rate signal can be fed directly into the actuator (without pitch rate feedback), and no change in the subsequent calculations will result. It is now desired to obtain the transfer function between the commanded pitch rate q_c and the indicated pitch angle θ_i employing the erection loop dynamics derived above.

A block diagram of the signal path between commanded pitch angle is shown in Figure 2.4.

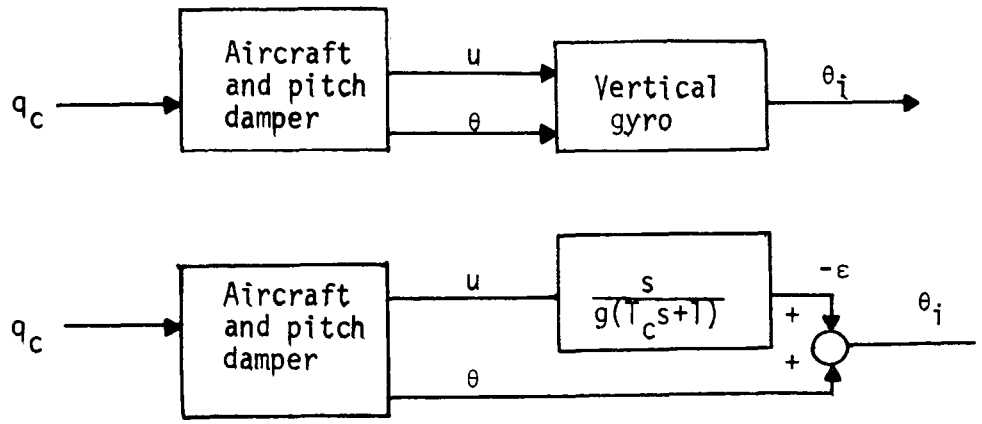

Figure 2.4 Signal path from commanded pitch rate to indicated pitch angle

From Figure 2.4 or Eqs. (2.4-5) and (2.4-9), it follows that

$$\theta_i = \frac{su}{g(T_e s+1)} + \theta \qquad (2.4\text{-}10)$$

The denominator of the transfer function from q_c to θ_i will contain the poles of the aircraft-pitch damper combination, that is actuator,

damped short period, and phugoid poles, plus the erection pole ($T_e s+1$). For closure of the pitch attitude loop, it is important to know the location of the transfer function zeros since the low-frequency closed-loop poles will approach these zeros. Thus, Eq. (2.4-10) will be written with a common denominator

$$\theta_i = \frac{(su+g\theta)+gT_e s\theta}{g(T_e s+1)} \tag{2.4-11}$$

From the aircraft X-axis force equation, it follows that

$$su + g\theta = X \tag{2.4-12}$$

where X denotes the sum of the nongravitational X-axis forces, that is, the X components of aerodynamic force and thrust, divided by the aircraft mass. Combining Eqs. (2.4-11) and (2.4-12) yields

$$\theta_i = \frac{X + gT_e s\theta}{(T_e s+1)} \tag{2.4-13}$$

Eq. (2.4-13) indicates how the zeros of the q_c, θ_i transfer function vary with the erection time constant T_e. If T_e is very large, the zeros approach the zeros of the normal q_c, θ transfer function with an extra zero at the origin which nearly cancels the erection pole, the latter being very close to the origin in this case. On the other hand, if the erection time constant is short, the zeros of the q_c, θ_i transfer function approach the zeros of X. It is desirable, at this point, to obtain an idea of the location of the q_c, X transfer

function zeros.

If elevator lift is ignored, there are two integrations between elevator deflection and X-force. Thus the q_c, X transfer function has two zeros. The X-force is not very strongly excited in the phugoid mode, the only significant phugoid frequency component of X-force being drag variation, which is small since the phugoid is lightly damped. That is, in the phugoid mode,

$$\delta\alpha \simeq 0 \tag{2.4-14}$$

$$\delta\dot{u} \simeq -g\delta\theta \tag{2.4-15}$$

$$\delta X = \delta\dot{u} + g\delta\theta \simeq 0 \tag{2.4-16}$$

Thus, one would expect that the zeros of the X transfer function nearly cancel the phugoid poles, and it is in fact true that the zeros of X are near the phugoid poles. If elevator lift is considered, X force is only one integration from elevator deflection, and X has a third zero with a very short time constant (a fraction of a second). This zero has little effect on pitch dynamics and will be ignored in the following discussion.

Root locus techniques may now be applied to (2.4-13) to plot the zeros of the q_c, θ_i transfer function as a function of the erection time constant. The θ transfer function has a fast zero with a time constant in the short period range, which corresponds to angle of attack adjustment with a pitch hold autopilot, and also a slow

zero with a time constant on the order of a minute, which corresponds to aircraft speed adjustment with a pitch hold autopilot. Figure 2.5 shows the locus of q_c, θ_i transfer function zeros as a function of erection time constant, T_e.

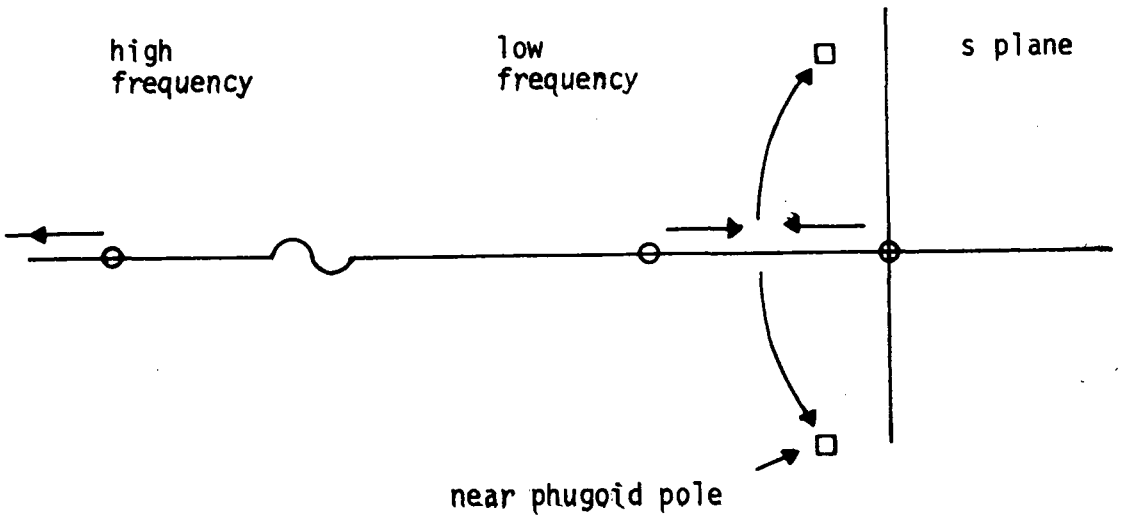

○ = θ transfer function zeros plus zero at origin

□ = X transfer function zeros

⟶ direction of zero locus with decreasing T_e (increasing erection loop gain).

Figure 2.5 Locus of q_c to θ_i transfer function zeros.

2.4.4 Dynamics of Pitch Hold Mode with Erection Loop Interaction

Figure 2.6 is the block diagram of a pitch hold autopilot.

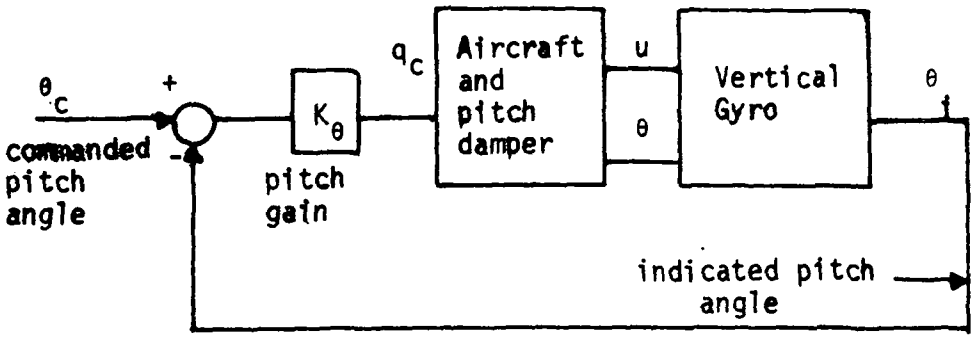

Figure 2.6 Pitch hold autopilot loop

In this autopilot mode, the difference between the commanded pitch angle and the pitch angle indicated by the vertical gyro is multiplied by the pitch gain K_θ and serves as the pitch rate command for the pitch damping loop.

For comparison purposes, Fig. 2.7 shows the root locus for the poles of the transfer function from commanded pitch angle to true pitch angle as a function of pitch gain with a perfect vertical gyro, that is with $T_e = \infty$.

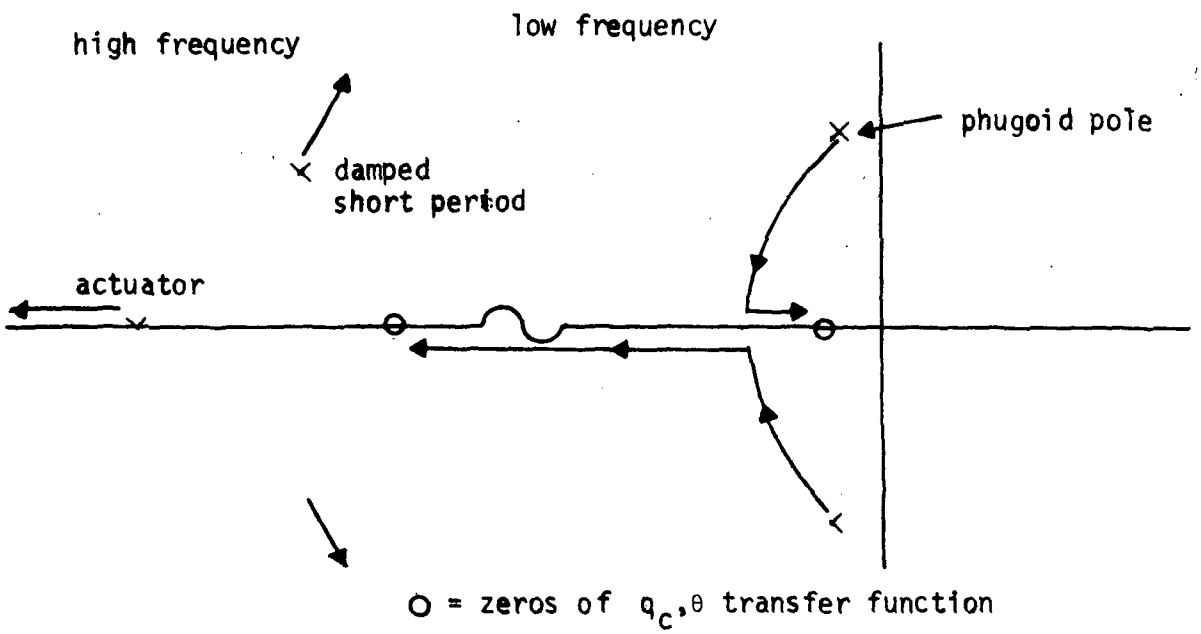

Figure 2.7 Root locus for pitch hold mode with perfect vertical gyro as a function of pitch gain

The only thing which is critical about the choice of the pitch gain in the perfect vertical gyro case is that it be chosen high enough so that the phugoid pole which remains in the low-frequency range is driven to within a few percent of the low-frequency zero. If this is not done, the residue on the low-frequency pole will be too high and the aircraft nose will appear to drift slowly for a long time following each command input.

The root locus for the case of a vertical gyro with a finite erection time constant follows much the same pattern except that there is an extra pole due to erection. Figure 2.8 shows the root locus for the pitch hold mode for the normal case when the erection time constant is somewhat longer than the time constant of the slow zero of the q_c to θ transfer function. Again, the poles remaining in the low-frequency region of the s-plane all approach zeros and if a sufficiently high pitch gain is employed so that the poles are driven

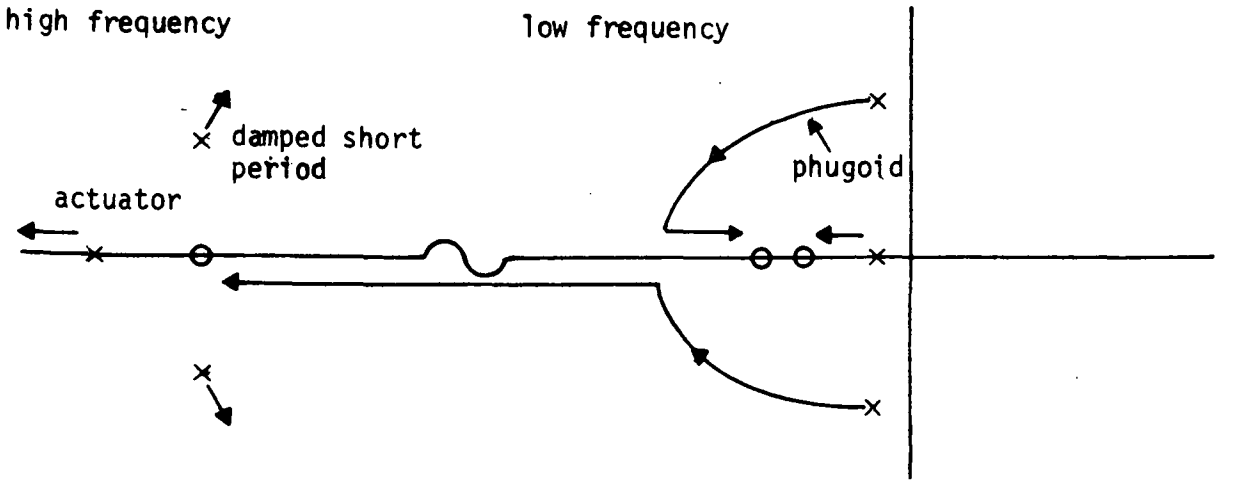

Figure 2.8 Root locus for pitch hold mode with finite vertical gyro erection time. Erection time constant several times longer than slow q_c,θ transfer function zero time constant

close to the zeros, the indicated pitch angle will track pitch angle commands without any slow drift following step commands. If an extremely short erection time constant is employed, the zeros of the q_c, θ_i transfer function lie near the phugoid poles with the result that closing the pitch hold loop no longer damps the phugoid. This root locus is shown in Figure 2.9. Such a short erection time constant would not be used in practice, but even in this case the indicated pitch angle would track the commanded pitch angle well.

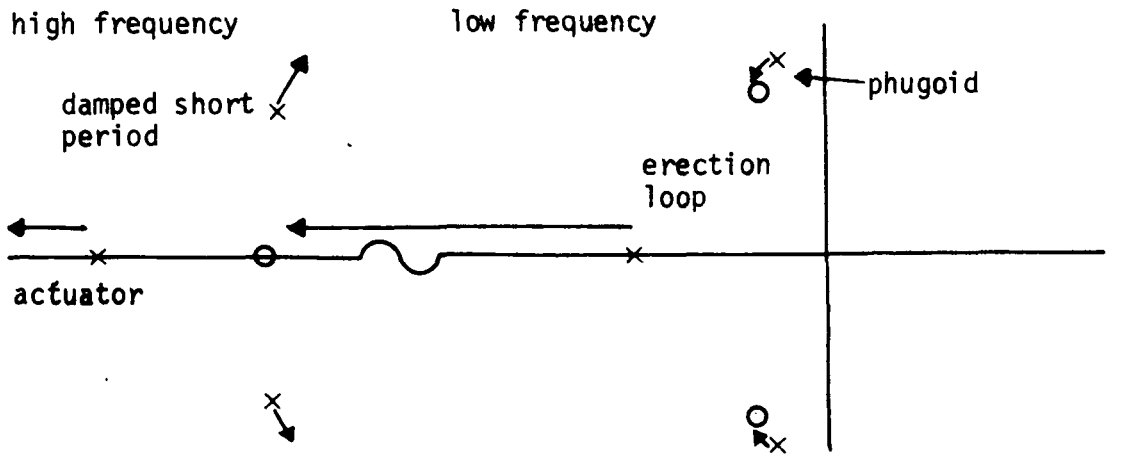

Figure 2.9 Root locus for pitch hold mode with very short erection time constant.

Now the transfer function relating commanded pitch angle, θ_c to true pitch angle θ will be calculated. It should be noted that the artificial horizon provides the pilot with the indicated pitch angle and that his only indication of true pitch angle is the actual horizon and anomalous airspeed and altitude behavior which does not relate well to the history of artificial horizon motion. From the block diagram of the pitch hold autopilot loop shown in Figure 2.6, it follows that the transfer function from commanded pitch angle to pitch rate command is

$$q_c = \left(\frac{K_\theta}{1+K_\theta T_{\theta_i/q_c}(s)} \right) \theta_c \qquad (2.4\text{-}17)$$

where T_{θ_i/q_c} denotes the q_c to θ_i transfer function derived above. Multiplying Eq. (2.4-17) by the q_c to θ transfer function, which will be denoted by T_{θ/q_c}, yields the desired transfer function from θ_c to true pitch angle θ:

$$\theta = \left(\frac{K_\theta T_{\theta/q_c}(s)}{1+K_\theta T_{\theta_i/q_c}(s)} \right) \theta_c \qquad (2.4\text{-}18)$$

Since $T_{\theta/q_c}(s)$ and $T_{\theta_i/q_c}(s)$ have the same denominator except that T_{θ_i/q_c} has an extra pole $(T_e s+1)$ from the erection loop, the denominators of the transfer functions in Eq. (2.4-18) cancel out, and the zeros of the θ_c to θ transfer function are the zeros of $T_{\theta/q_c}(s)$ plus a zero at the erection time constant. Finally, the poles of the θ_c to θ transfer function are the closed-loop pitch hold mode poles.

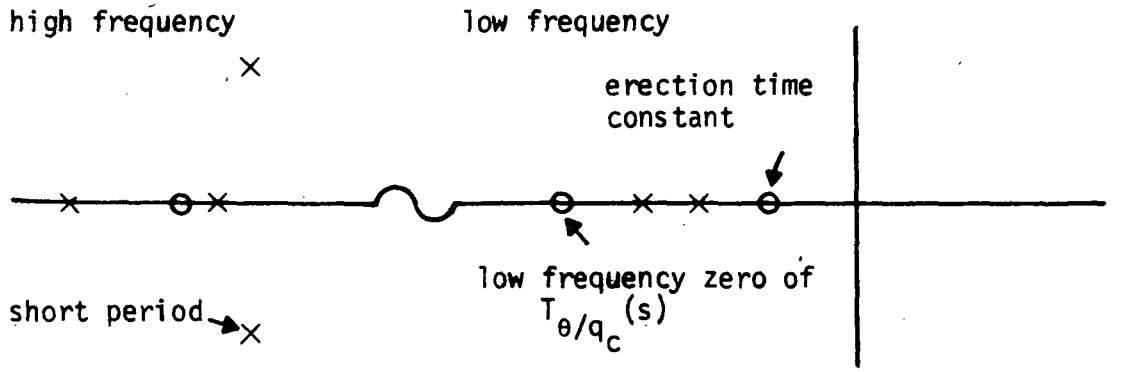

Figure 2.10 Poles and zeros of θ_c to θ transfer function for the case when erection time constant is several times longer than time constant of low frequency zero of $T_{\theta/q_c}(s)$.

Figure 2.10 is an s-plane plot of the poles and zeros of the θ_c to θ transfer function for the case illustrated in Fig. 2.8, in which the erection time constant is several times longer than the time constant of the low-frequency q_c to θ transfer function zero. Note that the two poles in the low-frequency region are not very close to the low-frequency zeros. These poles lie to the left of the right-most zero, which indicates that they participate in an over-shoot rather than a slow rise time when a step input is applied. These poles are particulary objectionable because they have time constants which are minutes long. Their effects last long after the command input has been applied and give the pilot the impression that the autopilot does not provide long-term attitude stabilization if he can detect their presence.

Figure 2.11 is an s-plane plot of the poles and zeros of the θ_c to θ transfer function for the case illustrated in Fig. 2.9, in which the erection time constant, T_e, is very short. In this case the phugoid poles are essentially the same as those of the bare airplane and are not near any zeros. Thus, when a step command is applied, the phugoid mode is strongly excited and then decays according to its small damping ratio. This case is included to show the direction of the trend of decreasing erection time constant but does not correspond to a practical system.

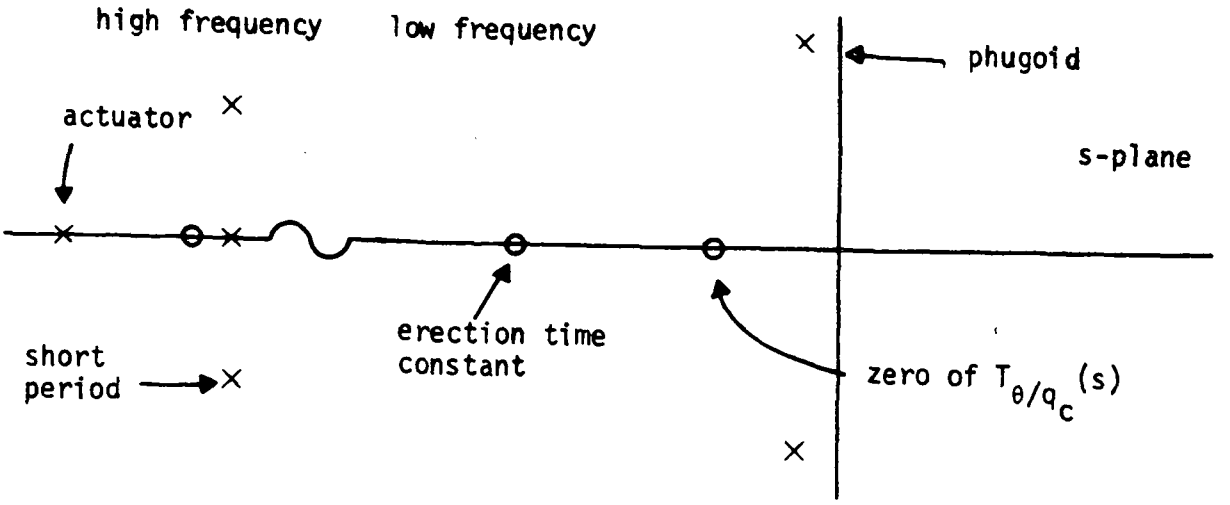

Figure 2.11 Poles and zeros of θ_c to θ transfer function for the case when erection time constant is very short.

2.4.5 Dynamics of Altitude Hold Mode with Erection Loop Interaction

In designing an altitude hold loop in which altitude error is to be fed to the elevator, the simplest approach would be to employ scaled altitude error as the pitch rate command, q_c, to the pitch damper. Unfortunately, there is too much phase lag at low frequencies between q_c and altitude, and this configuration does not provide a well damped altitude response. This difficulty can be removed in two ways. First, an altitude rate signal can be added to the altitude error signal to provide the necessary phase lead. This approach works well in the automatic landing mode where data from a radar altimeter and a vertical accelerometer are mixed to provide a good altitude rate signal. Since the vertical gyro does not furnish signals for this mode, the possibility of vertical gyro-autopilot interaction is eliminated. However, in cruise a good altitude rate signal may

not be available, and a second altitude hold configuration may be employed. In this configuration, the altitude error is scaled by an altitude gain, K_h, and used as a command input to the pitch hold mode. If the aircraft is operating on the front side of the power curve or if an auto-throttle loop is employed to keep airspeed constant by varying power setting, the phase lag between commanded pitch angle and altitude at low frequencies (on the order of the phugoid frequency) is less than ninety degrees and a well damped altitude hold loop results. This altitude hold loop configuration does leave open the possibility of vertical gyro-autopilot interaction and will be investigated below.

Figure 2.12 is a block diagram of the altitude hold loop. The transfer function between commanded pitch angle θ_c and altitude rate $\dot{h}$ will be derived in the same way that the θ_c and θ transfer function was obtained. Thus

$$\dot{h} = T_{\dot{h}/q_c}(s)\, q_c \tag{2.4-19}$$

and employing Eq. (2.4-17)

$$\dot{h} = \left(\frac{K_\theta T_{\dot{h}/q_c}(s)}{1+K_\theta T_{\theta_i/q_c}(s)} \right) \theta_c \tag{2.4-20}$$

The denominators of the transfer functions on the right hand side of Eq. (2.4-20) cancel each other except for the erection loop pole

$(T_e s+1)$, and the zeros of the θ_c to $\dot{h}$ transfer function are thus the zeros of $T_{\dot{h}/q_c}(s)$ plus a zero at the erection loop time constant. The poles of the θ_c to $\dot{h}$ transfer function are the closed-loop poles of the pitch hold loop. Ignoring elevator lift (which contributes two zeros with very short time constants), the q_c to $\dot{h}$ transfer function has a single zero which lies in the left half of the s-plane if the aircraft is operating on the "front" side of the power curve and lies in the right half plane if the aircraft is operating on the "back" side of the power curve. This zero has a long time constant, and, if it lies in the right half plane, its presence makes the design of any altitude hold loop difficult (although still theoretically possible). Normal practice is to employ an auto-throttle to control airspeed with power setting when operating the altitude hold mode on the back side of the power curve. The presence of the auto-throttle loop moves the θ_c to $\dot{h}$ zero into the left half plane, and, if the speed resolution of the auto-throttle is good so that airspeed really remains constant, the problem of vertical gyro-autopilot interaction is eliminated. Thus it will be assumed that the aircraft is operating on the front side of the power curve with a fixed power setting and hence the q_c to $\dot{h}$ transfer function zero lies in the left half plane.

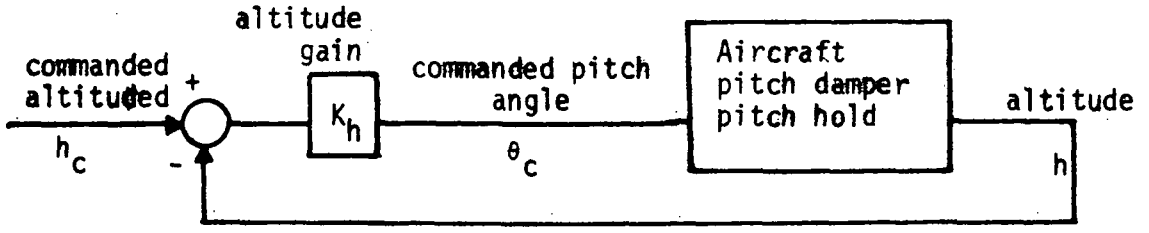

Figure 2.12 Block diagram of altitude hold loop.

For comparison purposes, Figure 2.13 shows the root locus for the closed loop poles of the altitude hold loop with a perfect vertical gyro ($T_e = \infty$) as a function of altitude gain, K_h.

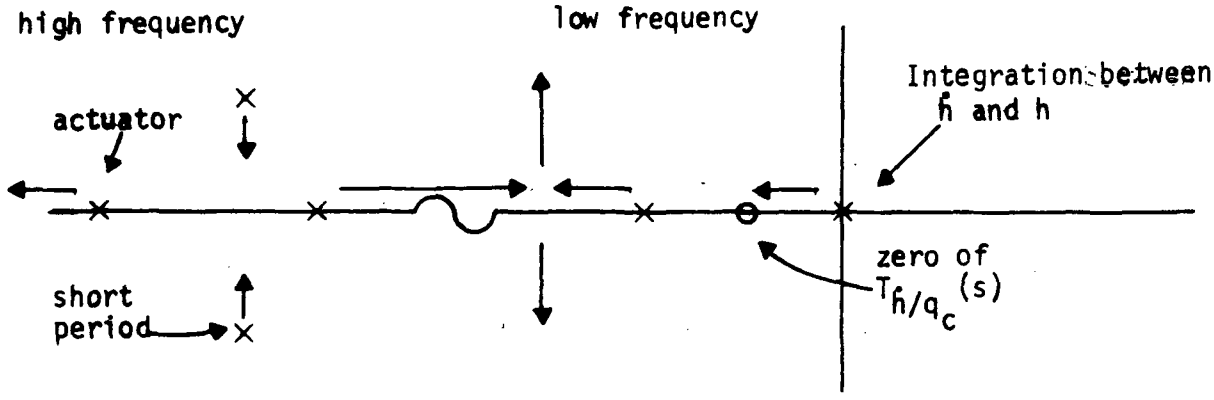

Figure 2.13 Root locus of altitude hold loop with perfect vertical gyro as a function of altitude gain, K_h.

The altitude gain must be chosen large enough so that the pole which was originally at the origin approaches within a few percent of the low-frequency zero. If K_h is not high enough, the residue of the low-frequency pole will not be small for a step input, and the altitude will take a long time to travel the last few percent of the way to its final value. Physically, what happens is that, if the autopilot is commanded to gain altitude, the aircraft loses speed while climbing and doesn't regain its level-flight equilibrium speed until long after the desired altitude has been reached. This speed error causes a small altitude error which slowly disappears as equilibrium speed is regained. If K_h is too high, the poles in the medium-frequency

range (which originally were the phugoid poles) will not be well damped. If this is a problem, lag-lead compensation can be included to provide high gain at low frequencies and medium gain at medium frequencies. An auto-trim mode is also useful for providing high gain at low frequencies.

Figure 2.14 shows the root locus for the closed-loop poles of the altitude hold loop with a finite erection time constant. The only difference in this case is that the extra zero at the erection time constant attracts the extra pole due to the erection loop, and the

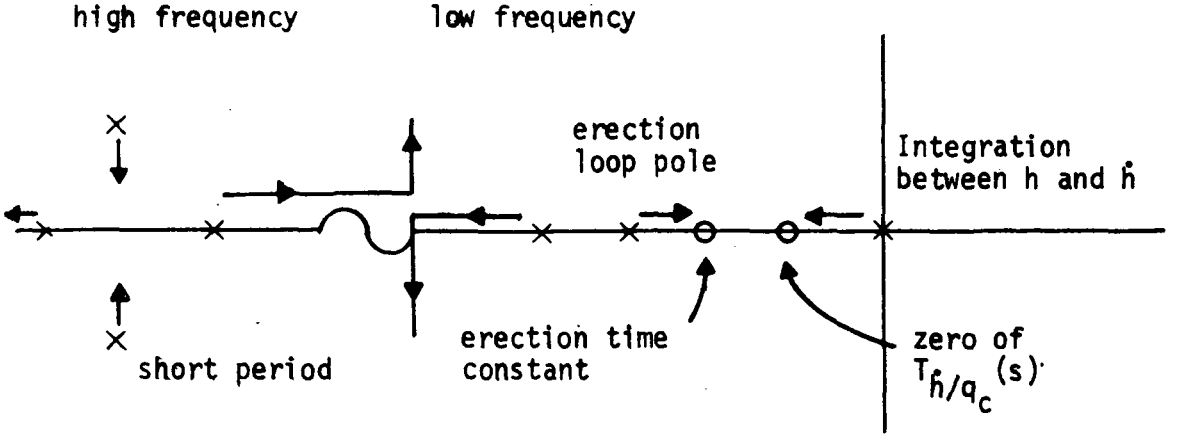

Figure 2.14 Root locus of altitude hold loop with finite erection time constant

altitude gain must be chosen high enough to ensure that both low-frequency poles are close to their respective zeros. Thus the pitch erection loop has little deleterious effect on altitude hold mode operation.

Dynamics of Mach Hold Mode with Erection Loop Interaction

In the Mach hold mode, the difference between actual

and commanded speed is scaled by a Mach gain K_m and employed as a pitch angle command. Figure 2.15 is a block diagram of this mode. The zeros of the transfer function from commanded pitch angle θ_c

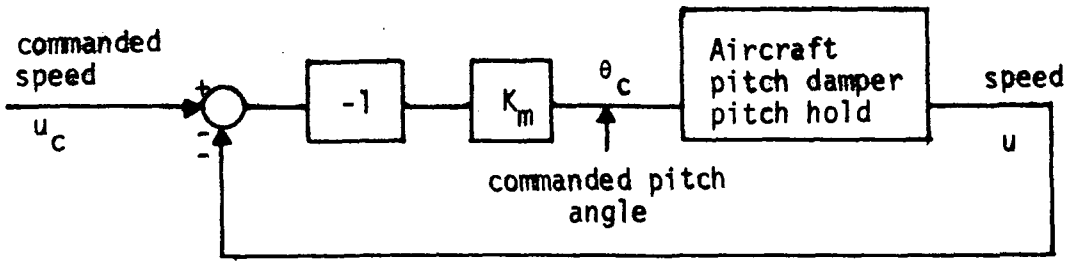

Figure 2.15 Block diagram of Mach hold mode.

to airspeed u are the zeros of the q_c to u transfer function plus a zero at the erection time constant. The poles of the θ_c to u transfer function are the closed-loop poles of the pitch hold mode. Neglecting elevator lift, the q_c to u transfer function has a single zero which lies in the short-period frequency range. Figure 2.16 shows the root locus of the Mach hold mode with a perfect vertical gyro ($T_e = \infty$) as a function of Mach gain K_m. The only limitation

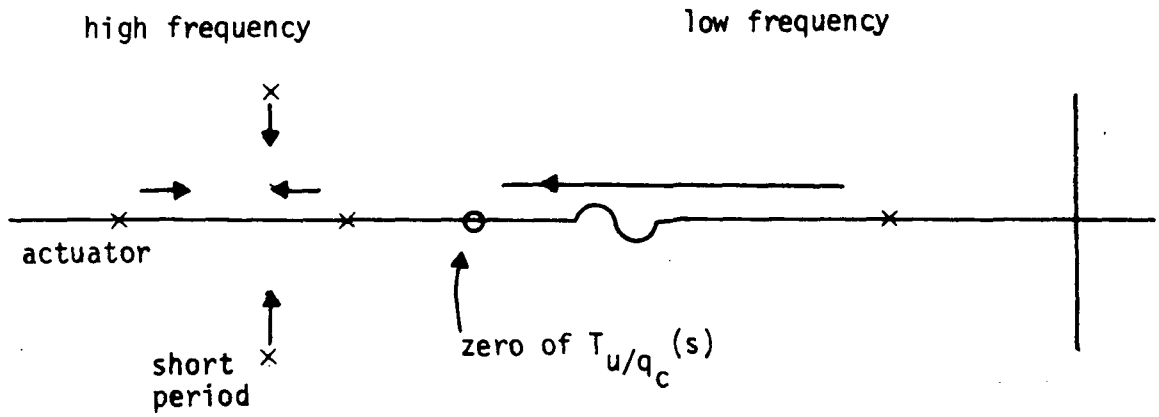

Figure 2.16 Mach hold mode root locus with perfect vertical gyro as a function of Mach gain

on Mach gain in this case is that it not be so high that the poles in the short-period frequency range are poorly damped. Figure 2.17 shows the root locus of the Mach hold mode with a finite erection time constant as a function of Mach gain K_m. In this case the Mach gain should be chosen high enough to drive the erection loop pole

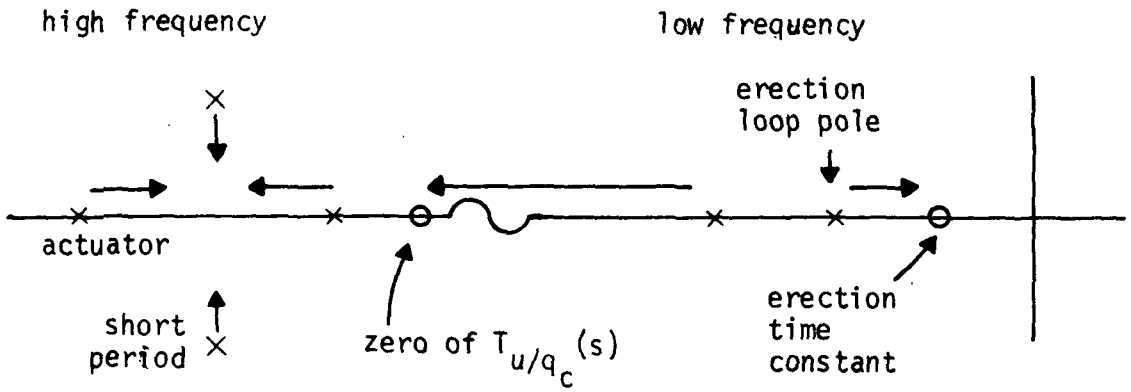

Figure 2.17 Mach hold mode root locus with finite erection time constant as a function of Mach gain.

close to the erection time constant zero in order to prevent this pole from causing a noticeable, slowly decaying speed overshoot. If such a high gain destabilizes the poles in the short-period frequency range, lag-lead compensation may be employed to provide high gain at low frequencies and low gain at high frequencies.

Thus, erection loop-autopilot interaction causes no serious problems in Mach hold loop design.

2.4.6 Approximate Time Constant of Low-Frequency Zero in θ Transfer Function

In order to obtain a simple model of the effect of vertical gyro erection on pitch hold mode dynamics, it is necessary to show that the low-frequency zero of the q_c to θ transfer function is closer to the s-plane origin than the q_c to X transfer function zeros which are near the phugoid poles. This allows the X zeros to be ignored. The approximation process also provides insight into the airspeed adjustment which takes place with pitch angle changes and leads to interaction with the vertical gyro.

The q_c to θ transfer function zeros are the characteristic roots of the aircraft equations of motion when the elevator deflection δe is adjusted to balance the pitching moment equation with θ remaining constant. That is, the zeros are the characteristic roots of the X and Z axis force equations with θ locked and the elevator lift calculated from the elevator deflection required to keep the pitching moment equation balanced. These characteristic roots correspond physically to the dynamics of the aircraft with a very tight pitch hold loop.

To analyze the aircraft dynamics in this case, consider a step increase in pitch angle. The excess lift caused by the jump in angle of attack causes the flight path angle to start to increase, decreasing the angle of attack until lift again equals weight at the current airspeed. This adjustment takes place rapidly and corresponds to the high-frequency zero of the q_c to θ transfer function. With the increased flight path angle, the component of gravity along the flight

path will be larger, and the airspeed will begin to decrease. As airspeed drops, the dynamic pressure decreases, lift becomes slightly less than weight, and the flight path angle decays toward its new equilibrium value in such a way that the increase in angle of attack keeps lift and weight nearly balanced. This slow airspeed decay corresponds to the low-frequency zero of the q_c to θ transfer function. Since the lift adjustment is rapid and results in lift being close to weight, it will be assumed for the approximate analysis of speed decay that lift equals weight. This determines angle of attack α as a function of airspeed u.

$$L_\alpha \delta\alpha + L_u \delta u = 0 \tag{2.4-21}$$

$$L_\alpha \delta\alpha + 2L \frac{\delta u}{u} = 0 \tag{2.4-22}$$

or

$$\delta\alpha = -2\left(\frac{L}{L_\alpha}\right) \frac{\delta u}{u} \tag{2.4-23}$$

Since the rate of change of airspeed is the sum of the forces per unit mass along the flight path and thrust is assumed to be constant,

$$\frac{d\delta u}{dt} = -g \frac{\partial\left(\frac{D}{L}\right)}{\partial u} \delta u - g \, \delta\gamma \tag{2.4-24}$$

where $\partial(D/L)/\partial u$ is the derivative, with respect to trim speed, of the drag-to-lift ratio as a function of trim speed (speed at which lift equals

weight for a given angle of attack), and γ is the flight path angle. Finally,

$$\delta\gamma = \delta\theta - \delta\alpha \tag{2.4-25}$$

and combining equations (2.4-23), (2.4-24), and (2.4-25) yields

$$\delta u = - \frac{gT_u}{T_u s+1} \delta\theta \tag{2.4-26}$$

where

$$\frac{1}{T_u} = g \frac{\partial\left(\frac{D}{L}\right)}{\partial u} + 2 \frac{g}{u} \left(\frac{L}{L_\alpha}\right) \tag{2.4-27}$$

T_u is an approximation to the low-frequency characteristic root of the aircraft dynamical equations in this case and thus approximates the low-frequency zero of the q_c to θ transfer function.

The angular frequency of the phugoid oscillation, ω_p, is given approximately by the formula

$$\omega_p = \sqrt{2} \frac{g}{u} \tag{2.4-28}$$

and thus

$$\frac{1}{T_u} = g \frac{\partial\left(\frac{D}{L}\right)}{\partial u} + \sqrt{2} \left(\frac{L}{L_\alpha}\right)\omega_p \tag{2.4-29}$$

If the aircraft is operating at the speed for maximum L/D, the contribution of the term $g(\partial(D/L))/\partial u$ to T_u will be zero, and if the aircraft is

flying faster than this speed, the $g(\partial(L/D))/\partial u$ term will increase T_u. Thus T_u can be expected to be roughly approximated by

$$T_u \simeq \frac{1}{\sqrt{2}} \frac{L_\alpha}{L} \left(\frac{1}{\omega_p}\right) \tag{2.4-30}$$

and since $L_\alpha/L \simeq 5$,

$$T_u \simeq \frac{3}{\omega_p} \tag{2.4-31}$$

This calculation indicates that the low frequency zero of the q_c to θ transfer function is several times closer to the s-plane origin than the phugoid poles. Eq. (2.4-26) also gives a fair approximation at low frequencies to the relationship between aircraft speed and true pitch angle with a tight pitch hold loop.

2.4:7 Approximate Low-Frequency Behavior of Pitch Hold Mode with Interaction

Let D(s) denote the characteristic polynomial of the aircraft-pitch damper combination, that is the product of the actuator, damped short period, and phugoid poles. Then at low frequencies the high-frequency zero of the q_c to θ transfer function may be ignored, and

$$T_{\theta/q_c}(s) \simeq \frac{C_\theta(T_u s+1)}{D(s)} \tag{2.4-32}$$

where C_θ is the q_c to θ static gain. Since the zeros of the q_c to X

transfer function lie near the phugoid poles and are, according to the analysis immediately above, several times farther from the s-plane origin than the low-frequency zero of $T_{\theta/q_c}(s)$, they will be ignored, and at low frequencies

$$T_{X/q_c}(s) \approx \frac{C_X}{D(s)} \tag{2.4-33}$$

where C_X is the q_c to X static gain. Since a constant q_c command yields a steady-state condition with constant elevator deflection, speed, and pitch angle, and since

$$X = \frac{du}{dt} + g\theta \tag{2.4-34}$$

it follows that

$$X_{\text{steady state}} = g\theta_{\text{steady state}} \tag{2.4-35}$$

and therefore that

$$C_X = gC_\theta \tag{2.4-36}$$

Substituting Eqs. (2.4-32), (2.4-33), and (2.4-36) into Eq. (2.4-13) yields

$$T_{\theta_i/q_c}(s) \approx \frac{gC_\theta\{T_e s(T_u s+1)+1\}}{(T_e s+1)D(s)} \qquad (2.4\text{-}37)$$

Under the assumption that the pitch gain in the pitch hold mode is fairly high, the closed-loop low-frequency poles will be close to the low frequency zeros of $T_{\theta_i/q_c}(s)$, and, ignoring the high-frequency closed-loop poles, the denominator of the commanded pitch angle θ_c to true pitch angle θ transfer function will be approximately

$$T_e s(T_u s+1) + 1 \qquad (2.4\text{-}38)$$

It was found in the discussion following Eq. (2.4-18) that the numerator of the θ_c to θ transfer function consists of the zeros of $T_{\theta/q_c}(s)$ plus a zero at the erection time constant. Thus, at low frequencies,

$$T_{\theta/\theta_c}(s) \approx \frac{C(T_u s+1)(T_e s+1)}{T_e s(T_u s+1)+1} \qquad (2.4\text{-}39)$$

where C is the θ_c to θ static gain. Unless automatic trim or some other form of pure integration is employed in the forward loop, the static gain C will be slightly less than one. However, for a tight pitch hold loop, C will be close to one, and thus

$$T_{\theta/\theta_c}(s) \approx \frac{(T_u s+1)(T_e s+1)}{T_e s(T_u s+1)+1} \qquad (2.4\text{-}40)$$

Before the properties of the approximate pitch hold mode transfer function given in Eq. (2.4-40) are discussed, the transfer function will be derived in another way which is easier to understand physically. In the pitch hold mode block diagram, Fig. 2.6, the pitch hold mode nulls the error signal

$$\theta_c - \theta_i = \theta_c - \theta + \varepsilon \tag{2.4-41}$$

where ε is the pitch component of the vertical indication error. With a tight pitch hold loop the low-frequency component of this error signal will be small, and it may be assumed that

$$0 \simeq \theta_c - \theta_i = \theta_c - \theta + \varepsilon \tag{2.4-42}$$

and the true pitch angle, θ, of the aircraft is given by

$$\theta \simeq \theta_c + \varepsilon \tag{2.4-43}$$

It has already been shown that, with a tight pitch hold loop, the speed of the aircraft is related to its true pitch angle by Eq. (2.4-26), which is repeated here

$$\delta u = - \frac{g T_u}{T_u s + 1} \delta\theta \tag{2.4-26}$$

Moreover, the pitch vertical indication error ε depends on aircraft

longitudinal acceleration and is given by Eq. (2.4-4)

$$\varepsilon = \left(\frac{-s}{T_e s+1}\right) \frac{u}{g} \tag{2.4-4}$$

Thus the vertical indication error ε is given by

$$\varepsilon = \frac{T_u s}{(T_u s+1)(T_e s+1)} \theta \tag{2.4-44}$$

and combining Eqs. (2.4-43) and (2.4-44) yields

$$T_{\theta/\theta_c}(s) = \frac{(T_u s+1)(T_e s+1)}{T_e s(T_u s+1)+1}$$

which is the same expression as Eq. (2.4-40). Combining Eqs. (2.4-40) and (2.4-44) yields

$$T_{\varepsilon/\theta_c}(s) = \frac{T_u s}{T_e s(T_u s+1)+1} \tag{2.4-45}$$

By either Eq. (2.4-43) or direct computation from the approximate $T_{\theta/\theta_c}(s)$ transfer function of Eq. (2.4-40), it follows that the transfer function relating pitch angle command θ_c to pitch following error $(\theta-\theta_c)$ is, to the order of approximation, the same as $T_{\varepsilon/\theta_c}(s)$. Thus, Eq. (2.4-45) will be used to determine the pitch following error. This makes sense physically since it implies that, with a tight pitch loop, the low-frequency pitch following error is caused entirely by the

vertical gyro inaccuracy.

The response of pitch angle following error, or equivalently vertical indication error, ε, will now be found for a step pitch command input. Let

$$R = \frac{T_e}{T_u} \tag{2.4-46}$$

and rescale time so that the time constant T_u of the low-frequency zero of the q_c to θ transfer function is the unit of time. With this time scale Eq. (2.4-45) becomes

$$T_{\varepsilon/\theta_e}(s) = \frac{s}{Rs^2+Rs+1} \tag{2.4-47}$$

and the response to a unit step is

$$\varepsilon(t) = \frac{2e^{-t/2}\sinh\left(\sqrt{1-\frac{4}{R}}\ \frac{T}{2}\right)}{R\sqrt{1-\frac{4}{R}}} \qquad \text{for } R > 4$$

$$\varepsilon(t) = \frac{t}{4}e^{-t/2} \qquad \text{for } R = 4 \tag{2.4-48}$$

$$\varepsilon(t) = \frac{2e^{-t/2}\sin\left(\sqrt{\frac{4}{R}-1}\ \frac{t}{2}\right)}{R\sqrt{\frac{4}{R}-1}} \qquad \text{for } R < 4$$

Finally, it follows from these expressions that for the critically

damped case when R = 4 the pitch overshoot is 1/2e, or 18%, and for the underdamped case of R = 2 the pitch overshoot is $(\sqrt{2} - 1)$, or 41%.

2.4.8 Conclusions

In the simplest type of attitude reference system the vertical drift due to earth angular velocity and motion of the aircraft around the earth is not compensated directly and must be nulled by the erection loops. Since this drift rate is on the order of 15 degrees per hour (angular velocity of the earth), it follows by Eq. (2.4-4) that the erection time constant cannot be chosen much longer than two minutes if the vertical indication error is to be held to an acceptable level such as one half degree. Furthermore, according to Eq. (2.4-27), for a true airspeed of 600 feet per second and $L_\alpha/L = 5$, the pitch hold speed decay zero time constant, T_u, will be on the order of 50 seconds. Thus, in cruise, the ratio of T_e to T_u will be near two, and the true pitch angle response of the pitch hold autopilot mode to a step pitch angle command will display a large overshoot, on the order of forty percent, which will take place over a time period of several minutes following the step input. Although the true pitch angle displays a large overshoot in this case, the indicated pitch angle tracks the pitch command input well, and the pilot of the aircraft would not be aware of the true pitch angle overshoot except through reference to the true horizon, or because airspeed and altitude variations do not correlate well with the indicated pitch angle displayed by the artificial horizon which is driven by the attitude reference system.

Since the pilot uses pitch angle as a reference to aid him in controlling airspeed and rate of climb rather than as a variable to be controlled for its own sake and since indicated pitch angle responds well to command inputs, it may be argued that the overshoot in true pitch angle does no harm, especially since it is so slow, and that, even with its relatively poor true pitch angle response, the performance of the pitch hold autopilot mode in this case is adequate.

If better true pitch angle response is desired, some means must be found to reduce the magnitude of pitch plane vertical indication errors caused by longitudinal acceleration. The most direct approach would be to include computed corrections or employ Schuler tuning to eliminate the vertical drift due to earth rotation and aircraft motion over the surface of the earth, so that the vertical erection loops are required only to null vertical drift due to gyro drift. Then, if good-quality gyros with drift rates of one tenth earth rate or better are employed, the erection time constant may be increased by a factor of ten, and vertical indication errors due to longitudinal acceleration will be reduced by a factor of ten, and the true pitch angle response to step inputs will display only a small overshoot. If Schuler tuning is employed with good-quality gyros, vertical erection loops may not be required at all, since the Schuler tuning loops tend to bound the errors caused by vehicle motion and earth rotation.

Another approach, which will reduce the true pitch angle overshoot for large pitch commands, is to limit the magnitudes of the erection signals. Since in subsonic flight the true vertical will never

rotate faster than thirty degrees per hour due to aircraft motion and earth rotation, the magnitude of the erection signals can be limited to this value. With a large step pitch angle command, the component of the erection signal caused by longitudinal acceleration will be larger than thirty degrees per hour, and part of the false erection signal will be removed by the limiting action.

It would also be possible to sense rate of change of airspeed with a pressure instrument and apply this signal to the vertical gyro as an additional erection signal to null out the longitudinal acceleration sensed by the erection loop accelerometer. This extra signal provides weak negative feedback so that, even if the scale factor of the sensor is incorrect, it should not cause a stability problem. However, since this sensor drives the vertical gyro, which in turn drives the artificial horizon display, the output of the sensor would need to be fairly reliable. This sensor would be sensitive to changes in the longitudinal component of wind velocity , and this sensitivity might be an undesirable error source.

Finally, if the pitch hold mode is operated in conjunction with an airspeed hold mode (auto-throttle) which maintains constant speed by adjusting power setting, the interaction between the vertical gyro and the pitch hold mode will be eliminated.

When the pitch hold loop is employed as an inner loop for automatic altitude or speed control, the outer loop dynamics are not significantly degraded by the interaction between the vertical gyro and the pitch hold mode. However, altitude or airspeed command inputs will cause true airspeed variations which will tilt the vertical gyro and result

in incorrect pitch angle indication on the artificial horizon. This vertical gyro tilt appears in the transfer functions for the altitude and mach hold modes as the closed loop pole which lies near the zero located at the erection time constant.

2.5 System Configurations

Two attitude reference systems are proposed for use with the digital autopilot. The first configuration is a system providing light computer loading. This system employs an inertial platform for navigation and as a primary attitude source and two vertical gyros and two directional gyros as backup attitude sources. Comparison between various attitude angle sources for failure detection and isolation would be done in the digital computer since dissimilar attitude sources must be compared. This system would tolerate only one gyro failure since the second failure might not be identifiable. If it were desired to be able to tolerate two gyro failures, another directional gyro and vertical gyro would be added. Body-mounted rate gyros and accelerometers would be mounted with three sensor input axes parallel to each aircraft body axis with their output signals voted to provide simplicity of data processing. This approach requires nine rate gyros, but the saving of one rate gyro would not justify the extra complexity of the eight gyro system described in Section 2.3 if only a single gyro failure is to be tolerated. If two rate gyro failures must be tolerated, the eight instrument configuration of Section 2.3 would be employed.

The second proposed configuration involves more development risk and employs a small number of sensors while requiring a large data processing capability. Attitude information would be obtained

by integrating the outputs of body mounted rate gyros as described in Section 2.2. Six gyros would be employed as body-mounted rate gyros in the first redundancy configuration described in Section 2.3. Three gyros would be of high quality and their outputs would be employed for navigation as well as attitude reference while the other three gyros would be less expensive lower quality gyros to provide a backup for attitude determination in case of primary gyro failures. Six accelerometers would also be employed in the first redundancy configuration described in Section 2.3. Three of the accelerometers would be of high quality for use in navigation while the remaining three accelerometers would be of lower quality to provide backup erection signals for attitude determination and backup acceleration signals for autopilot use in case of primary accelerometer failures. This system will tolerate two gyro and two accelerometer failures.

CHAPTER III

THE DIGITAL COMPUTER

The core of a digital autopilot is the central computing element, which consists of one or more general-purpose digital computer processors. The aggregate unit must provide both the computing power and the reliability required to perform the delicate and complex tasks demanded of advanced autopilots.

Any of several currently available flight computers can provide the necessary computational power. Examples are the IBM 4 PI and the Data General Nova (flight packaged). Unfortunately, although a single such processor does provide the necessary computational power, it does not provide the required reliability. It is concluded therefore that the central computing element must consist of three identical processors configured so as to provide backup capacity in the event of failure of any single processor. Systems employing only two processors fall short of a full "fail-operational, fail-passive" specification.

Within the three-processor system, consideration has been given to a configuration which allows use of current machines with a minimum of modification. Hardware modifications are minimized in order to avoid unnecessary complications and to preserve the already limited reliability of a single processor.

3.1 Reliability Requirements

In conventional analog autopilots the various operational modes are implemented by setting up several control loops. The feedback con-

trol devices are constructed of analog components and dedicated solely to the control of a single loop. While cross links among such loops occur, these loops remain sufficiently distinct so that various components are labeled, for example, the pitch control computer, yaw computer, roll computer, automatic throttle/speed control computer, etc. When mode sequencing or variable gains are required, specialized hardware is constructed and often designated by such names as sequencing computer, flap limiter, programmer computer, and so on. A digital autopilot replaces the dedicated hardware used in implementing each of the many separate control functions with a single piece of hardware, a digital computer.

The digital computer serves as the heart of the control system. By time-sharing the computational capacity among the several loops, the computer serves as the feedback control element for many separate processes. These processes may range in complexity from simple pitch control to fully automatic landing control. In addition, the computer may serve as the control element in nested control loops. As an example, navigation computations are used to provide aircraft positional information. The guidance control loop uses this information to generate a desired heading for the aircraft. This heading command then serves as the input to the heading control loop of the autopilot. The same computer may serve as the control element to close both loops.

It is clear that a digital computer failure presents the prospect of simultaneous breakdown in all control loops. With so much of the control centered in a single component, it is not surprising that

great reliability is demanded of that component. An interesting contrast develops here between analog and digital implementation. Within an analog design, effort can be concentrated on particular elements of the system so as to enhance overall safety. For example, basic stability augmentation functions may be implemented with redundant hardware and with high-cost, high-reliability components. Functions that do not affect flight safety may be implemented by less costly means, with overall operating ease and convenience, as balanced against cost, being the decisive factor governing the final choice of components for these subsystems. In a digital design the central computer will provide a uniform level of reliability for all the tasks it performs. This level must be high enough to meet the requirements of the most demanding task. The primary point to be made here is that a digital counterpart does not really exist for the so-called "non-safety-related failures" in analog systems.

Unfortunately, the required reliability cannot be achieved with a single non-redundant computer. If we assume a mean time before failure (MTBF) of 10^4 hours for a single computer, there is a probability of about 10^{-3} of a computer failure during a single day of average use (10 hrs). There is, of course, a much smaller chance that a failure will occur while the plane is in a critical maneuver. For example, if a plane makes four landings a day and the landing maneuver takes about 6 minutes per landing, there is a probability of 4×10^{-5} of an autopilot failure during a landing. Over a twenty-year lifetime with a fleet of 500 planes, several failures during landing become almost a certainty.

Reliability can be increased if there are two or more computers aboard the aircraft. The object is to detect a failure on the first computer and then to allow the standby computer to take over the function of the first computer. From a reliability viewpoint it is desirable to keep all standby computers in a powered-down state in order to increase component life. Typically the failure rate of unpowered components is lower than that for fully powered units. However, the task of detecting a computer failure quickly is not a trivial one; thus it will probably be necessary to keep the spare computers "powered up" and operating, solely to aid in the detection of failures. The increased rate of failures in the spares is an unfortunate consequence of the need for their continuous operation.

3.2 Single Computer Failure Detection.

In order to show that active spares are necessary, let us first examine mechanisms whereby a single computer might recognize a failure within itself. If the failure is a minor one, the computer may be able to recognize it solely by subjecting certain critical calculations to reasonableness checks. However, some minor and even transient computer failures can generate spurious branches in the execution sequences of a program, resulting in total collapse of the computer-supplied functions. If this happens, reasonability checks on calculations are not performed; even the control calculations themselves are not performed. The straightforward solution to this problem is to

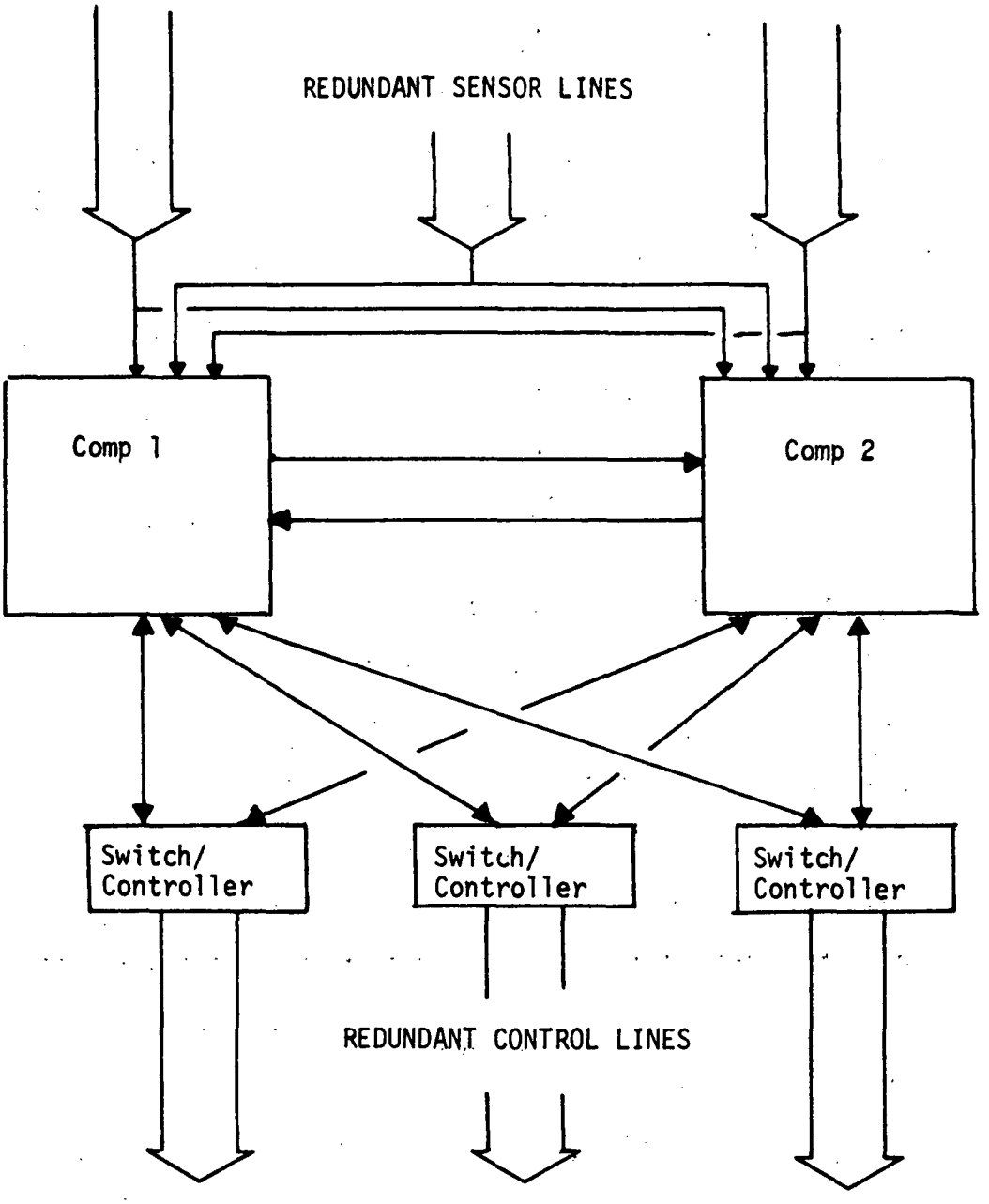

Figure 3.1 Dual Computer Configuration

provide a hardware "night watchman". The night watchman is a simple timing device which must be visited periodically by the programming. If more than a few milliseconds pass without the device being reset, it signals a failure. Thus disastrous failures are also detected.

In the grey area between total failure and minor failure, detection cannot be assured. This grey area can be made smaller at the cost of more numerous and more complex reasonableness checks, but in the end even this may prove inadequate. Also, as a greater percentage of the computer's time is designed into non-productive work, the processor power must be increased in order to provide the necessary level of useful work. The more powerful processor may cause further reliability problems, as large processors naturally tend to be less reliable than smaller ones. From the considerations above, one might estimate that somewhere between 50% and 95% of all failures can be detected by a single computer operating alone. Even the higher figure of 95% seems woefully inadequate.

3.3 Dual Computer Configuration

Two identical processors may be connected together as shown in Figure 3.1. Each has access to all sensor inputs and can manipulate all control channels to the aircraft. In addition each processor can communicate with the other over a direct link. In a normal mode of operation Computer 1 would control the aircraft, and Computer 2 would monitor its performance. If a failure is detected,

both computers would enter extensive self-check routines in an effort to locate the failure in either Computer 1 or Computer 2. Since this self-check is non-recurring, it could be much more extensive than that which might be possible if only a single active computer were used and self check were continually run as the error detection mechanism. After the location of the failure has been pinpointed, the affected computer is disengaged, and the remaining computer continues autopilot functions alone. In order to assure a high probability of fail-passive capability, the remaining computer will be forced to execute self-check procedures continuously. Since a maximum of reliability is required for such aircraft maneuvers as automatic landing, it is suggested that all non-safety-related functions, such as navigation and data logging, be abandoned after detection of the first failure in order to allow a maximum amount of time for self-check procedures in the remaining computer.

This system has two major weaknesses. First, after detection of the first failure there is a small probability that it will be impossible to pinpoint which computer is the source of the failure. Under these circumstances, one may be forced to make an arbitrary choice which could result in placing the failed unit into service and removing the good unit. Secondly, fail-passive operation of the single unit, after a failure has been isolated, is not certain since the detection of the second failure occurs only through reasonableness testing.

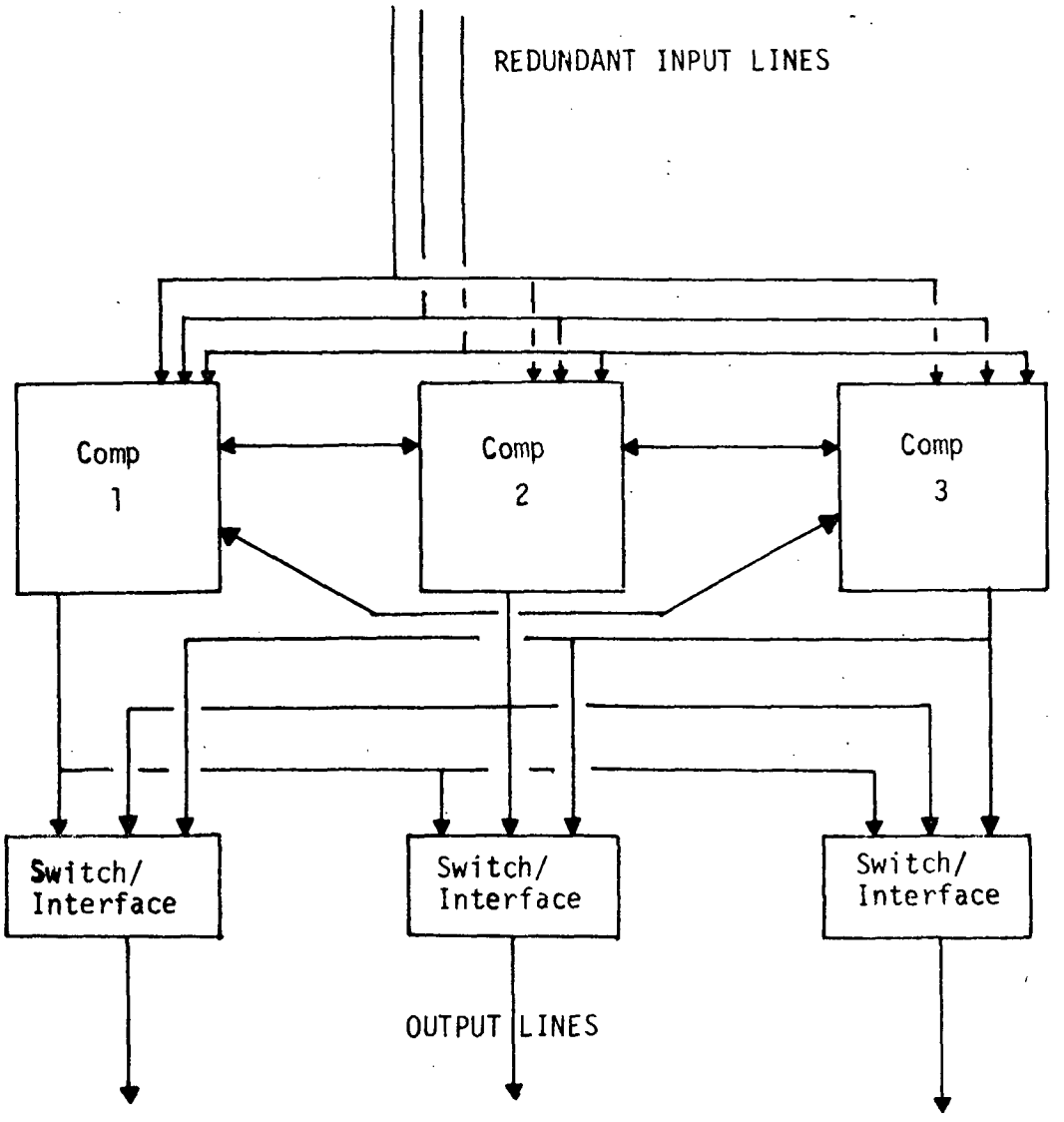

Figure 3.2 Triple redundant computer.

3.4 Triple Computer Configuration

A triple computer configuration provides a means of overcoming these problems. The most immediate gain from the triple configuration is the simplification of error detection and identification. In a dual system, if computer outputs are compared and found to differ, there is no way to tell, without self-checks, which computer is at fault. Thus, while the error is known to have occurred, it is impossible to say, without further knowledge, which computer is still good and should continue to be used. With three computers, this problem is solved by using majority voting, or "2 out of 3 voting", as it is more commonly referred to.

In addition to simplifying error location, the triple configuration enables the loss of a single computer to be more readily tolerated. In such a situation, one can fall back to a dual system and still retain most of the system capabilities. Finally, as system capability remains high even after a failure, maintenance can be postponed to a regularly scheduled period, and the impact of the failure on overall aircraft performance is minimized.

An example of a triple redundant computer configuration is shown in Fig. 3.2. As in the dual configuration, all inputs are available to all computers, and all control lines can be reached from any computer. Also, as in the dual arrangement, direct links exist among all processors. Unlike the basic dual system, two of the three processors operating in unison can deactivate or turn off the faulty third processor.

Because of the difficulty in providing for hardware synchronization of all three computers, this is not attempted. The synchronization which is necessary is provided via software convention by means of the direct links between computers. For example, without absolute synchronization, time skew on the reading of input lines could cause each processor to get a different value. These small differences in input make a direct comparison between the outputs of the processors difficult. In order to eliminate this problem without requiring tight synchronization, one processor will read the input lines and distribute the values to other processors, which will read an input line only to verify the reasonableness of the value delivered to them. After verifying the correctness of the inputs received from the partner computer, they will use it for all calculations. Thus, all computers will have identical inputs and should therefore produce identical outputs. A similar arrangement at the output provides for software voting on the output commands to the control lines, thereby eliminating hardware voting devices. Two of the three processors can lock the other processor out of the system at any time.

This system provides the means of detecting at least the first fault and locating its source exactly. Operation may then fall back to a dual configuration except that now only fail-safe operation of the dual system is required. As noted in the section on dual systems, fault detection is reasonably sound. Since the need for fault location after the detection is reduced, such a system functions adequately as a backup mode of operation.

Thus a triple system provides full fail-operational, fail-passive capabilities. Since two failures are now required to undo the system, a significant increase in reliability is realized over a single computer system during the six-minute landing phase. In addition, an even greater margin of safety is provided since the probability of undetected failures in the triple computer system is smaller than in the single or dual systems; that is, the three-computer system is more likely to fail passive after an incapacitating set of failures than the other systems.

3.5 Conclusions

The computer configuration recommended for the autopilot is a three-processor redundant system providing full fail-operational, fail-passive operation. The processors operate independently, with loose synchronization being provided by software conventions and by use of the inter-processor data links. Voting on redundant inputs and outputs is provided by means of the software. The concentration of error detection functions into software as opposed to hardware is more flexible and economical in this early stage of development, although greater reliance on hardware may be feasible with future computers designed for fault detection and isolation. It is expected that almost any of the modern flight computers could serve as the processor base of such a triple-processor system.

Chapter IV

4.1 Introduction

This chapter describes a digital flight control system (D.F.C.S.) for cruise flight operation of the Boeing KC-135. A program structure of the flight control system has been developed and coded in FORTRAN. Two basic modes of operation are provided, manual and automatic. In the manual mode pitch and roll rates are commanded by deflecting the control stick, with pitch and roll attitude being held when the stick is returned to neutral. In automatic operation attitude or Mach number feedback loops are closed around the pitch attitude loop to provide attitude or Mach hold modes of operation, depending on the mission requirement. For lateral control a heading feedback loop is closed around the roll angle loop to provide a heading hold system.

The preliminary autopilot gains have been selected assuming the vehicle to be rigid. Root locus analysis was carried out in the s domain, and the difference equations for the filters have been generated by obtaining the z transforms of the s domain compensation functions assuming a sampling frequency of 20 cycles/sec. This appears to be the most practical design approach for cases like this one in which autopilot bandwidth requirements are quite low, autopilot compensation is of low order, and the autopilot sampling rate is determined by the requirement that control surface motion be smooth.

4.2 Choice of Flight Condition

A complete digital autopilot design would include a schedule of autopilot gains for all cruising flight conditions with the gains stored as a function of a set of variables such as true airspeed, air density and Mach number. For the C-135, which was designed for ease of manual control, no unusual autopilot design problems are likely to be encountered in cruising flight, and sufficient information about the requirements for a digital autopilot will be obtained by determining the autopilot gains for a single flight condition in the cruise range. The criterion employed in choosing this flight condition is described below.

For design of the altitude hold mode the flight condition has been chosen such that the aircraft speed is on the front (high speed) side of the minimum thrust-required speed. This selection has been made because it is normal practice to operate the altitude hold mode in conjunction with an autothrottle control loop, which controls airspeed by varying engine power setting, when the aircraft is flown near or below the minimum thrust speed, while the goal in the present chapter is to design a satisfactory altitude hold mode which operates alone, with no control of power setting being attempted. The performance of the altitude hold mode without an autothrottle near or below the minimum thrust required speed would be poor for the following reasons. First, at the minimum thrust required speed steady-state altitude cannot be controlled with the elevator since, at this speed, elevator deflection causes an initial altitude transient following

which the aircraft returns to its original altitude. Second, when the aircraft speed is below the minimum thrust required speed, a nose-down attitude must be commanded in order to obtain a steady rate of climb. This relationship between pitch angle and rate of climb results in an undershoot in response to a step altitude command and hence a poor altitude response containing either a long time delay or a large undershoot.

Figures (4.1) and (4.2) show the thrust and power required characteristics for the aircraft at 40,000 ft and 35,000 ft respectively. On the basis of these data the equilibrium cruise flight condition for the aircraft was chosen to be 800 feet per second at 35,000 feet.

4.3 Aircraft Transfer Functions

Tables (4.1) and (4.2) present the transfer functions for the aircraft longitudinal and lateral dynamics. These transfer functions are derived for the flight condition selected above from aerodynamic and other aircraft data presented in Ref. (1) using linearized equations of motion as presented in Ref. (2).

4.4 Longitudinal Control System Configuration and Design Criteria

A functional diagram of the basic longitudinal attitude control system for manual mode operation is shown in Fig.(4.3a), while Fig. (4.3b) shows an s domain transfer function model of the same system. The purpose of the absolute square nonlinearity is to provide higher

$$G_{A[\delta_e,\theta]} = \frac{-0.8322\left[\frac{s}{0.588}+1\right]\left[\frac{s}{0.00697}+1\right]}{D_A}$$

$$G_{A[\delta_e,'\alpha]} = \frac{-0.66\left[\frac{s}{110}+1\right]\left[\left(\frac{s}{0.05646}\right)^2+2(0.04516)\left(\frac{s}{0.05646}\right)+1\right]}{D_A}$$

$$G_{A[\delta_e,'u]} = \frac{4.8\left[\frac{s}{-2.2.5}+1\right]\left[\frac{s}{0.894}+1\right]}{D_A}$$

where

$$D_A = \left[\left(\frac{s}{2.308}\right)^2+2(0.4135)\left(\frac{s}{2.303}\right)+1\right]$$

$$\cdot\left[\left(\frac{s}{0.05365}\right)^2+2(0.0451)\left(\frac{s}{0.05365}\right)+1\right]$$

Table 4.1 Summary of Aircraft Longitudinal Transfer Functions

$$G_{A[\delta r,\omega_z]} = \frac{-24.62\left[\frac{s}{1.3357}+1\right]\left[\left(\frac{s}{0.427}\right)^2+2(-0.112)\left(\frac{s}{0.427}\right)+1\right]}{\left[\left(\frac{s}{1.7841}\right)^2+2(0.069446)\frac{s}{1.7841}+1\right]\left[\frac{s}{1.252}+1\right]\left[\frac{s}{0.00443}+1\right]}$$

$$G_{A[\delta r,\beta]} = \frac{-1.16\left[\frac{s}{63.2899}+1\right]\left[\frac{s}{1.2394}+1\right]\left[\frac{s}{-0.009332}+1\right]}{\left[\left(\frac{s}{1.7841}\right)^2+2(0.069446)\left(\frac{s}{1.7841}\right)+1\right]\left[\left(\frac{s}{1.252}\right)+1\right]\left[\frac{s}{0.00443}+1\right]}$$

$$G_{A[\delta_a,\phi]} = \frac{458.92\left[\left(\frac{s}{1.7213}\right)^2+2(0.0893)\left(\frac{s}{1.7213}\right)+1\right]}{\left[\left(\frac{s}{1.7841}\right)^2+2(0.069446)\left(\frac{s}{1.7841}\right)+1\right]\left[\frac{s}{1.252}+1\right]\left[\frac{s}{0.00443}+1\right]}$$

$$G_{A[\delta_a,\psi]} = \frac{19.263\left[\left(\frac{s}{2.299}\right)^2+2(-0.5457)\left(\frac{s}{2.299}\right)+1\right]\left[\frac{s}{2.125}+1\right]}{\left[\left(\frac{s}{1.784}\right)^2+2(0.069446)\left(\frac{s}{1.7841}\right)+1\right]\left[\frac{s}{1.252}+1\right]\left[\frac{s}{0.00443}+1\right]}$$

Table 4.2 Summary of Aircraft Lateral Transfer Functions

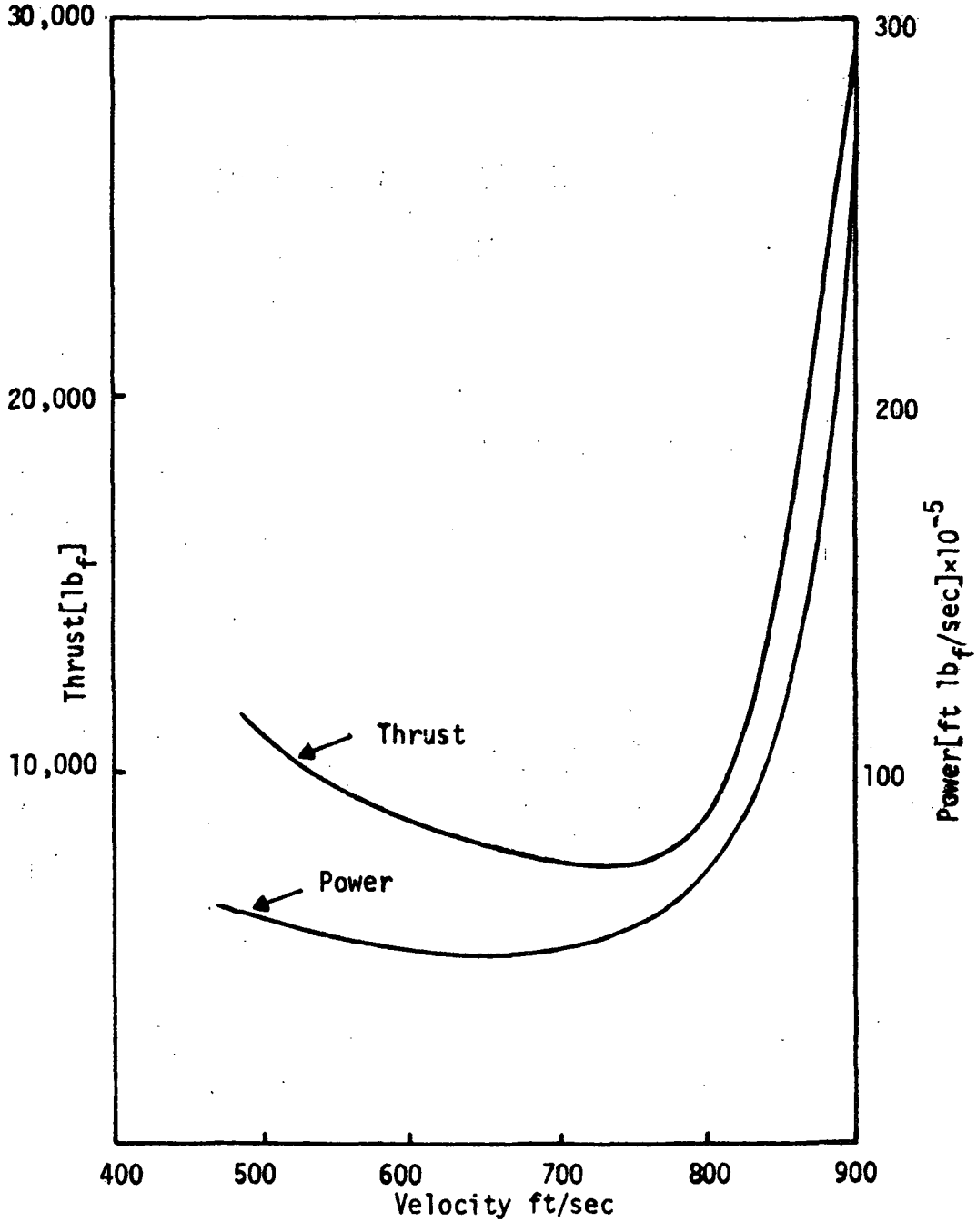

Figure 4.1 C-135 thrust and power required characteristics at 40,000 ft.

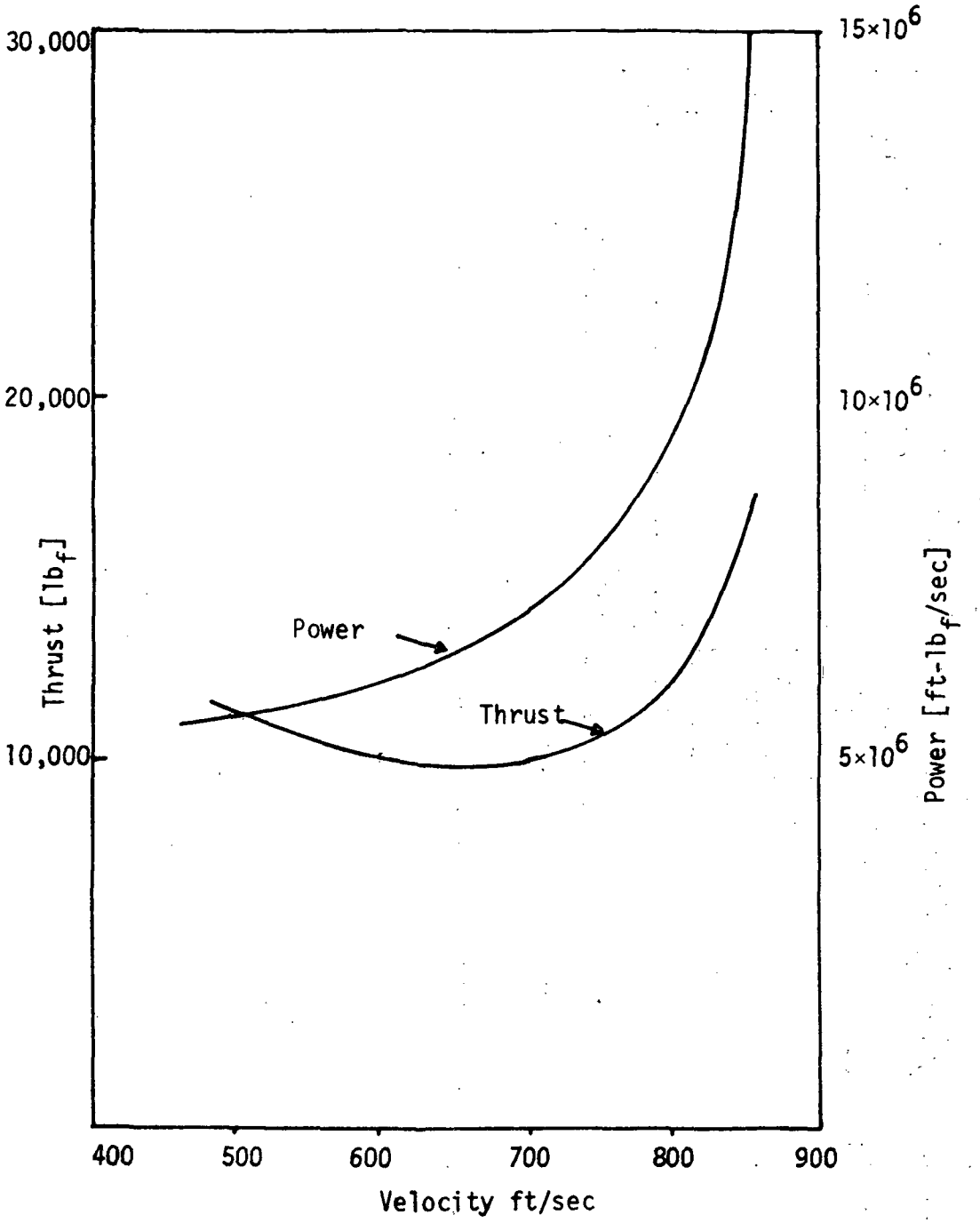

Figure 4.2 C-135 power and thrust required characteristics at 35,000 ft.

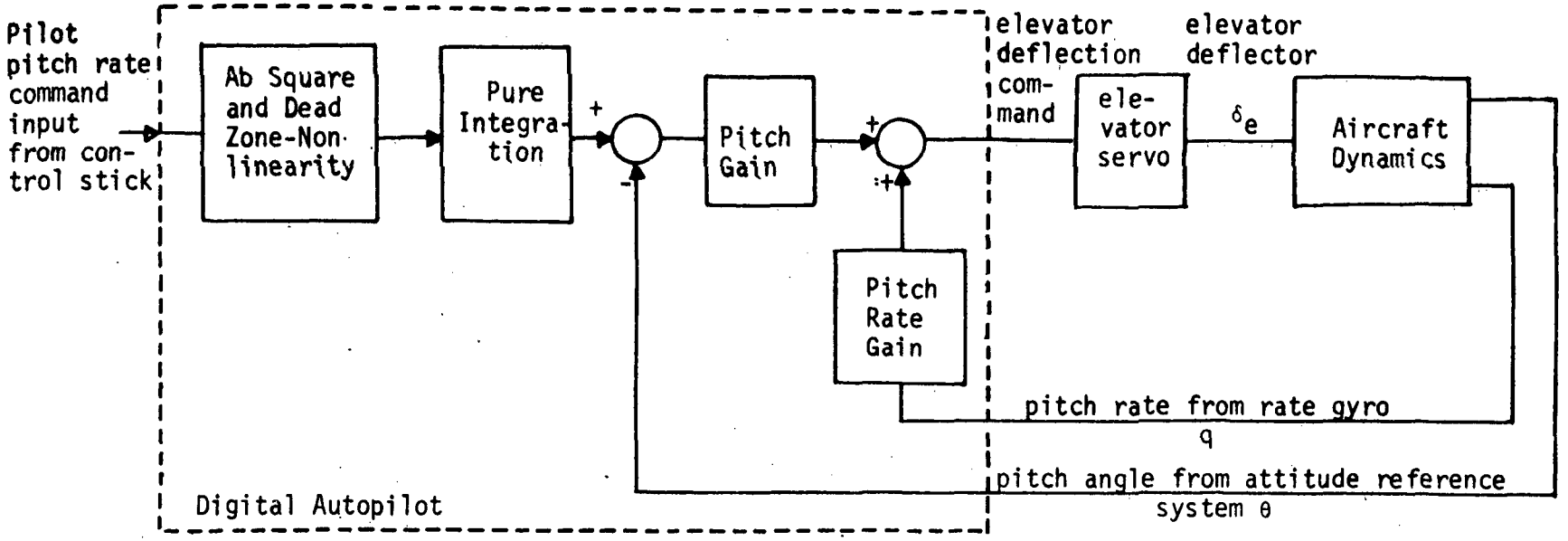

Figure 4.3a Functional diagram of pitch-rate control mode of digital autopilot for KC-135.

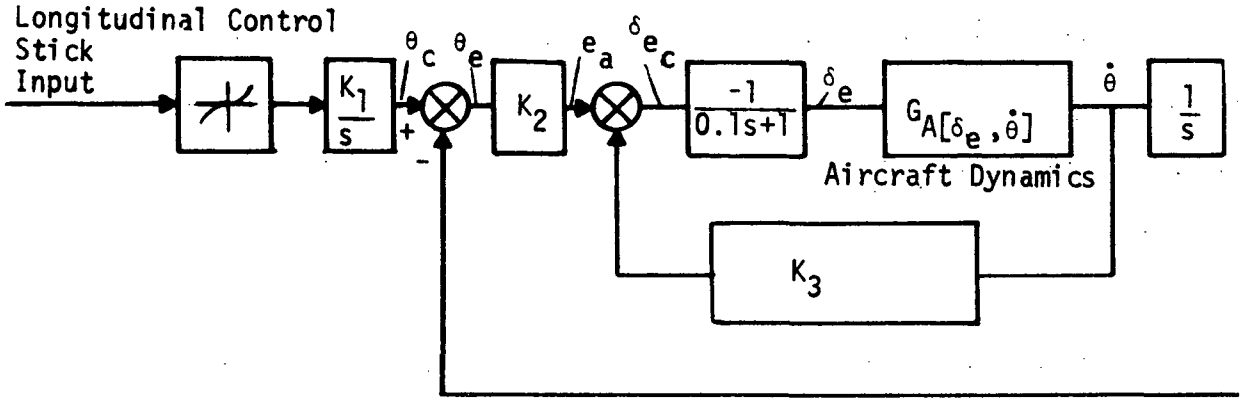

Figure 4.3b s Domain Transfer Function Block Diagram of Pitch Attitude Control System

stick sensitivity for large stick deflections. The dead zone is included to ensure that no stick bias signal is passed to the integrator when the stick is centered.

The rate gyro sensitivity K_3 is selected to provide adequate damping of the short-period oscillation when the pitch attitude loop is closed. A root locus diagram of the short period-roots is shown in Fig. (4.4). The phugoid poles are not affected appreciably when the pitch rate feedback loop is closed and are not indicated in this diagram. Fig. (4.5) shows the locus of the short-period roots as a function of outer loop gain K_2 for two values of the inner loop gain. This diagram indicates that for a given outer loop gain greater damping of the short-period mode is obtained by using a higher gain for the pitch damping loop. Based on these trends and computer simulation runs, the inner loop gain selected corresponds to a value of rate gyro sensitivity of K_3=200 degrees of δ_e/radian per sec. of $\dot{\theta}$.

Referring to Fig. (4.5) and (4.6), the pitch gain K_2 is selected to make the low-frequency phugoid pole close up on the low-frequency zero while keeping the frequency and damping of the short-period mode acceptable. The need for the closure requirement may be appreciated by observing that the time constant of the low-frequency phugoid pole is of the order of 100 seconds. If there is appreciable separation between this pole and the neighboring zero, there results a significant residue for this pole and consequently a very slow convergence to steady state conditions

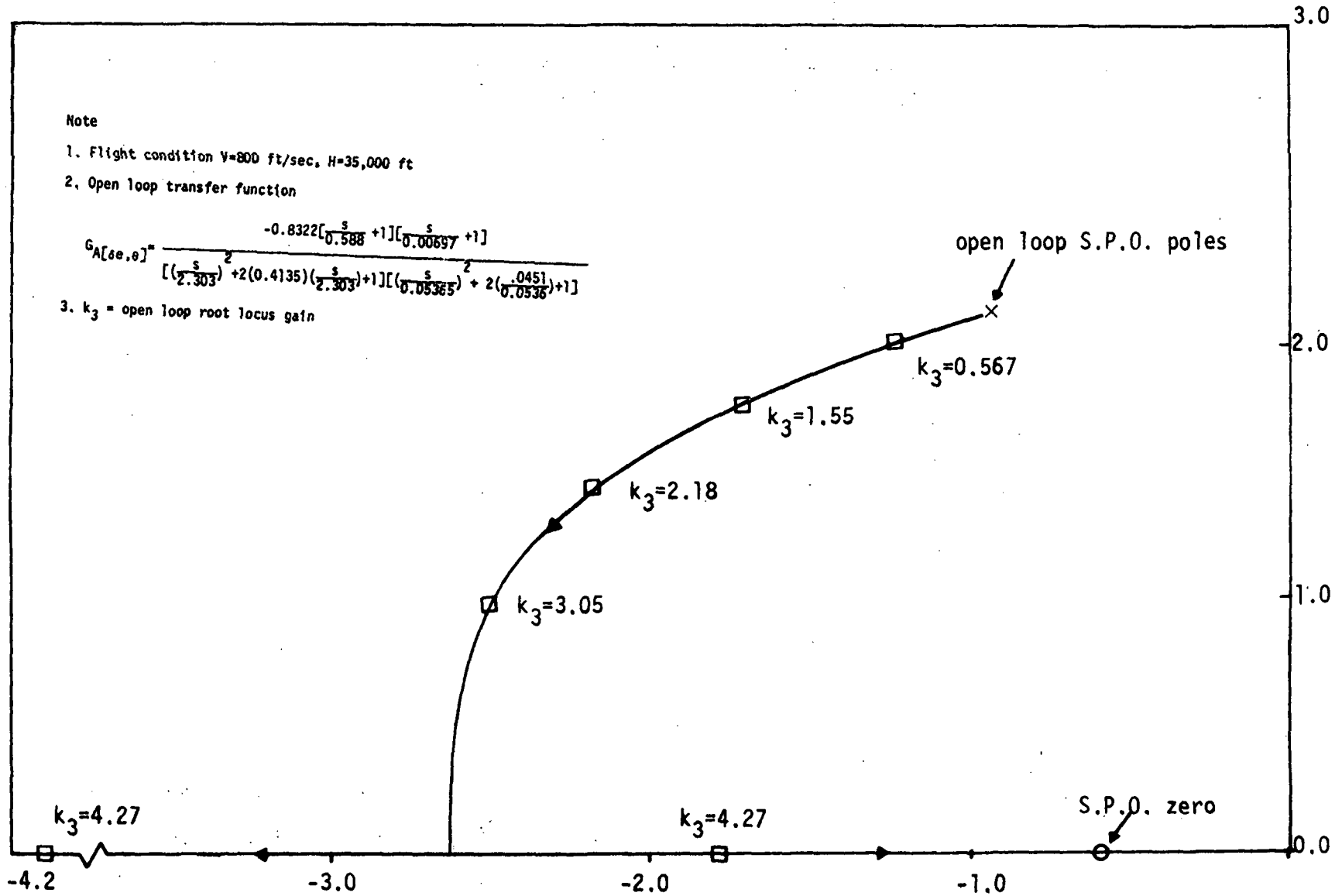

Figure 4.4 Locus of S.P.O. roots for pitch damping loop as a function of pitch damping gain.

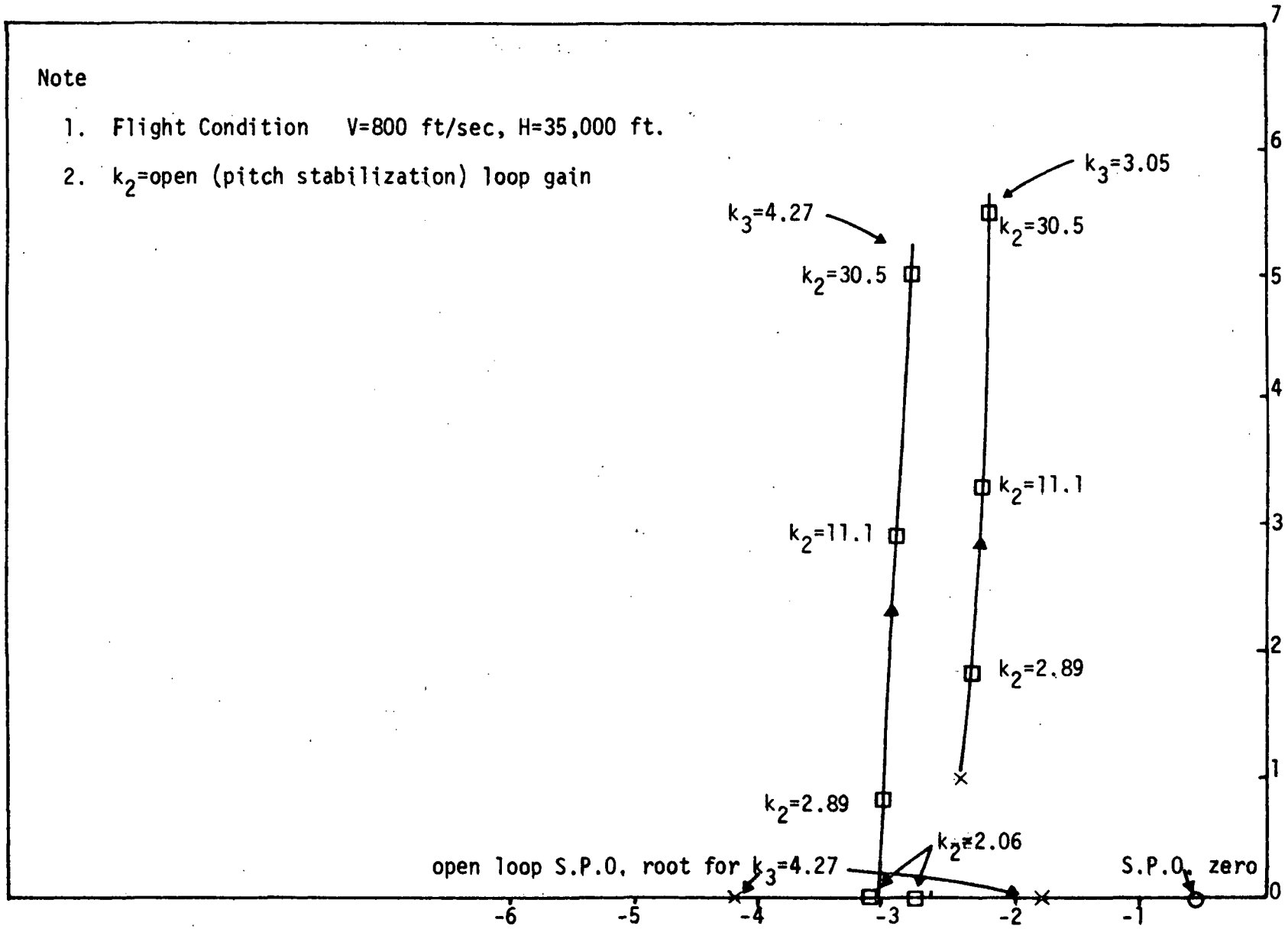

Figure 4.5 Locus of S.P.O. roots for pitch stabilization loop as a function of pitch attitude gain

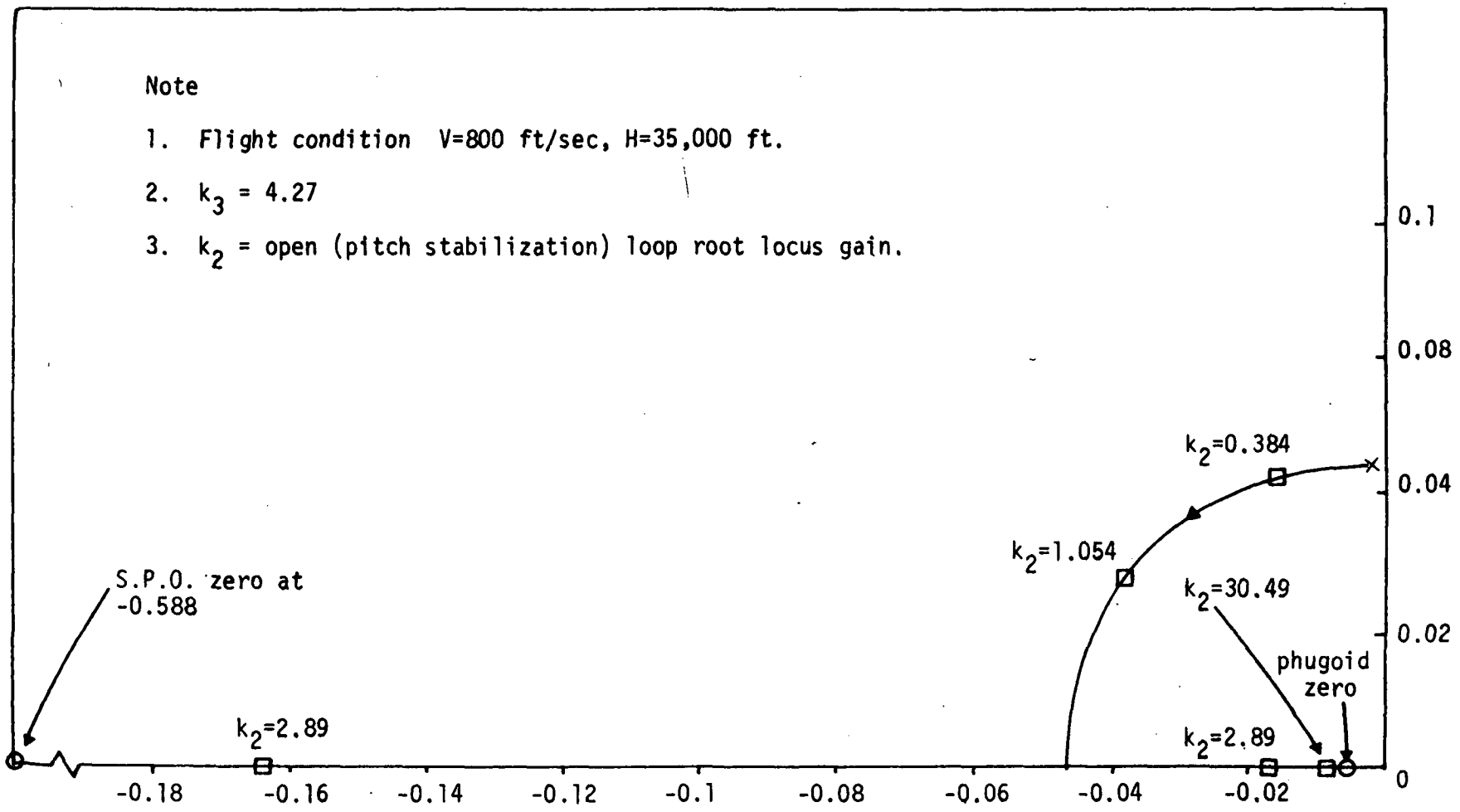

Figure 4.6 Locus of phugoid poles for pitch attitude stabilization loop as a function of pitch altitude gain k_2

following a step command input. Another requirement calling for high pitch attitude loop gain is that of minimizing steady-state error. Based on these considerations, the value of outer loop gain selected from the root locus and computer simulation runs corresponds to K_2=500 degrees of e_a/radian of θ_e. The chart recording of Fig. (4.18) shows the response to a pulse stick input. A fast response with a slight overshot is indicated.

In addition to the manual pitch attitude hold mode, the D.F.C.S. has two automatic longitudinal modes of operation. These are the altitude hold and Mach hold modes. As mentioned earlier, with the aircraft flying on the "front" side of the power curve it is possible to provide acceptable altitude control by deflecting the elevator. The altitude hold control system configuration is shown in Fig. (4.7), where an altitude feedback loop is closed around the pitch attitude loop through an altitude gain. The reference altitude command is an input from the control console. The root locus for the short-period and phugoid roots for the altitude hold loop is shown in Figs. (4 8) and (4.9) with altitude gain K_4 as the parameter. The rate gyro sensitivity is 81.366 degrees of δe/rad per sec. of $\dot{\theta}$. From Figs. (4.8) and (4.9) the altitude gain K_4 is selected high enough to minimize steady-state error without destabilizing the phugoid poles. The value of K_4 selected is 0.00011 rads. of θ_c/ft. of altitude error. Fig. 4.19 shows the response to a 200 ft. step change in altitude. Very little overshoot is apparent here.

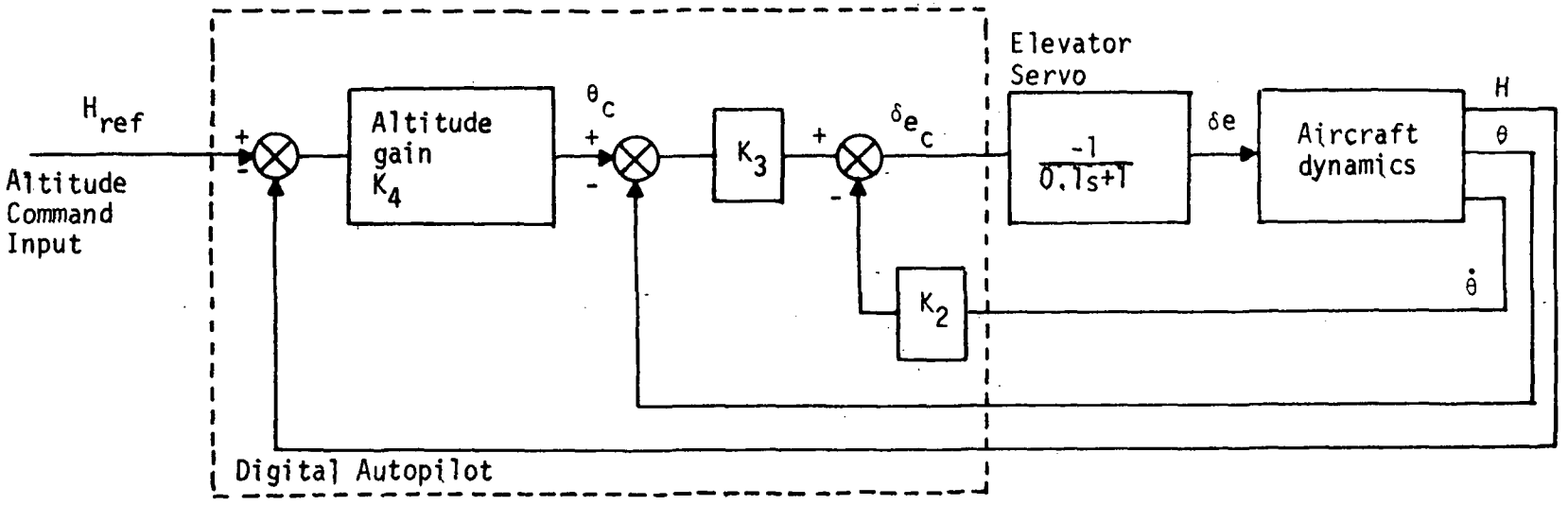

Figure 4.7 Block diagram of Altitude Hold Control Mode.

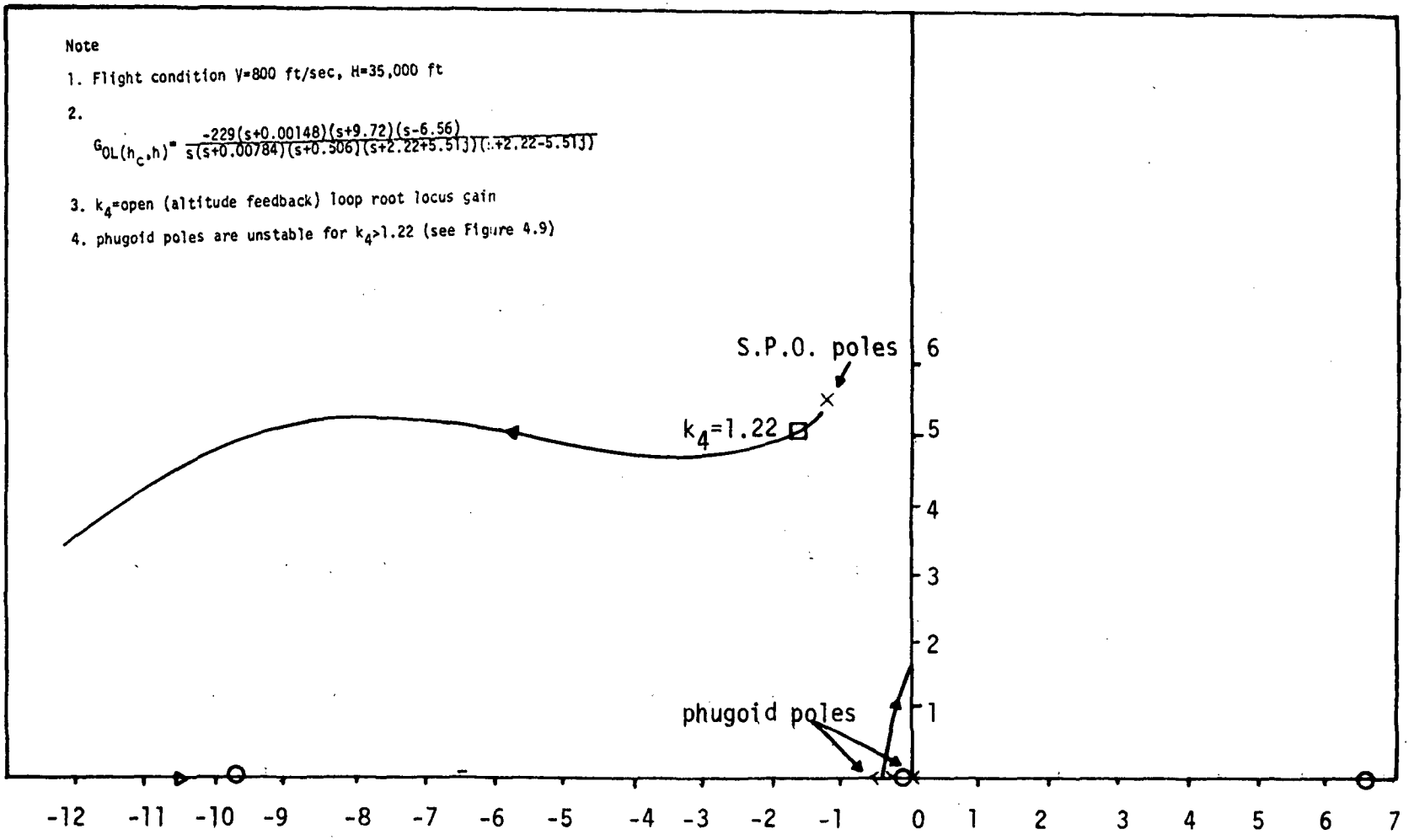

Figure 4.8 Locus of S.P.O. root for altitude hold loop as a function of altitude gain k_4.

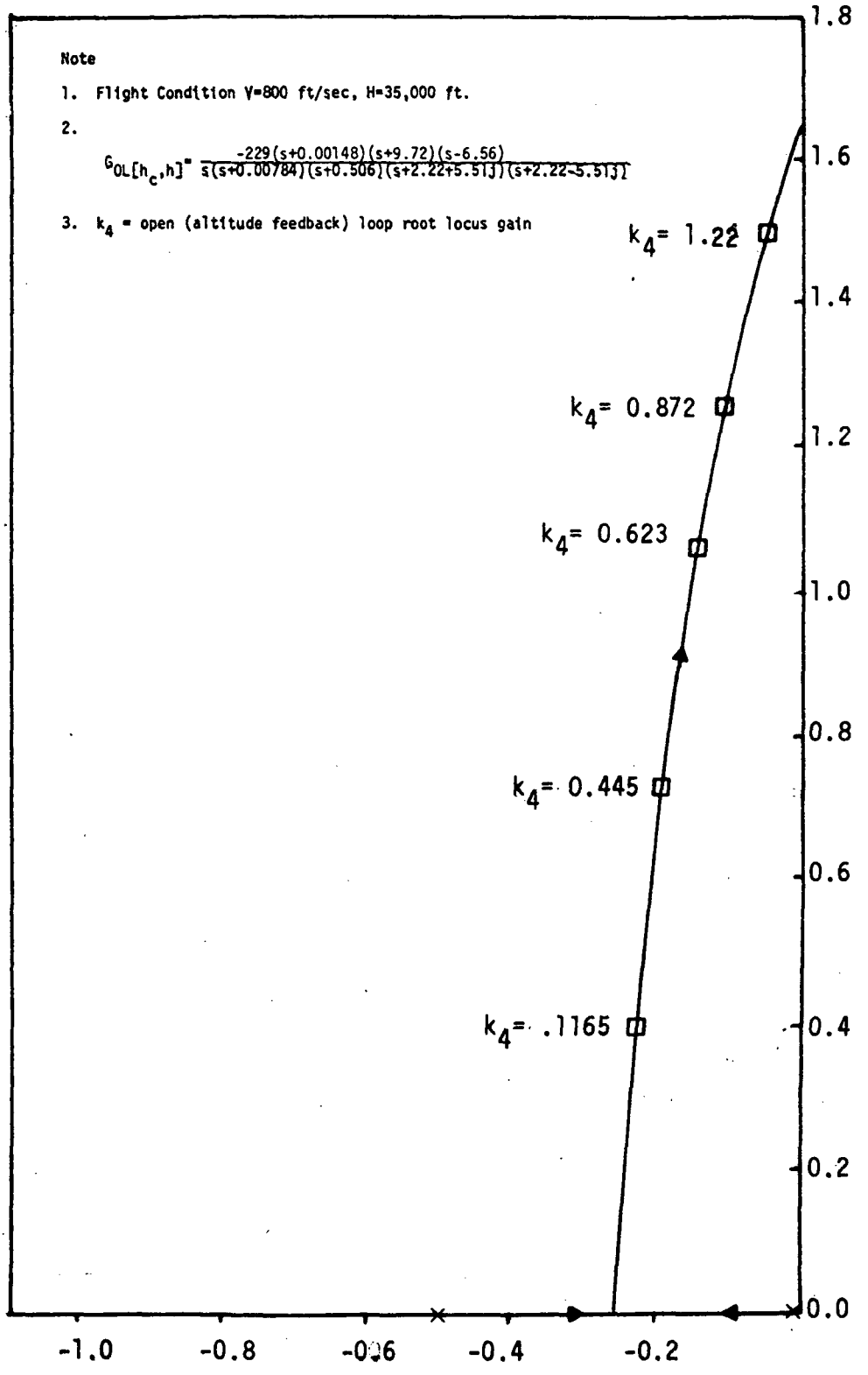

Figure 4.9 Locus of phugoid root for altitude hold loop as a function of altitude gain k_4.

The automatic mach hold control system configuration is the same as that shown in Fig. (4.7). The altitude feedback loop is replaced by a Mach number feedback loop, and the reference Mach number command is inserted from the control console. In addition, the altitude gain is replaced by the Mach number gain K_5=-3.5 rads. of θ_c/unit Mach no. error. The design considerations here are to minimize steady state error while retaining adequate damping of the short-period oscillation. Fig. (4.10) is the root locus for the Mach hold loop as a function of the Mach number gain with K_3=81.66 degrees of δe/rad. per sec. of $\dot{\theta}$. Fig. (4.20) shows the response for a 0.01 step change in reference Mach number. As for the altitude hold case, there is practically no overshoot.

4.5 Lateral Control

Manual and automatic modes for lateral control are provided. Fig. (4.11) shows the lateral control system configuration for manual operation. The pilot commands a roll rate by deflecting the stick. When the stick is centered, the roll angle is held. In automatic operation, a heading loop is closed around the roll angle feedback loop as shown in Fig. (4.12). Here the command to the aileron is generated from the a heading error. In this mode the aircraft returns to wings-level flight when the heading error goes to zero. Completely automatic cruising flight is possible by engaging the altitude hold or Mach hold mode of the longitudinal control system and the heading hold mode of the lateral control system.

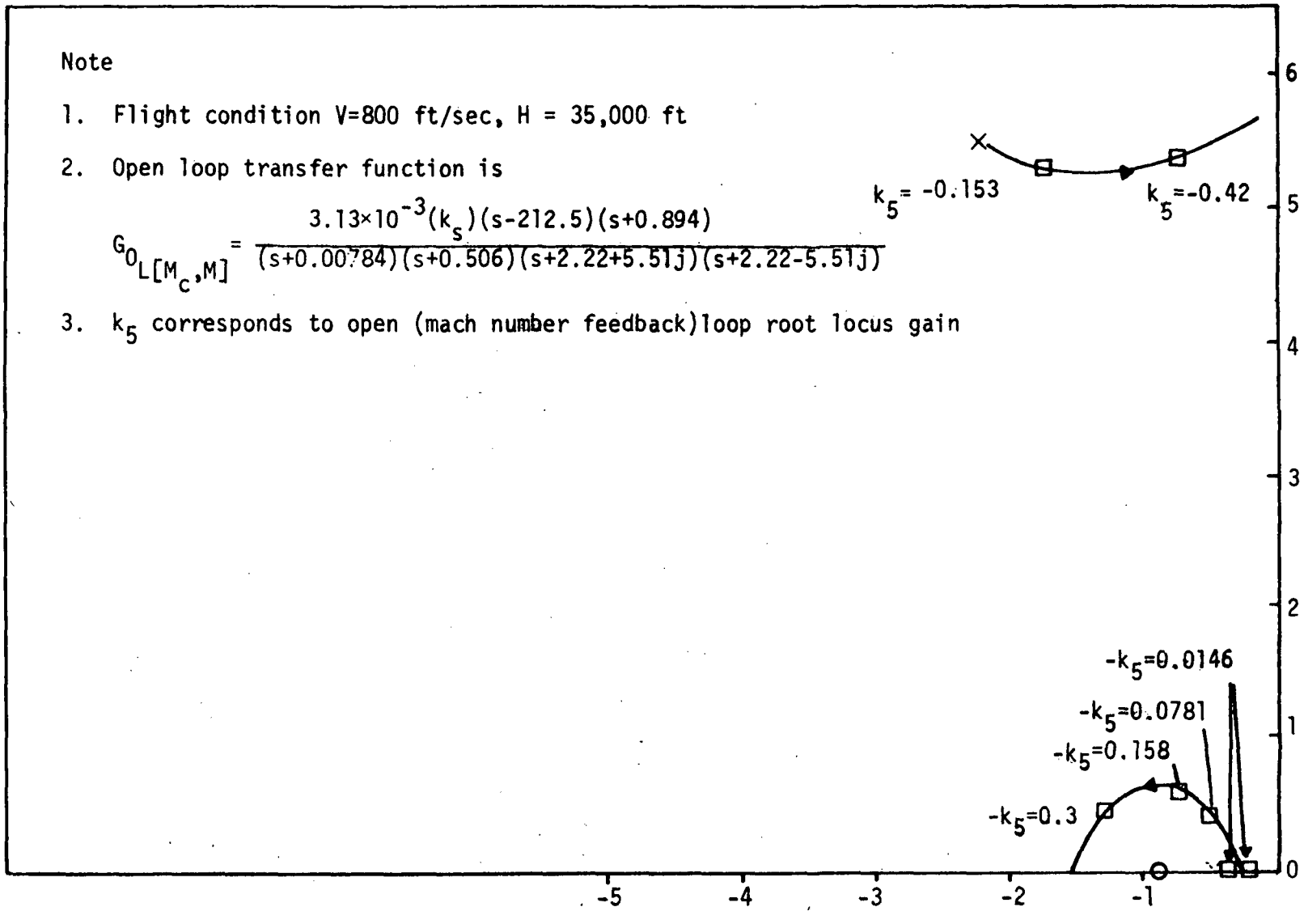

Figure 4.10 Locus of roots for Mach hold loop as a function of Mach number gain k_5

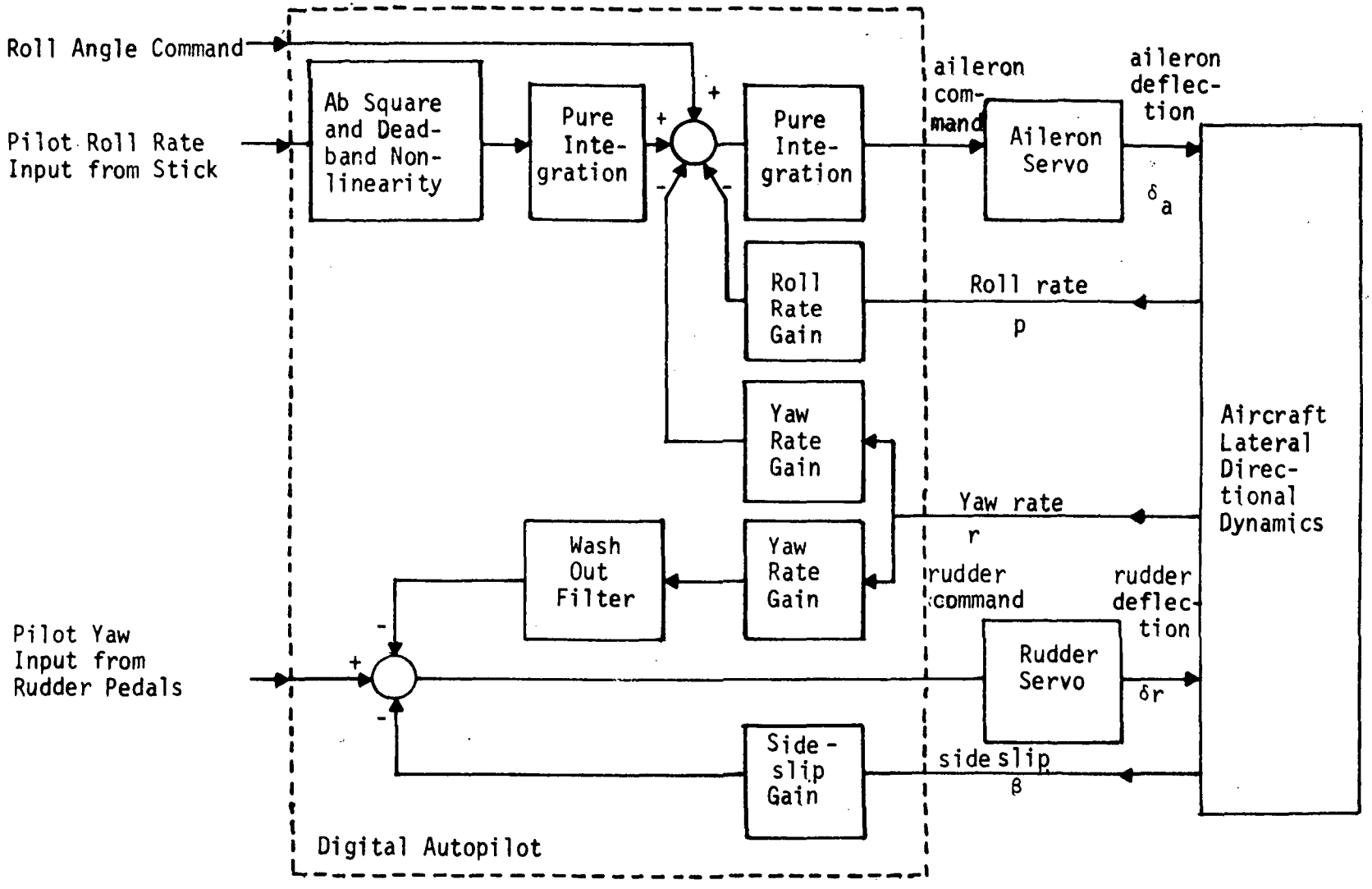

Figure 4.11 Functional diagram of manual lateral control mode of digital autopilot.

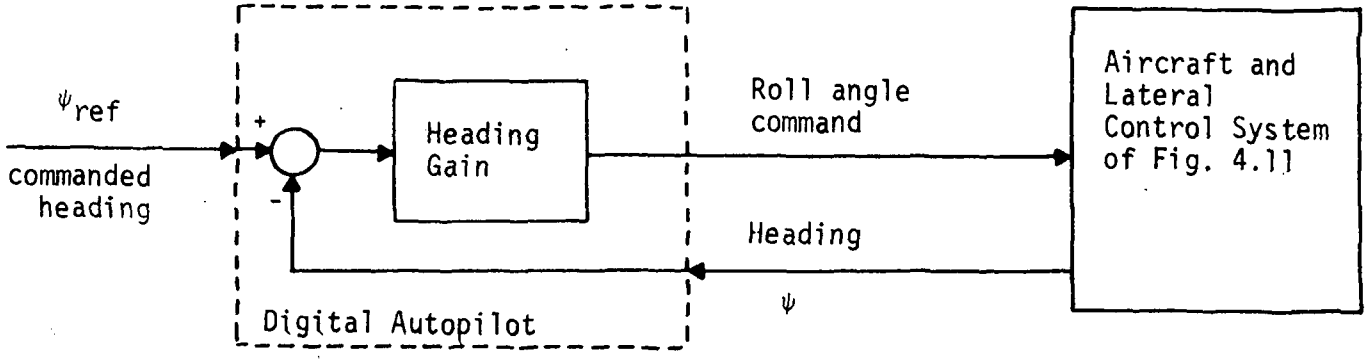

Figure 4.12 Functional diagram of heading hold system.

Fig. (4.13) shows the s domain transfer function block diagram for the manual mode lateral control system. The function of the high-pass, wash-out filter in the yaw-rate-to-rudder feedback loop is to eliminate the constant yaw rate signal which would be present during a steady turn. The elimination of this signal reduces the gain required in the sideslip-to-rudder loop and thus simplifies the problem of obtaining an acceptable frequency and damping ratio in the closed-loop Dutch roll poles. Fig. (4.14) shows the root locus for the lateral oscillation roots of the yaw-rate-to-rudder feedback loop as a function of yaw gain K_8. The locus is drawn for two values of the washout filter time constant. From this diagram it is seen that a long time constant is preferable from the point of view of increasing the damping of the lateral oscillation. However, too large a time constant leads to a very slow attenuation of the low-frequency yaw rate feedback. The larger value of τ = 2.5 sec. was chosen for the time constant of the washout filter.

Coordination of the aircraft during a turn is achieved by feeding back sideslip to the rudder. Fig. (4.15) shows the root locus for the sideslip feedback loop as a function of the sideslip gain K_9. While a high sensitivity is preferred, it is seen that this would lead to a high-frequency, lightly damped lateral oscillation. In practice [1], the sensitivity of the sideslip sensor must be kept low enough to minimize the effects of noise.

In addition to the lateral oscillation damping and sideslip coordination loops, yaw rate is fed to the aileron. The effect of yaw rate feedback is similar to that of roll angle feedback. The function of this loop is to hold roll angle constant when a command

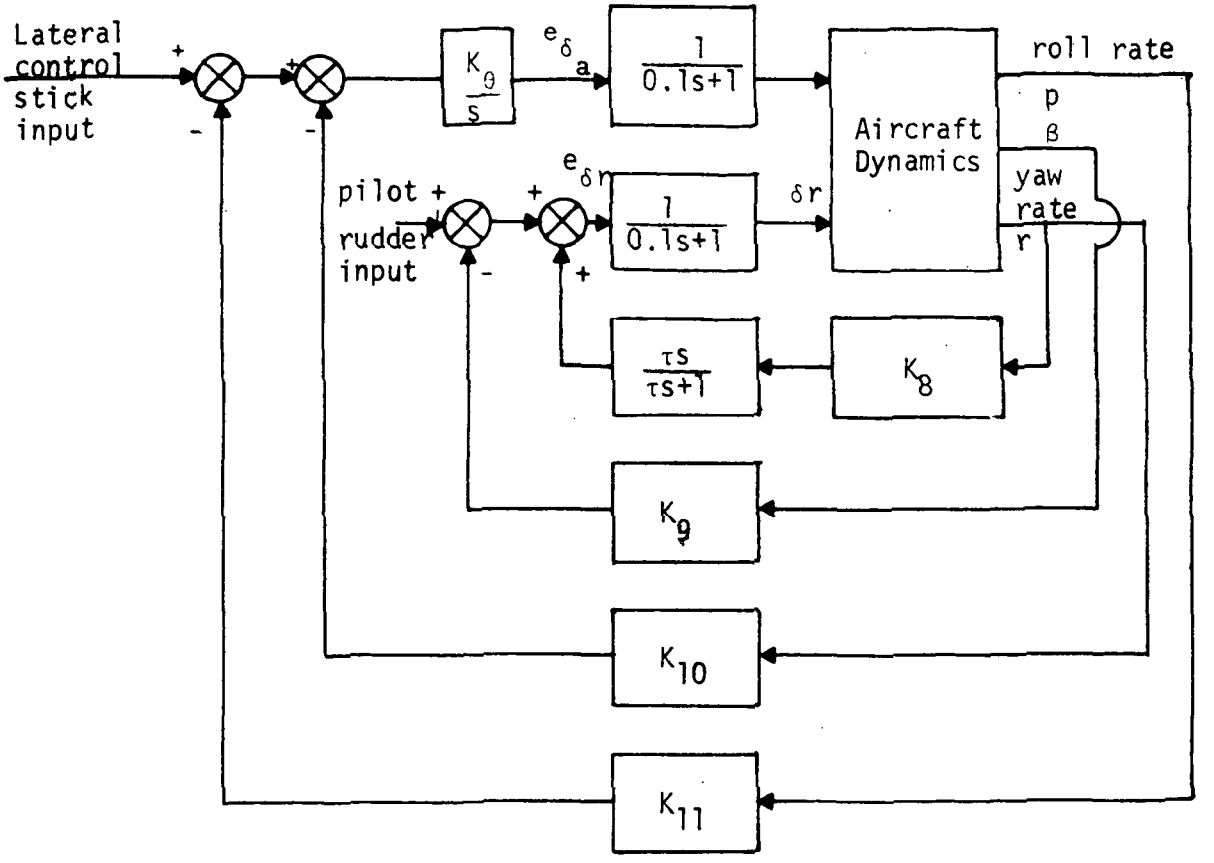

Fig. 4.13 s domain transfer function block diagram of the lateral control system (manual mode).

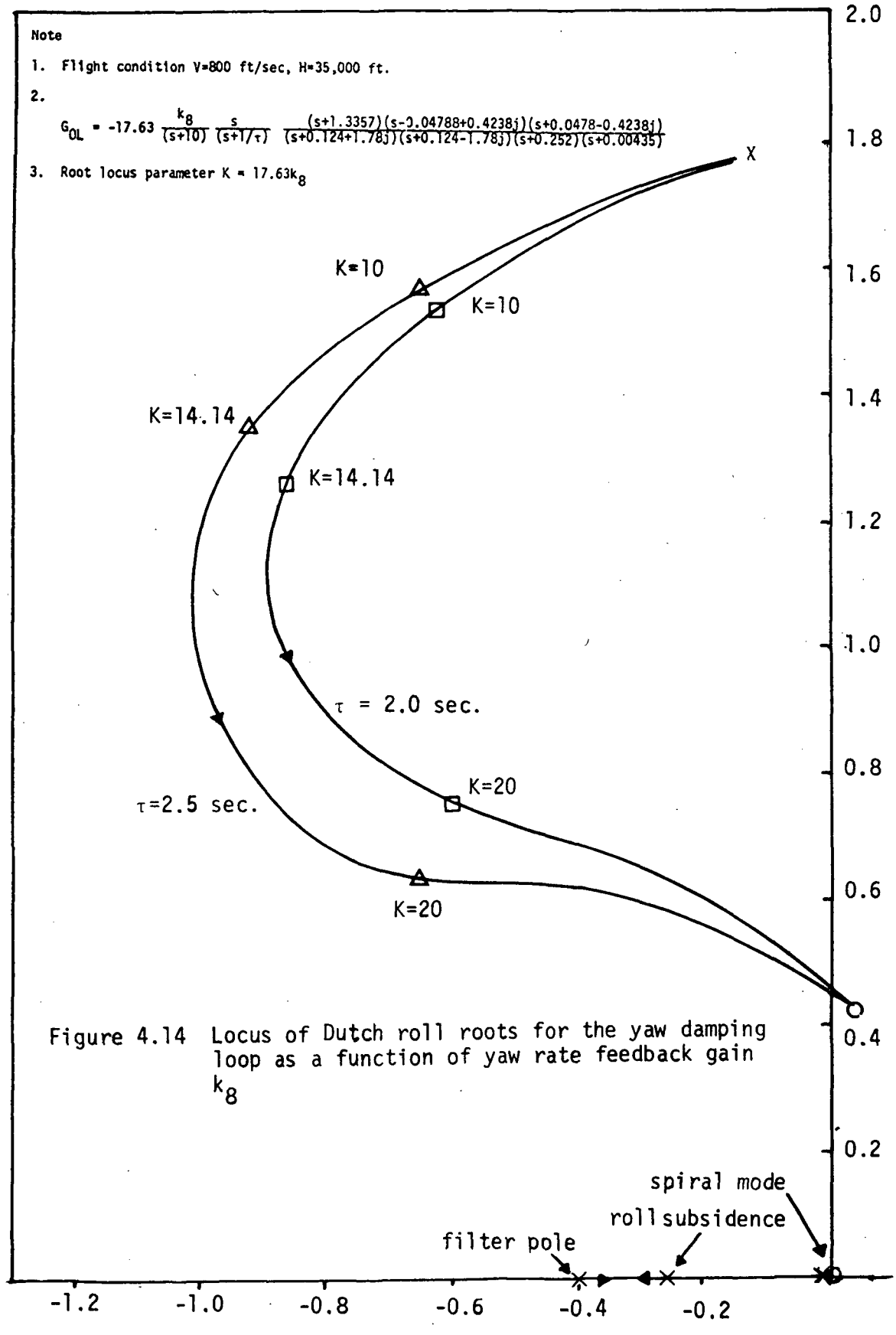

Figure 4.14 Locus of Dutch roll roots for the yaw damping loop as a function of yaw rate feedback gain k_8

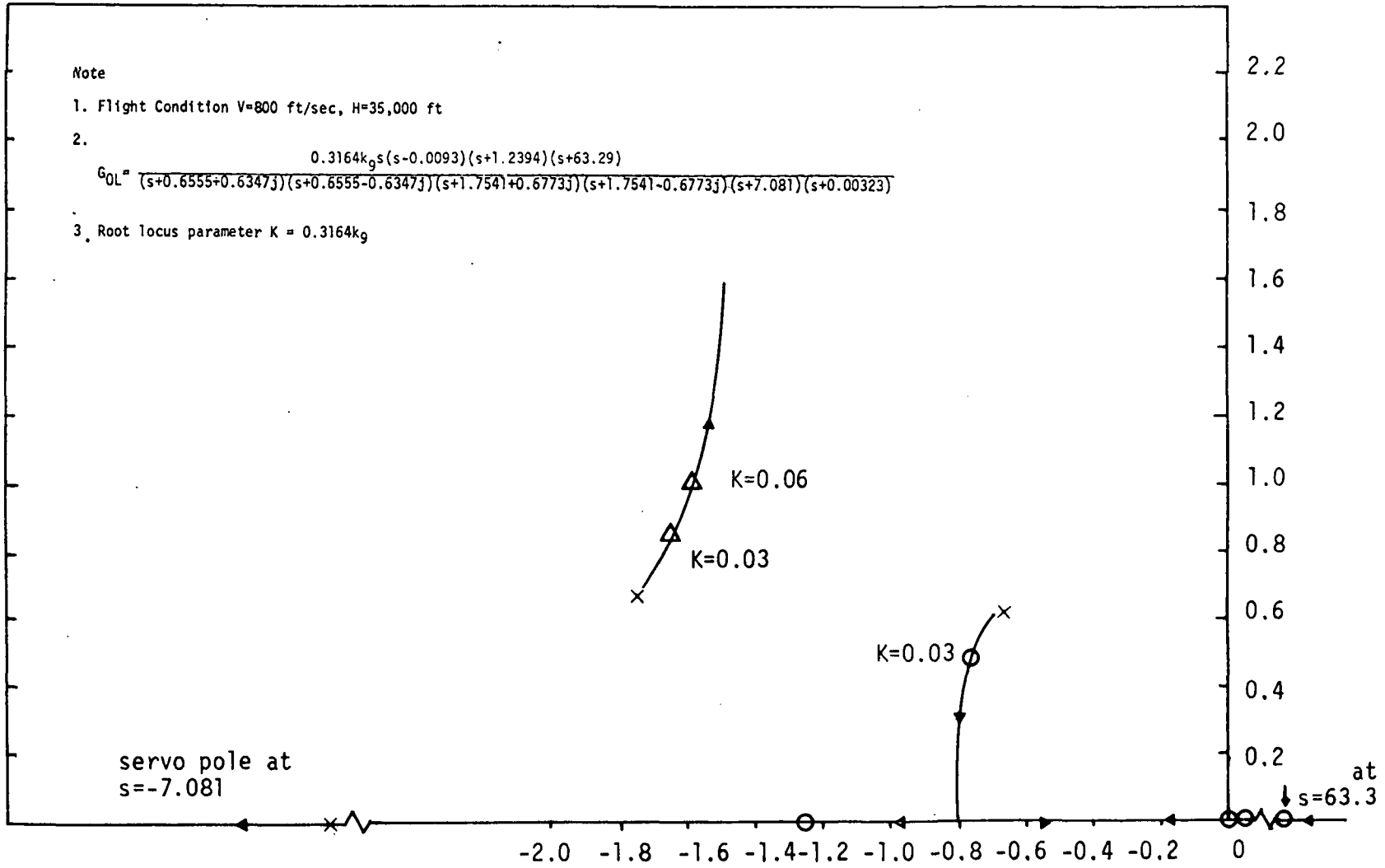

Figure 4.15 Root locus gain for sideslip feedback loop as a function of sideslip gain k_θ for filter time constant = 2.5 sec.

input from the stick is absent. Roll rate is also fed back to the aileron to provide roll damping.

From the root locus diagrams of Fig. (4.14) and (4.15), the yaw rate gain is selected to be K_8=1.15 rads. per sec. of e_{rg}/rad. per sec. of ω_z, and the sideslip gain K_9 is taken to be K_9= 0.12 rad of e_{δ_r}/rad. of β. The gains K_6 and K_{11} were determined from computer simulation runs to give as fast a roll response as possible without an excessive overshoot. These values are K_6=0.4 and K_{11}=0.35.

Figure (4.21) shows the response of the manual mode to a pulse stick input. This response is rather sluggish and would probably not receive a good pilot rating. Since the roll subsidence mode of the aircraft has a time constant of 1.25 seconds, a faster roll response, with a time constant on the order of one second, could be obtained without introducing stability problems by removing the pure integration between the roll rate and yaw rate summation point and the aileron command and readjusting the roll and yaw rate gains. The large initial sideslip error is caused by the absence of any yawing moment to provide yaw acceleration when a turn is initiated. The sideslip transient could be nearly eliminated by providing a cross-feed in the digital autopilot from the lateral control stick input to the rudder deflection command.

Figure (4.22) shows the response of the automatic heading mode to a ten degree step change in the commanded heading. This response is well damped with a slight roll angle overshoot.

4.6 Method Employed to Construct Autopilot Difference Equations

The analysis of the vehicle dynamics as well as the selection of the

autopilot gains and filters was carried out in the s domain. The preliminary analysis also assumed the vehicle to be rigid. Aeroelastic effects would introduce high-frequency lightly damped modes which could be destabilizing, particularly if the sampling frequency is not sufficiently high [3].

The highest frequencies of the vehicle dynamics occur in the short-period and Dutch roll modes and are of the order of 5 radians per second. Using the general rule that the sampling frequency be about ten times the highest frequency of the plant, a sampling frequency of 50 rads/sec (a sample period of T = 0.125 sec. or a sampling frequency of 8 cycles/sec.) is required for control of the rigid vehicle dynamics The sampling frequency employed in the digital autopilot is 20 cycles/sec. This sampling rate was chosen because the C-135 digital autopilot equations are quite simple, consisting, in the majority of cases, of scaling and summing the inputs to produce the desired output quantities. Therefore, the most economical method of obtaining the varying outputs required to prevent jerkiness in the motion of the aircraft control surfaces is to sample the autopilot equations at a high cyclic rate. If the autopilot equations were so complex that a single equation update cycle required more time than was available in the interval between outputs required for smoothness, provision would have to be made for generating outputs at several intermediate points within the basic equation update cycle. The s plane transfer functions to be generated in the digital autopilot were converted to z plane transfer functions employing the following transformation:

$$D(z) = (1 - \frac{1}{z}) Z\left(\frac{G(s)}{s}\right)$$

D(z) denotes the z plane transfer function, G(s) the s plane transfer function, and the operator Z( ) represents the operation of replacing the poles and zeros of the s plane transfer function with poles and zeros in the z plane located at the exponential function of the sample time times the original pole or zero. That is, if

$$F(s) = \frac{K(s-a_1)\ldots(s-a_m)}{(s-b_1)\ldots(s-b_n)}$$

then

$$Z\left(F(s)\right) = \frac{K(z-e^{a_1 T})\ldots(z-e^{a_m T})}{(z-e^{b_1 T})\ldots(z-e^{b_n T})}$$

where T denotes the sample time.

To illustrate this procedure, the z domain equivalent of the s domain washout filter is derived.

$$G_f(s) = \frac{s}{s+\frac{1}{\tau}}$$

$$D_f(z) = (1-z^{-1}) Z\left(\frac{G_f(s)}{s}\right)$$

$$D_f(z) = (1-z^{-1}) Z\left(\frac{1}{s+\frac{1}{\tau}}\right)$$

$$D_f(z) = (1-z^{-1}) \frac{z}{z-e^{-T/\tau}} = \frac{(z-1)}{z-e^{-T/\tau}}$$

calling RI(z) the filter input and RO(z) the filter output, then

$$\frac{RO(z)}{RI(z)} = \frac{z-1}{z-e^{-T/\tau}}$$

The corresponding difference equation is

$$RO(I) = e^{-T/\tau}RO(I-1)+RI(I)-RI(I-1)$$

where the index I refers to the value of the variable at the current sampling instant.

The simulation results presented earlier were all obtained employing autopilot equations derived as described above with a sampling rate of twenty times per second.

4.7 Autopilot Structure

Block diagrams of the longitudinal and lateral autopilots with digital compensations are shown in Figures (4.16) and (4.17). The mode select switches in these diagrams are represented in the D.F.C.S. program by the integer variables MODE and MODE1. The autopilot mode is selected by setting these mode select switch variables according to Table 4.3. Table 4.4 presents a summary of the autopilot gains for the various modes.

The D.F.C.S. computer program has been coded in FORTRAN. The program has been structured for use with the M.I.T. Draper Laboratory hybrid simulator (Aero-Sim). In its present form D.F.C.S. consists of

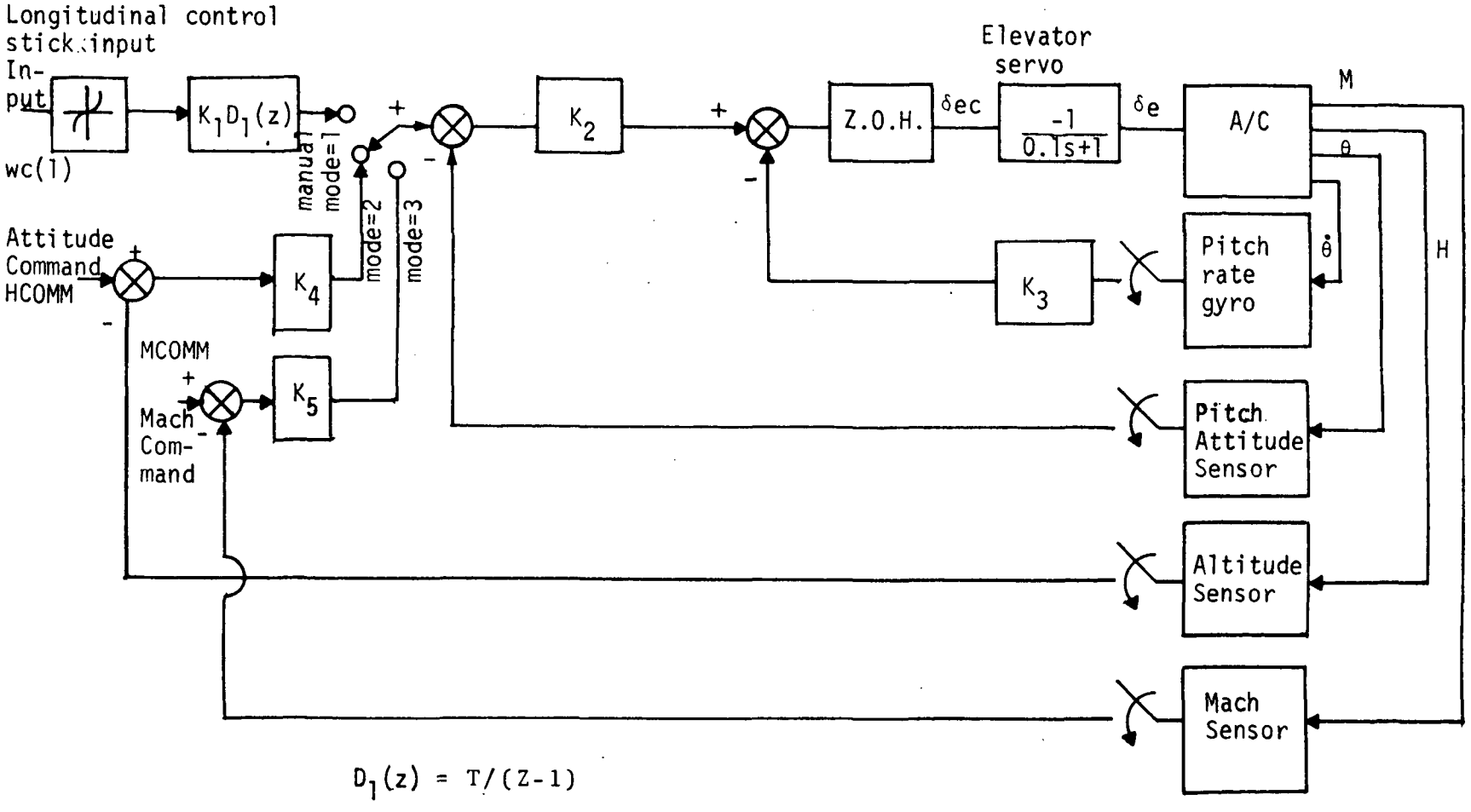

Figure 4.16 Block diagram of longitudinal digital control system

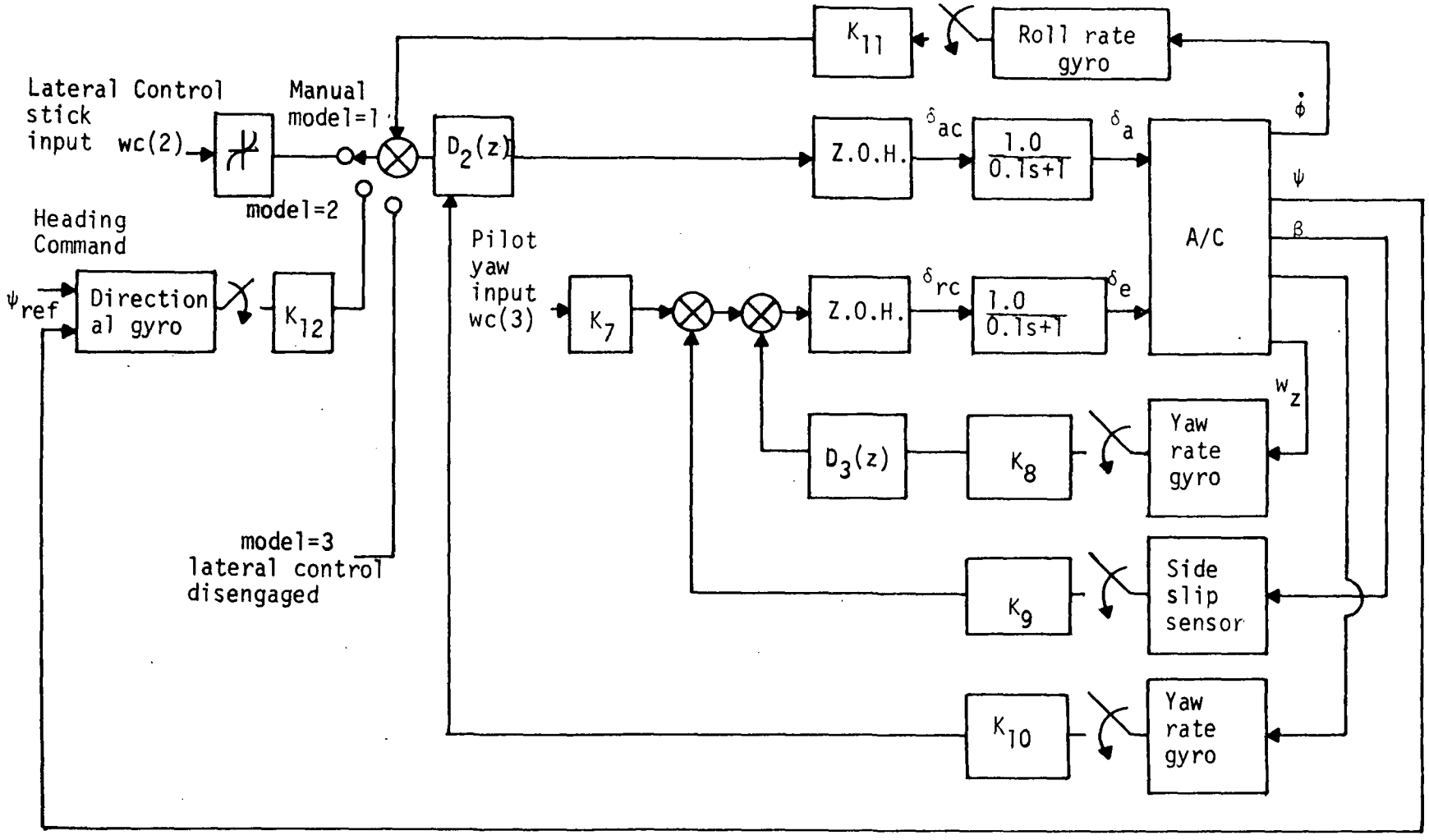

$$D_2(z) = \frac{K_6 T}{z-1} \qquad D_3(z) = \frac{z-1}{z-e^{-T/\tau}}$$

Figure 4.17 Block diagram of lateral control system with digital compensations

Table 4.3 Mode Select Switch Settings

Longitudinal Autopilot Mode	Lateral Autopilot Mode	MODE	MODE1
Attitude Hold (AHOLD) (Manual)	Disengaged	1	3
Altitude Hold (HHOLD) (Automatic)	Disengaged	2	3
Mach Hold (MHOLD) (Automatic)	Disengaged	3	3
Attitude Hold (AHOLD) (Manual)	Roll Attitude Hold (Manual)	1	1
Altitude Hold (HHOLD) (Automatic)	Heading Hold (DHOLD) (Automatic)	2	2

Table 4.4 Summary of Gains for Various D.F.C.S. Modes

Gain	Pitch Attitude Hold Manual C.S.S. MODE=1, MODE1=3	Altitude Hold MODE=2 MODE1=3	Mach Hold MODE=3 MODE1=3	Lateral C.S.S. MODE1=1	Lateral Heading Hold MODE1=2
K(1)	0.50				
K(2)	500	500	500		
K(3)	200	200	200		
K(4)		0.00011	-		
K(5)			-3.5		
K(6)				0.4	0.4
K(7)				0.698	0.698
K(8)				1.15	1.15
K(9)				0.12	0.12
K(10)				0.9	0.9
K(11)				0.36	0.36
K(12)					0.035
G(1)				0.98	0.98

the following four subroutines

a. AUTOCARD: This subroutine is used to assign fixed D.F.C.S. data and to type declare and dimension the variables and arrays. In addition, all D.F.C.S. variables that are interfaced with the Aero-Sim executive routine are placed in common here. The D.F.C.S. mode select switches MODE and MODE1 are called for by this routine and are typed in according to Table 4.3. While this subroutine is required to interface the D.F.C.S. with the Aero-Sim executive routine, it would not be included in an actual flight control implementation.

b. AUTOINIT: This subroutine is called by the Aero Sim executive routine fifty times a second during the trim calculation phase of the executive routine. The purpose of this routine is to set the autopilot command signals so that they correspond to trim values of control surface deflections and throttle settings when the flight phase is entered. In an actual flight control implementation, such a routine would be included to initialize autopilot outputs and internal variables when the autopilot is switched to a new mode.

c. AUTOTTY: This subroutine is called once prior to entering the flight phase. This subroutine is used to input the D.F.C.S. gains for the mode selected by the mode switches, MODE and MODE1.

d. AUTOPILO: This subroutine contains the autopilot equations. The relations between the inputs and outputs of the filters and integrators are written as difference equations of the type obtained in the previous section for the yaw rate washout filter.

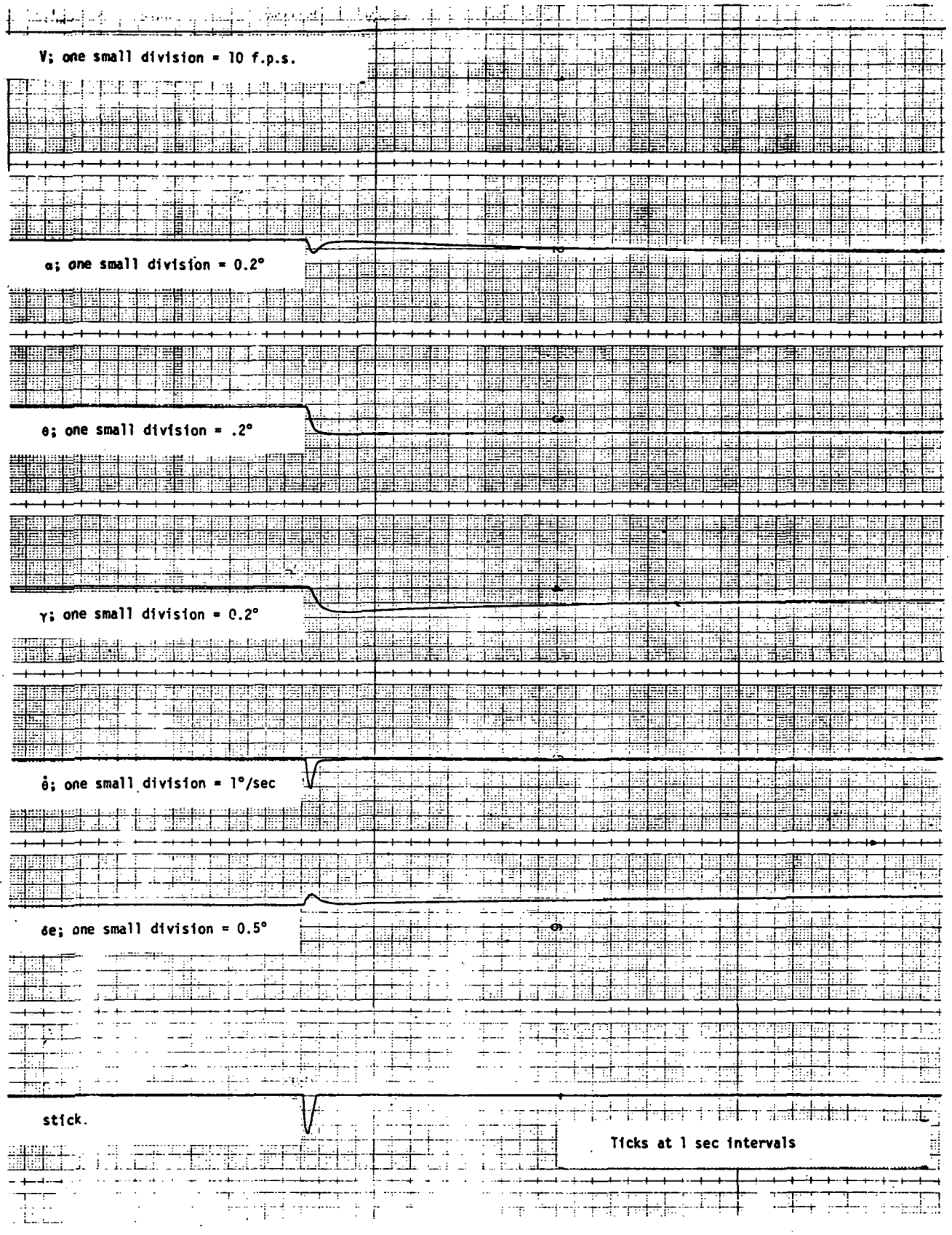

Figure 4.18 Longitudinal C.S.S. Attitude Hold Response

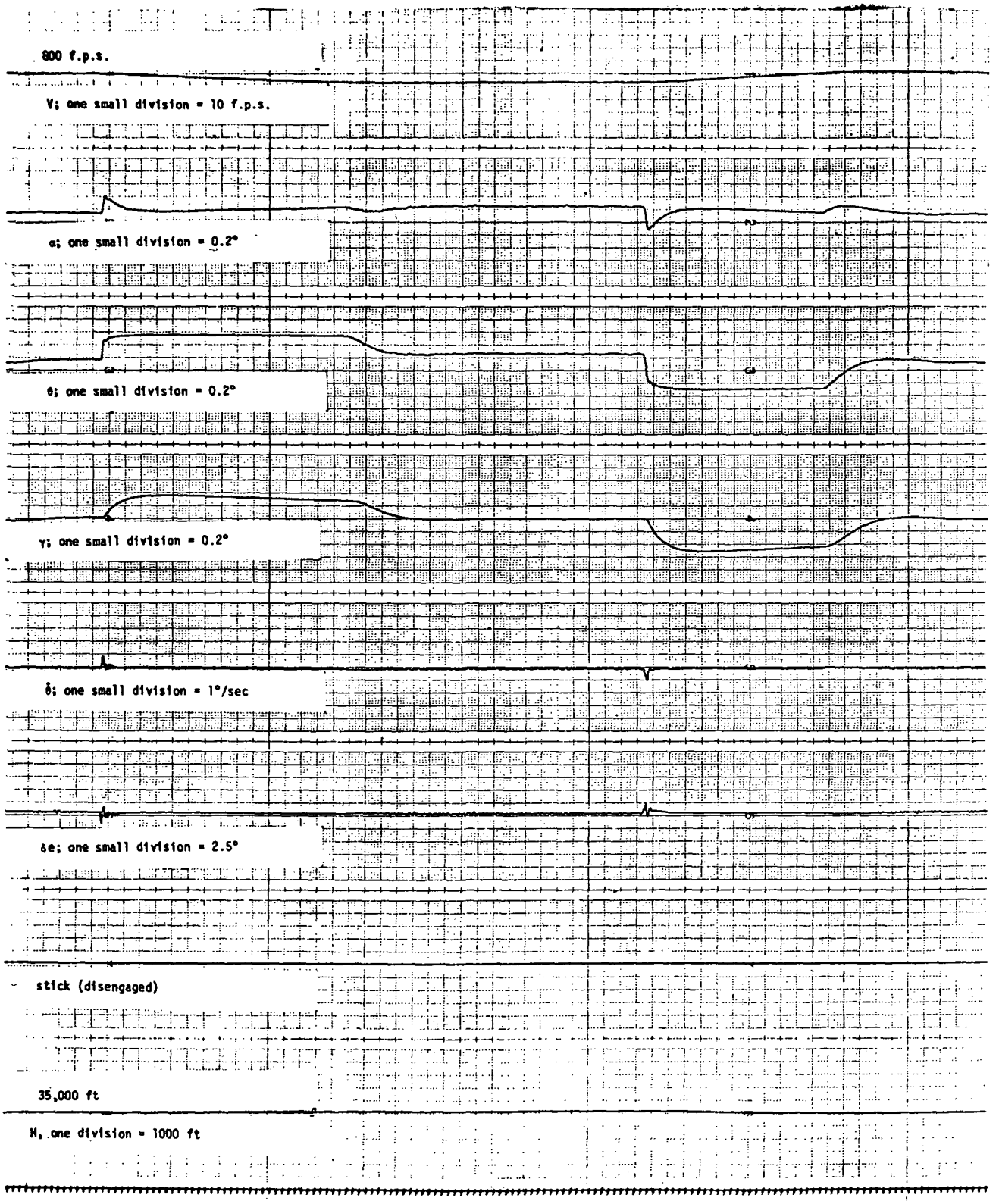

Figure 4.19 Altitude hold response for 1000 ft step changes in reference attitude

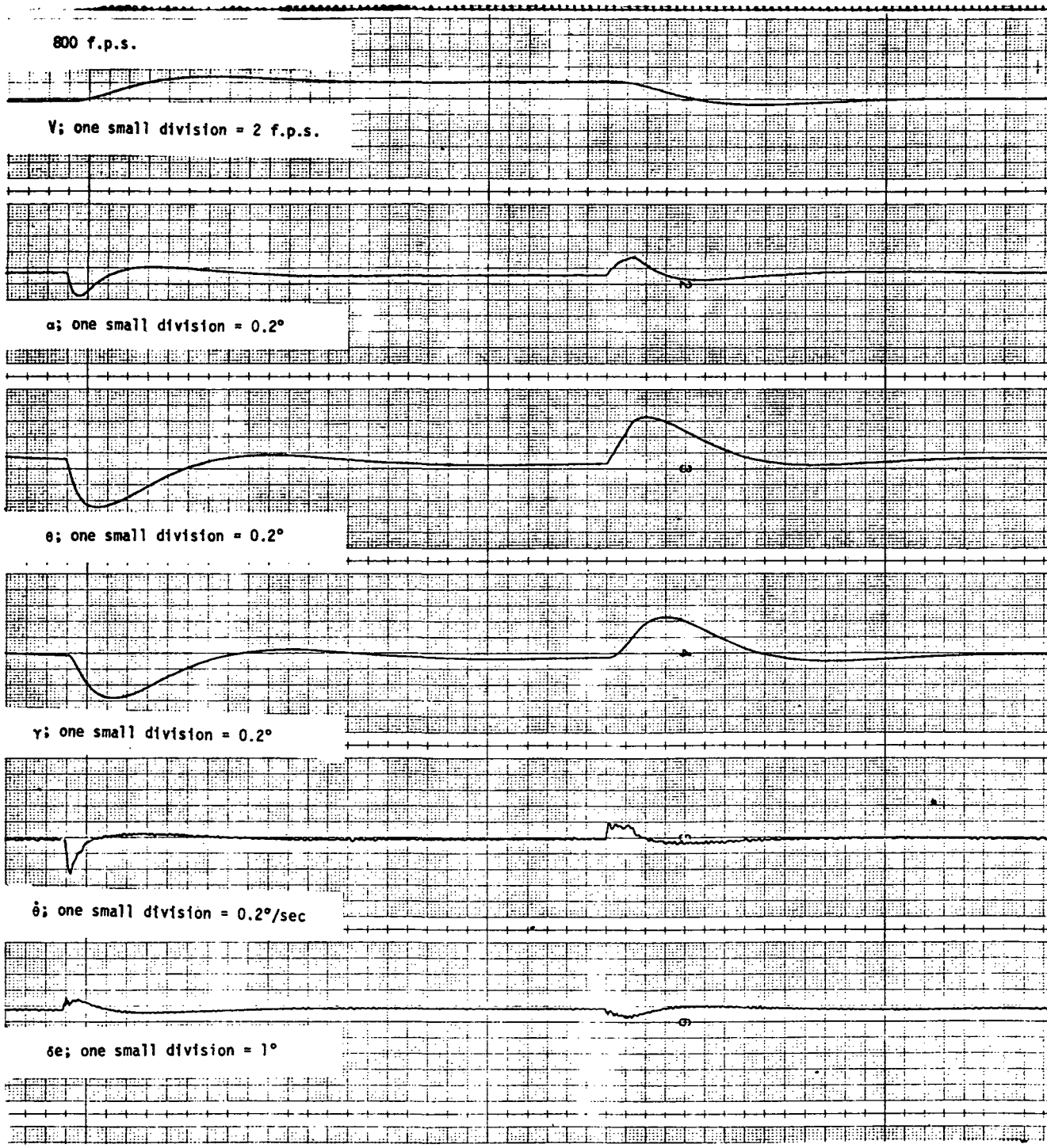

Figure 4.20 Mach hold response for 0.01 step change in mach number.

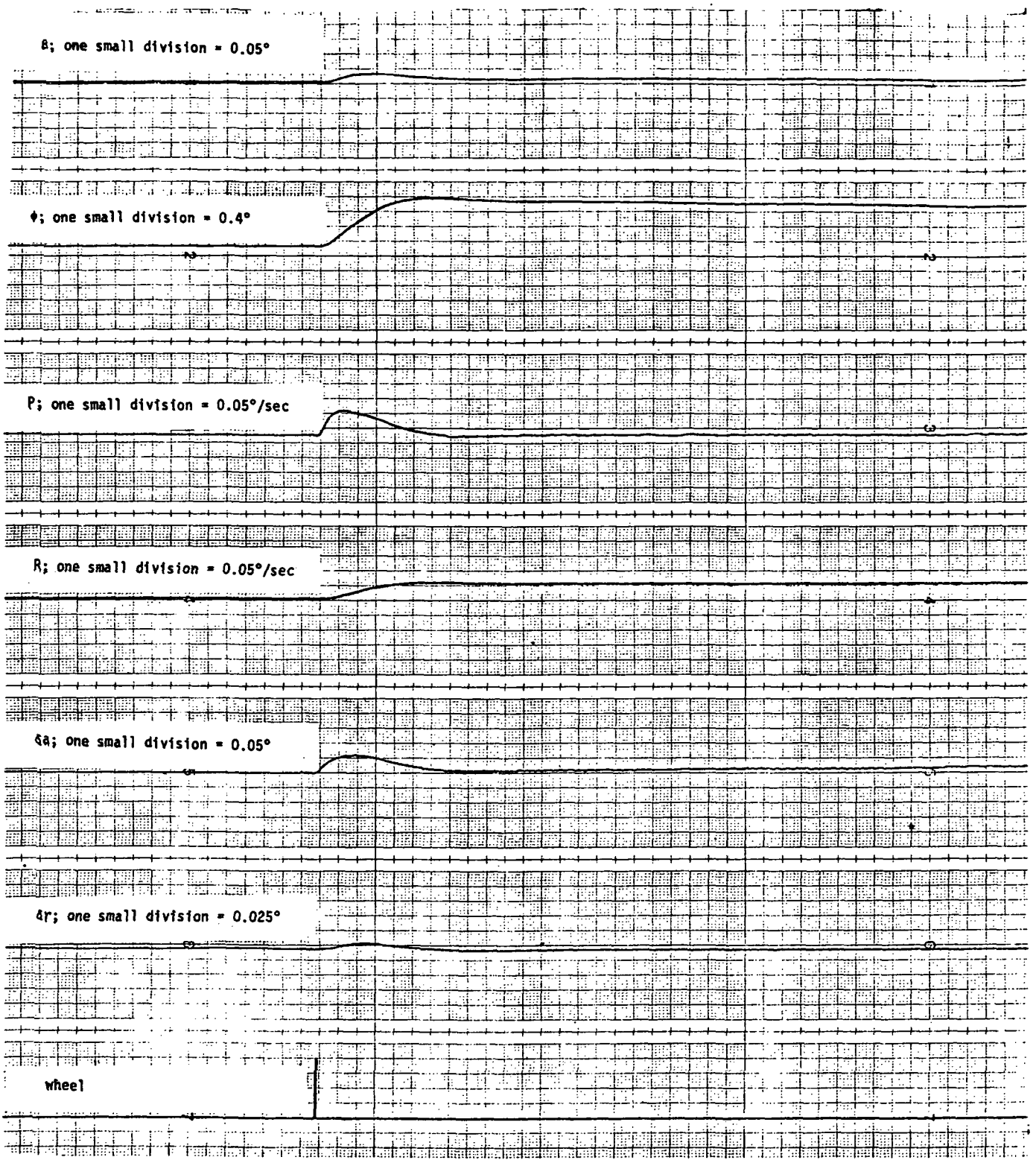

Figure 4.21 Lateral C.S.S. Impulse Response

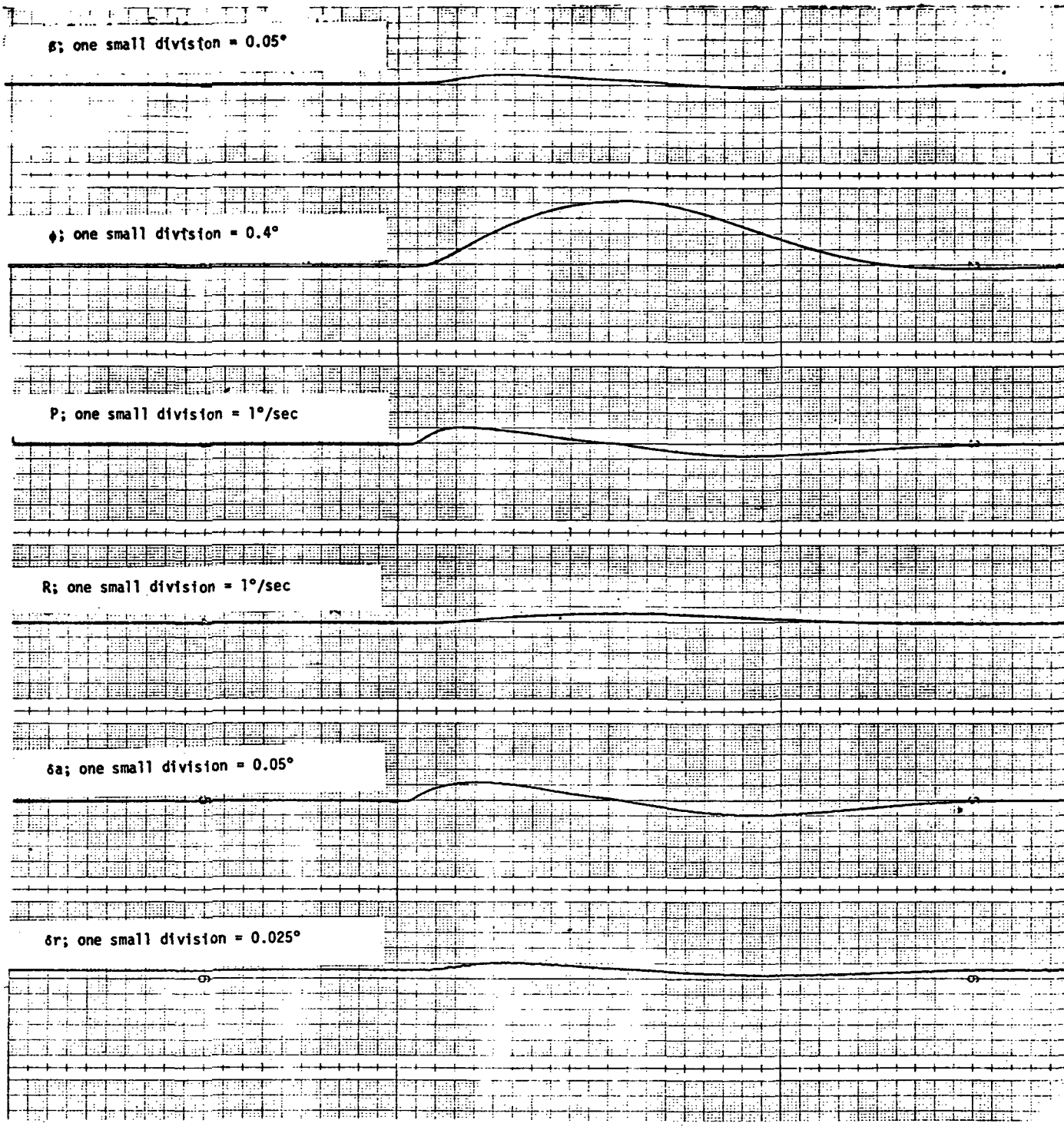

Figure 4.22 Lateral heading hold response for 10° change in reference heading

References

1. Aerodynamic Data for the C-135A Simulator, Boeing Company Document no. D6-7612

2. Blakelock, J.H., Automatic Control of Aircraft and Missiles, John Wiley and Son, Inc, 1965.

3. Penchuk, A. and Schlundt, R.W., Cruise Phase Autopilots for Straight Wing Orbiter Vehicle, M.I.T. C.S. Draper Laboratory Memo No. 71-23C-4.

4. Ragazzini and Franklin, Sampled Data Control Systems, McGraw Hill Book Company, 1958.

Chapter V

AIRCRAFT FLIGHT SIMULATOR

5.1 Introduction

A flight simulator has been designed to serve as a test-bed for the digital autopilot. A hybrid computer facility, consisting of a Beckman, 2200 Series, analog computer and a Xerox Data Systems, 9300 Series, digital computer, was used for the simulation.

Aerodynamic data for the Boeing KC-135 airplane were used in setting up the simulator, but the scaling is such that any large subsonic transport-type aircraft (excluding VTOL's) can be simulated with virtually no modification of the basic analog patchboards.

The computation is nonlinear; it covers the complete flight regime from stall speed to maximum permissible speed and from take-off to touch-down. The assumptions made in linearized computers are not made in this mechanization; no "small angle" or "small perturbation" assumptions are made, and longitudinal and lateral modes are coupled to the extent indicated by the aircraft data.

The choice of analog versus digital computation is made such that the strong features of each are exploited. Thus, aircraft dynamics is handled primarily on the analog computer, and nonlinear function generation is done on the digital computer.

In the solution of the equations of motion the earth is assumed to be non-rotating and flat; also, the aircraft is assumed to have constant mass and constant mass distribution.

The following sections indicate the equations used and the way that these equations have been implemented in the hybrid computer.

5.2 Equations of Motion

The six basic equations of aircraft motion can be divided into two groups of three each. The first three describe the translational motion of the aircraft center of mass; these are known as the "force equations". The other three describe the aircraft's rotational motion about its center of mass; these are the "moment equations".

Each group of three equations can be represented by a single vector equation. In the vector equations below, a vector is indicated by underlining, and the standard dot ($\cdot$) and cross ($\times$) are used for the dot product and the cross product, respectively. The letter p preceding a vector signifies the time rate of change of that vector. The subscript appended to the p indicates the coordinate system relative to which the rate is taken; thus, $p_j\underline{V}$ is the time rate of change of vector $\underline{V}$ relative to coordinate system j.

If wind effects are neglected, the vector equation for the translational motion of a constant-mass aircraft flying over a flat, non-rotating earth is

$$p_j\underline{V} = \frac{1}{m}\underline{F} + \underline{g} - \underline{\omega}_{ij} \times \underline{V} \qquad (5.2\text{-}1)$$

$\underline{V}$ is the true airspeed vector, i.e., the velocity of the aircraft relative to the ambient air mass. $\underline{g}$ is the acceleration due to gravity. $\underline{F}$ is the resultant non-gravitational force on the craft. m is the aircraft mass. Subscripts j and i refer to a moving and an inertial coordinate system, respectively. $\underline{\omega}_{ij}$ is the angular velocity of the moving system relative to the inertial system.

The vector equation of rotational motion is

$$p_j \underline{H}_C = \underline{M}_C - \underline{\omega}_{ij} \times \underline{H}_C \qquad (5.2\text{-}2)$$

$\underline{H}_C$ is the angular momentum of the aircraft with respect to its center of mass C. $\underline{M}_C$ is the external moment applied about C.

Note that the moving coordinate system denoted by subscript j in Eq. (5.2-2) need not be the same moving coordinate system as that of Eq. (5.2-1); thus, $\underline{\omega}_{ij}$ in the second equation is, in general, not equal to $\underline{\omega}_{ij}$ in the first equation. In the next section several moving coordinate systems are described, each with its individual subscript.

5.3 Coordinate Frames

Implementation of the vector equations of motion depends on the choice of the coordinate frame with respect to which each of the vector equations is resolved into component equations. Coordinate frames of interest are the following:

1. Navigation	(symbol n)	3. Stability	(symbol s)
2. Body	(symbol b)	4. Wind	(symbol w)

The origin of the navigation frame is at a point fixed relative to the earth. The origin of all the other frames is at the aircraft center of mass. All frames are orthogonal.

In the navigation frame the positive x axis (i.e., the x_n axis) points north, the y_n axis points east, and the z_n axis points down. For a non-rotating, flat earth the navigation frame may be regarded as an inertial frame.

The body frame is fixed to the aircraft, which is assumed to be a rigid body. It is also assumed that the craft has a plane of symmetry. The x_b and z_b axes lie in that plane, and the y_b axis is perpendicular to the plane. The positive x_b axis points forward and is parallel to the fuselage reference line. The positive y_b axis points out along the right wing. The positive z_b axis points in the downward direction in level flight.

The stability frame is displaced from the body frame by the angle of attack α, an angle that is measured in the plane of symmetry. Thus, the x_s and z_s axes, like the x_b and z_b axes, lie in the plane of symmetry. Also, the y_s axis coincides with the y_b axis. The x_s axis, positive forward, lies along the projection of the velocity vector $\underline{V}$ in the plane of symmetry. The positive z_s axis points downward in level flight.

The wind frame is displaced from the stability frame by the side-

slip angle β. The z_w and z_s axes coincide and are positive in the same direction. The x_w axis is parallel to $\underline{V}$ and is positive in the direction that $\underline{V}$ is positive. The y_w axis is in the cross-wind direction; its positive direction is to the right.

5.4 Coordinate Transformations

The transformation of any of the vector quantities of Section 5.2 from one coordinate frame to another is accomplished by means of a three-by-three transformation matrix. Since all the coordinate frames being considered are orthogonal, the transformation matrices are orthogonal.

A superscript will be used to indicate the coordinate frame in which the components of a vector are expressed. If we know the components of a vector $\underline{x}$ in two coordinate frames, the i frame and the j frame, and if we designate the matrix that transforms a vector from the i frame to the j frame as $C_i{}^j$, then we have the defining matrix equation

$$\underline{x}^j = C_i{}^j \underline{x}^i \tag{5.4-1}$$

Conversely,

$$\underline{x}^i = C_j{}^i \underline{x}^j \tag{5.4-2}$$

Since the matrices are orthogonal,

$$C_j^{\ i} = (C_i^{\ j})^{-1} = (C_i^{\ j})^T \qquad (5.4\text{-}3)$$

where superscript -1 denotes the matrix inverse and superscript T denotes the matrix transpose.

We are concerned with the transformation matrices which relate the coordinate frames of Section 5.3. The body frame b is related to the navigation frame n by the three body axis Euler angles ψ, θ, ϕ. Three rotations are involved in going from the n frame to the b frame, first about the positive z_n axis through the heading angle ψ, then about the rotated positive y axis through the pitch angle θ, finally about the resulting positive x axis (which has undergone two rotations) through the roll angle ϕ.

The stability frame s is obtained from the b frame by rotation about the negative y_b axis through the angle of attack α. The wind frame w is obtained from the s frame by rotation about the positive z_s axis through the sideslip angle β.

The elements of the transformation matrices are shown below.

$$C_n^{\ b} = \begin{bmatrix} 1 & 0 & 0 \\ 0 & \cos\phi & \sin\phi \\ 0 & -\sin\phi & \cos\phi \end{bmatrix} \begin{bmatrix} \cos\theta & 0 & -\sin\theta \\ 0 & 1 & 0 \\ \sin\theta & 0 & \cos\theta \end{bmatrix} \begin{bmatrix} \cos\psi & \sin\psi & 0 \\ -\sin\psi & \cos\psi & 0 \\ 0 & 0 & 1 \end{bmatrix}$$

$$C_n^b = \begin{bmatrix} \cos\theta\ \cos\psi & \cos\theta\ \sin\psi & -\sin\theta \\ -\cos\phi\ \sin\psi & \cos\phi\ \cos\psi & \sin\phi\ \cos\theta \\ +\sin\phi\ \sin\theta\ \cos\psi & +\sin\phi\ \sin\theta\ \sin\psi & \\ \sin\phi\ \sin\psi & -\sin\phi\ \cos\psi & \cos\phi\ \cos\theta \\ +\cos\phi\ \sin\theta\ \cos\psi & +\cos\phi\ \sin\theta\ \sin\psi & \end{bmatrix} \quad (5.4\text{-}4)$$

$$C_b^s = \begin{bmatrix} \cos\alpha & 0 & \sin\alpha \\ 0 & 1 & 0 \\ -\sin\alpha & 0 & \cos\alpha \end{bmatrix} \quad (5.4\text{-}5)$$

$$C_s^w = \begin{bmatrix} \cos\beta & \sin\beta & 0 \\ -\sin\beta & \cos\beta & 0 \\ 0 & 0 & 1 \end{bmatrix} \quad (5.4\text{-}6)$$

$$C_b^w = C_s^w\, C_b^s = \begin{bmatrix} \cos\beta\ \cos\alpha & \sin\beta & \cos\beta\ \sin\alpha \\ -\sin\beta\ \cos\alpha & \cos\beta & -\sin\beta\ \sin\alpha \\ -\sin\alpha & 0 & \cos\alpha \end{bmatrix} \quad (5.4\text{-}7)$$

$$C_n^w = C_b^w\, C_n^b = \begin{bmatrix} c_{11} & c_{12} & c_{13} \\ c_{21} & c_{22} & c_{23} \\ c_{31} & c_{32} & c_{33} \end{bmatrix} \quad (5.4\text{-}8)$$

$$c_{11} = \cos\beta \cos\alpha \cos\theta \cos\psi - \sin\beta \cos\phi \sin\psi$$
$$+ \sin\beta \sin\phi \sin\theta \cos\psi + \cos\beta \sin\alpha \sin\phi \sin\psi$$
$$+ \cos\beta \sin\alpha \cos\phi \sin\theta \cos\psi \qquad (5.4\text{-}8a)$$

$$c_{12} = \cos\beta \cos\alpha \cos\theta \sin\psi + \sin\beta \cos\phi \cos\psi$$
$$+ \sin\beta \sin\phi \sin\theta \sin\psi - \cos\beta \sin\alpha \sin\phi \cos\psi$$
$$+ \cos\beta \sin\alpha \cos\phi \sin\theta \sin\psi \qquad (5.4\text{-}8b)$$

$$c_{13} = -\cos\beta \cos\alpha \sin\theta + \sin\beta \sin\phi \cos\theta$$
$$+ \cos\beta \sin\alpha \cos\phi \cos\theta \qquad (5.4\text{-}8c)$$

$$c_{21} = -\sin\beta \cos\alpha \cos\theta \cos\psi - \cos\beta \cos\phi \sin\psi$$
$$+ \cos\beta \sin\phi \sin\theta \cos\psi - \sin\beta \sin\alpha \sin\phi \sin\psi$$
$$- \sin\beta \sin\alpha \cos\phi \sin\theta \cos\psi \qquad (5.4\text{-}8d)$$

$$c_{22} = -\sin\beta \cos\alpha \cos\theta \sin\psi + \cos\beta \cos\phi \cos\psi$$
$$+ \cos\beta \sin\phi \sin\theta \sin\psi + \sin\beta \sin\alpha \sin\phi \cos\psi$$
$$- \sin\beta \sin\alpha \cos\phi \sin\theta \sin\psi \qquad (5.4\text{-}8e)$$

$$c_{23} = \sin\beta \cos\alpha \sin\theta + \cos\beta \sin\phi \cos\theta$$
$$- \sin\beta \sin\alpha \cos\phi \cos\theta \qquad (5.4\text{-}8f)$$

$$c_{31} = -\sin\alpha \cos\theta \cos\psi + \cos\alpha \sin\phi \sin\psi + \cos\alpha \cos\phi \sin\theta \cos\psi \quad (5.4\text{-}8g)$$

$$c_{32} = -\sin\alpha \cos\theta \sin\psi - \cos\alpha \sin\phi \cos\psi + \cos\alpha \cos\phi \sin\theta \sin\psi \quad (5.4\text{-}8h)$$

$$c_{33} = \sin\alpha \sin\theta + \cos\alpha \cos\phi \cos\theta \quad (5.4\text{-}8i)$$

5.5 Angular Velocity Vectors

The transformations of the last section can be used to obtain the components of the angular velocity vectors that are of interest. We start by designating the components of $\underline{\omega}_{nb}{}^{b}$ (the angular velocity of the b frame with respect to the n frame, with components expressed in the b frame) as P, Q, and R. In column matrix form,

$$\underline{\omega}_{nb}{}^{b} = \begin{bmatrix} P \\ Q \\ R \end{bmatrix} \quad (5.5\text{-}1)$$

The angular velocity of the s frame relative to the b frame is

$$\underline{\omega}_{bs}{}^{b} = \begin{bmatrix} 0 \\ -\dot{\alpha} \\ 0 \end{bmatrix} = \underline{\omega}_{bs}{}^{s} \quad (5.5\text{-}2)$$

The dot over the scalar function α denotes the time derivative of that scalar function. The angular velocity of the w frame with respect to the s frame is

$$\underline{\omega}_{sw}^{\ s} = \begin{bmatrix} 0 \\ 0 \\ \dot{\beta} \end{bmatrix} = \underline{\omega}_{sw}^{\ w} \tag{5.5-3}$$

By vector addition of angular velocities, we get

$$\underline{\omega}_{bw}^{\ w} = C_s^{\ w}\,\underline{\omega}_{bs}^{\ s} + \underline{\omega}_{sw}^{\ w} = \begin{bmatrix} -\dot{\alpha} & \sin\beta \\ -\dot{\alpha} & \cos\beta \\ & \dot{\beta} \end{bmatrix} \tag{5.5-4}$$

$$\underline{\omega}_{ns}^{\ s} = C_b^{\ s}\,\underline{\omega}_{nb}^{\ b} + \underline{\omega}_{bs}^{\ s} = \begin{bmatrix} P\cos\alpha + R\sin\alpha \\ Q - \dot{\alpha} \\ -P\sin\alpha + R\cos\alpha \end{bmatrix} \tag{5.5-5}$$

$$\underline{\omega}_{nw}^{\ w} = C_b^{\ w}\,\underline{\omega}_{nb}^{\ b} + \underline{\omega}_{bw}^{\ w}$$

$$= \begin{bmatrix} P\cos\beta\ \cos\alpha + (Q - \dot{\alpha})\sin\beta + R\cos\beta\sin\alpha \\ -P\sin\beta\ \cos\alpha + (Q - \dot{\alpha})\cos\beta - R\sin\beta\sin\alpha \\ -P\sin\alpha + R\cos\alpha + \dot{\beta} \end{bmatrix} \tag{5.5-6}$$

5.6 Component Equations of Translational Motion

The three scalar equations represented by the force vector equation (5.2-1) are to be solved for the three fundamental aerodynamic variables V, α, and β. The form of the solution depends on the choice of a coordinate frame. In this section we shall examine the equations resulting from the selection of each of the three moving frames described in Section 5.3 and weigh their relative advantages and disadvantages.

Because of the way in which the coordinate frames have been defined, the velocity vector has only one non-zero component in the wind frame, and the gravity vector has only one non-zero component in the navigation frame.

$$\underline{V}^w = \begin{bmatrix} V \\ 0 \\ 0 \end{bmatrix} \tag{5.6-1}$$

$$\underline{g}^n = \begin{bmatrix} 0 \\ 0 \\ g \end{bmatrix} \tag{5.6-2}$$

Data on the non-gravitational force $\underline{F}$ are usually presented with respect to stability axes, so that the vector is most simply represented as

$$\underline{F}^s = \begin{bmatrix} X^s \\ Y^s \\ Z^s \end{bmatrix} \tag{5.6-3}$$

where X, Y, and Z are force components along the corresponding axes.

The derivative $p_j\underline{V}$ in Equation (5.2-1), if resolved in the j coordinate system, is equal to $p\underline{V}^j$, the derivative of each of the components of $\underline{V}^j$.

$$(p_j\underline{V})^j = p\underline{V}^j \tag{5.6-4}$$

Finally, since the navigation frame is an inertial frame, angular velocity $\underline{\omega}_{ij}$ may be replaced by $\underline{\omega}_{nj}$.

In the j coordinate system Equation (5.2-1) becomes

$$p\underline{V}^j = \frac{1}{m} C_s{}^j\underline{F}^s + C_n{}^j\underline{g}^n - \left[\underline{\omega}_{nj}{}^j x\right]\underline{V}^j \tag{5.6-5}$$

This is the matrix form of the vector equation. If the components of $\underline{\omega}_{nj}{}^j$ are ω_x, ω_y, ω_z, then $[\underline{\omega}_{nj}{}^j x]$ is the three-by-three anti-symmetric matrix shown below.

$$[\underline{\omega}_{nj}{}^j x] = \begin{bmatrix} 0 & -\omega_z & \omega_y \\ \omega_z & 0 & -\omega_x \\ -\omega_y & \omega_x & 0 \end{bmatrix} \tag{5.6-6}$$

In the body frame,

$$\underline{V}^b = C_w{}^b \underline{V}^w = (C_b{}^w)^T \underline{V}^w = \begin{bmatrix} V\cos\beta\ \cos\alpha \\ V\sin\beta \\ V\cos\beta\ \sin\alpha \end{bmatrix} = \begin{bmatrix} u \\ v \\ w \end{bmatrix} \tag{5.6-7}$$

The last column is meant to indicate that the components of $\underline{V}^b$ are frequently referred to as u, v, w in aerodynamic parlance. With b replacing j, Equation (5.6-5) becomes

$$p\underline{V}^b = \frac{1}{m} C_s{}^b \underline{F}^s + C_n{}^b \underline{g}^n - \left[\underline{\omega}_{nb}{}^b x\right] \underline{V}^b \tag{5.6-8}$$

The derivative may be written as

$$p\underline{V}^b = \begin{bmatrix} \dot{u} \\ \dot{v} \\ \dot{w} \end{bmatrix} = \begin{bmatrix} \dot{V}\cos\beta\ \cos\alpha - V\dot{\beta}\sin\beta\ \cos\alpha - V\dot{\alpha}\cos\beta\ \sin\alpha \\ \dot{V}\sin\beta + V\dot{\beta}\cos\beta \\ \dot{V}\cos\beta\ \sin\alpha - V\dot{\beta}\sin\beta\ \sin\alpha + V\dot{\alpha}\cos\beta\ \cos\alpha \end{bmatrix} \tag{5.6-9}$$

The cross-product is

$$\left[\underline{\omega}_{nb}{}^b x\right]\underline{V}^b = \begin{bmatrix} -Rv + Qw \\ Ru - Pw \\ -Qu + Pv \end{bmatrix} = V \begin{bmatrix} -R\sin\beta + Q\cos\beta\ \sin\alpha \\ (R\cos\alpha - P\sin\alpha)\cos\beta \\ -Q\cos\beta\ \cos\alpha + P\sin\beta \end{bmatrix} \tag{5.6-10}$$

In terms of u, v, w, the component equations are

$$\dot{u} = \frac{1}{m} (X^S \cos \alpha - Z^S \sin \alpha) - g \sin \theta + Rv - Qw \tag{5.6-11}$$

$$\dot{v} = \frac{1}{m} Y^S + g \sin \phi \cos \theta - Ru + Pw \tag{5.6-12}$$

$$\dot{w} = \frac{1}{m} (X^S \sin \alpha + Z^S \cos \alpha) + g \cos \phi \cos \theta + Qu - Pv \tag{5.6-13}$$

The equations are integrated to obtain, u, v, w. The desired variables V, α, β are derived from u, v, w as follows:

$$V = + (u^2 + v^2 + w^2)^{1/2} \tag{5.6-14}$$

$$\alpha = \tan^{-1} \left(\frac{w}{u}\right) \tag{5.6-15}$$

$$\beta = \tan^{-1} \left(\frac{v}{+(u^2 + w^2)^{1/2}}\right) \tag{5.6-16}$$

The inverse tangents in the last two equations do not cause ambiguities because the magnitude of both α and β is assumed to be less than $\frac{\pi}{2}$ radians.

The square root and inverse tangent computations pose some difficulties for the analog computer, and it is this computer that we should like to use for integration of the force equations because of its wide dynamic range. The difficulties are not insurmountable; i.e., the computations can be performed, but there is likely to be some static inaccuracy. An alternative formulation of the body-axis

equations permits us to integrate directly to get V, α, β, without any square root or inverse tangent determination. This formulation is given below.

$$\dot{V} = \frac{1}{\cos\beta \cos\alpha}\left[\frac{1}{m}(X^S \cos\alpha - Z^S \sin\alpha) - g \sin\theta\right]$$

$$+ V\left[\left(\frac{1}{\cos\alpha} R + \dot{\beta}\right)\tan\beta - (Q - \dot{\alpha})\tan\alpha\right] \qquad (5.6\text{-}17)$$

$$\dot{\beta} = \frac{1}{V\cos\beta}\left(\frac{1}{m} Y^S + g \sin\phi \cos\theta - \dot{V}\sin\beta\right)$$

$$- R\cos\alpha + P\sin\alpha \qquad (5.6\text{-}18)$$

$$\dot{\alpha} = \frac{1}{V\cos\beta\cos\alpha}\left[\frac{1}{m}(X^S \sin\alpha + Z^S\cos\alpha) + g\cos\phi\cos\theta\right]$$

$$- \frac{1}{V}\dot{V}\tan\alpha - \frac{1}{\cos\alpha} P\tan\beta + \dot{\beta}\tan\beta\tan\alpha + Q \qquad (5.6\text{-}19)$$

Although the integrations are direct, there is a significant increase in the number of multiplications, another source of inaccuracy (particularly when the desired product is zero, or near zero, as it normally is for many of the terms on the right-hand sides of the equations).

In the stability frame we have

$$p\underline{V}^S = \frac{1}{m}\underline{F}^S + C_n{}^S\underline{g}^n - \left[\underline{\omega}_{ns}{}^S x\right]\underline{V}^S \qquad (5.6\text{-}20)$$

$$\underline{V}_s = C_w^{\,s}\underline{V}^w = (C_s^{\,w})^T\underline{V}^w = \begin{bmatrix} V\cos\beta \\ V\sin\beta \\ 0 \end{bmatrix} = \begin{bmatrix} V_x^{\,s} \\ V_y^{\,s} \\ 0 \end{bmatrix} \tag{5.6-21}$$

$$p\underline{V}^s = \begin{bmatrix} \dot{V}_x^{\,s} \\ \dot{V}_y^{\,s} \\ 0 \end{bmatrix} = \begin{bmatrix} \dot{V}\cos\beta - V\dot{\beta}\sin\beta \\ \dot{V}\sin\beta + V\dot{\beta}\cos\beta \\ 0 \end{bmatrix} \tag{5.6-22}$$

$$\left[\underline{\omega}_{ns}^{\,s}x\right]\underline{V}^s = \begin{bmatrix} (P\sin\alpha - R\cos\alpha)\,V_y^{\,s} \\ (-P\sin\alpha + R\cos\alpha)\,V_x^{\,s} \\ -(Q-\dot{\alpha})\,V_x^{\,s} + (P\cos\alpha + R\sin\alpha)\,V_y^{\,s} \end{bmatrix}$$

$$= V\begin{bmatrix} (P\sin\alpha - R\cos\alpha)\sin\beta \\ (-P\sin\alpha + R\cos\alpha)\cos\beta \\ -(Q-\dot{\alpha})\cos\beta + (P\cos\alpha + R\sin\alpha)\sin\beta \end{bmatrix} \tag{5.6-23}$$

$$C_n^{\,s}\,\underline{g}^n = C_b^{\,s}\,\underline{g}^b = g\begin{bmatrix} -\cos\alpha\ \sin\theta + \sin\alpha\ \cos\phi\ \cos\theta \\ \sin\phi\ \cos\theta \\ \sin\alpha\ \sin\theta + \cos\alpha\ \cos\phi\ \cos\theta \end{bmatrix} \tag{5.6-24}$$

The first two component equations may be integrated to get the velocity components $V_x^{\,s}$ and $V_y^{\,s}$, and from these we get V and β in a matter analogous to that used for the body-axis system. The equations are

$$\dot{V}_x^S = \frac{1}{m} X^S + g\,(-\cos\alpha\ \sin\theta + \sin\alpha\ \cos\phi\ \cos\theta)$$

$$+ (-P \sin\alpha + R \cos\alpha)\, V_y^S \qquad (5.6\text{-}25)$$

$$\dot{V}_y^S = \frac{1}{m} Y^S + g \sin\phi\ \cos\theta - (-P \sin\alpha + R \cos\alpha) V_x^S \qquad (5.6\text{-}26)$$

$$V = + \left[(V_x^S)^2 + (V_y^S)^2\right]^{1/2} \qquad (5.6\text{-}27)$$

$$\beta = \tan^{-1} \left[\frac{V_y^S}{V_x^S}\right] \qquad (5.6\text{-}28)$$

Again there is the disadvantage associated with analog computation of the square root and the inverse tangent. The formulation involving direct integration of $\dot{V}$, $\dot{\beta}$, $\dot{\alpha}$ is the following:

$$\dot{V} = \frac{1}{\cos\beta} \left[\frac{1}{m} X^S + g\,(-\cos\alpha\ \sin\theta + \sin\alpha\ \cos\phi\ \cos\theta)\right]$$

$$+ V\,(-P \sin\alpha + R \cos\alpha + \dot{\beta}) \tan\beta \qquad (5.6\text{-}29)$$

$$\dot{\beta} = \frac{1}{V \cos\beta} \left(\frac{1}{m} Y^S + g \sin\phi\ \cos\theta - \dot{V} \sin\beta\right) + P \sin\alpha - R \cos\alpha \qquad (5.6\text{-}30)$$

$$\dot{\alpha} = \frac{1}{V \cos\beta} \left[\frac{1}{m} Z^S + g\,(\sin\alpha\ \sin\theta + \cos\alpha\ \cos\phi\ \cos\theta)\right]$$

$$+ Q - (P \cos\alpha + R \sin\alpha) \tan\beta \qquad (5.6\text{-}31)$$

The vector equation in the wind frame is

$$p\underline{V}^W = \frac{1}{m} C_s{}^W\underline{F}^S + C_n{}^W\underline{g}^n - [\underline{\omega}_{nw}{}^W X]\ \underline{V}^W \tag{5.6-32}$$

where

$$p\underline{V}^W = \begin{bmatrix} \dot{V} \\ 0 \\ 0 \end{bmatrix} \tag{5.6-33}$$

$$C_s{}^W\underline{F}^S = \begin{bmatrix} X^S \cos\beta + Y^S \sin\beta \\ -X^S \sin\beta + Y^S \cos\beta \\ Z^S \end{bmatrix} \tag{5.6-34}$$

$$C_n{}^W\underline{g}^n = g \begin{bmatrix} c_{13} \\ c_{23} \\ c_{33} \end{bmatrix} \tag{5.6-35}$$

$$[\underline{\omega}_{nw}{}^W X]\ \underline{V}^W = V \begin{bmatrix} 0 \\ -P \sin\alpha + R \cos\alpha + \dot{\beta} \\ (P \cos\alpha + R \sin\alpha) \sin\beta - (Q - \dot{\alpha}) \cos\beta \end{bmatrix} \tag{5.6-36}$$

The component equations, solved for $\dot{V}$, $\dot{\beta}$, $\dot{\alpha}$, are

$$\dot{V} = \frac{1}{m}(X^S \cos\beta + Y^S \sin\beta) + g\,(-\cos\beta\ \cos\alpha\ \sin\theta + \sin\beta\ \sin\phi\ \cos\theta + \cos\beta\ \sin\alpha\ \cos\phi\ \cos\theta) \tag{5.6-37}$$

$$\dot{\beta} = \frac{1}{V}\left[\frac{1}{m}(-X^S \sin\beta + Y^S \cos\beta) + g(\sin\beta \cos\alpha \sin\theta + \cos\beta \sin\phi \cos\theta - \sin\beta \sin\alpha \cos\phi \cos\theta)\right] + P \sin\alpha - R \cos\alpha \quad (5.6\text{-}38)$$

$$\dot{\alpha} = \frac{1}{V \cos\beta}\left[\frac{1}{m} Z^S + g(\sin\alpha \sin\theta + \cos\alpha \cos\phi \cos\theta)\right] - (P \cos\alpha + R \sin\alpha) \tan\beta + Q \quad (5.6\text{-}39)$$

In comparing the formulations in the three coordinate frames, we shall confine the discussion to the equations that are solved for $\dot{V}$, $\dot{\beta}$, and $\dot{\alpha}$ directly. We note that, since the y_b and y_s axes coincide, the $\dot{\beta}$ equation in the s frame is the same as the $\dot{\beta}$ equation in the b frame. Also, since the z_s and z_w axes coincide, the $\dot{\alpha}$ equation is the same in the s and w frames.

As we go from the b frame to the s frame to the w frame, the components of the gravity vector become more complex, and the components of $(\underline{\omega} \times \underline{V})$ become simpler. The computational complexity caused by the gravity components can be reduced if aircraft attitude is determined by integration of the direction cosines; this subject is discussed in detail in a later section.

The $(\underline{\omega} \times \underline{V})$ components become simpler because $\underline{V}$ has only one non-zero component in the w frame. This fact more than compensates for the increased complexity of $\underline{\omega}$ in the w frame.

The apparent simplicity of the components of $\underline{F}$ in the s frame may be illusory; it depends on the assumption that aerodynamic and thrust data are normally presented in terms of stability-axis components. However, the data can be pre-processed to effect a transformation into any desired moving frame.

Finally, we note that there are $\dot{V}$ terms on the right-hand sides of the $\dot{\beta}$ and $\dot{\alpha}$ equations in the b and s frames, but no $\dot{V}$ terms on the right-hand sides of the w-frame equations.

The wind frame formulation has been selected for implementation in the simulator, the primary consideration being the reduced number of $(\underline{\omega} \times \underline{V})$ terms.

5.7 Component Equations of Rotational Motion

In order to resolve the rotational vector equation, (5.2-2), into scalar component equations, we shall derive an expression for angular momentum $\underline{H}_C$ as a function of angular velocity. It will become clear that the body frame has decided advantages over the other moving frames in the rotational equations.

The aircraft is assumed to be rigid, with constant mass and constant mass distribution. It may be regarded as a system of n particles, with the k-th particle having mass m_k and being located at position $\underline{r}_{Ck}$ relative to center of mass C. From the definition of angular momentum and the Coriolis theorem,

$$\underline{H}_C = \sum \underline{r}_{Ck} \times m_k \, (p_i \underline{r}_{Ck}) = \sum \underline{r}_{Ck} \times m_k \, (p_j \underline{r}_{Ck} + \underline{\omega}_{ij} \times \underline{r}_{Ck}) \qquad (5.7\text{-}1)$$

where $\sum$ represents the summation with respect to k from k = 1 to k = n.

The term $p_j \underline{r}_{Ck}$ is the velocity of the k-th particle with respect to the center of mass. This velocity is zero in the body frame, but non-zero in the other two moving frames. Hence a significant simplification of the equations is effected by using the body frame. In the body frame,

$$\underline{H}_C^b = \sum \underline{r}_{Ck}^b \times m_k \, (\underline{\omega}_{nb}^b \times \underline{r}_{Ck}^b) = -\sum m_k \underline{r}_{Ck}^b \times (\underline{r}_{Ck}^b \times \underline{\omega}_{nb}^b) \qquad (5.7\text{-}2)$$

In matrix notation, a triple vector product of the form $\underline{a} \times (\underline{a} \times \underline{b})$ may be expanded as follows:

$$[\underline{a} \times][\underline{a} \times]\underline{b} = (\underline{a}\,\underline{a}^T - \underline{a}^T\,\underline{a}\, I)\,\underline{b} \qquad (5.7\text{-}3)$$

where $\underline{a}\,\underline{a}^T$ is a dyad and I is the three-by-three identity matrix. With this expansion the angular momentum becomes

$$\underline{H}_C^b = \sum m_k \left[(\underline{r}_{Ck}^b)^T (\underline{r}_{Ck}^b)\, I - (\underline{r}_{Ck}^b)\, (\underline{r}_{Ck}^b)^T \right] \underline{\omega}_{nb}^b \qquad (5.7\text{-}4)$$

The summation operating on angular velocity vector $\underline{\omega}_{nb}^b$ is the inertia matrix, which we shall denote by K^b. If the components

of $\underline{r}_{Ck}{}^{b}$ are x_k, y_k, z_k, the inertia matrix is given by

$$K^b = \begin{bmatrix} \sum m_k(y_k{}^2 + z_k) & -\sum m_k x_k y_k & -\sum m_k x_k z_k \\ -\sum m_k y_k x_k & \sum m_k(z_k{}^2 + x_k{}^2) & -\sum m_k y_k z_k \\ -\sum m_k z_k x_k & -\sum m_k z_k y_k & \sum m_k(x_k{}^2 + y_k{}^2) \end{bmatrix}$$

$$= \begin{bmatrix} I_{xx} & -I_{xy} & -I_{xz} \\ -I_{xy} & I_{yy} & -I_{yz} \\ -I_{xz} & -I_{yz} & I_{zz} \end{bmatrix} \qquad (5.7\text{-}5)$$

I_{xx}, I_{yy}, and I_{zz} are the moments of inertia in the body frame, and I_{xy}, I_{xz}, and I_{yz} are the products of inertia in that frame. Because the $x_b z_b$ plane is assumed to be a plane of symmetry, I_{xy} and I_{yz} are identically zero, and I_{yy} is a principal moment of inertia.

It is possible to achieve a further simplification of the inertia matrix by establishing a new body-fixed frame in which all three coordinate axes are principal axes and all three products of inertia are zero. Then K^b becomes a diagonal matrix. The new x and z axes would be rotated by an angle ε from the x_b and z_b axes of the conventional body frame. This rotation was not used in the layout of the flight simulator because it was felt that the design improvement obtained was not sufficient to offset the labor (and probable confusion) that would be involved in re-processing some of the aerodynamic data.

We return now to the vector equation of rotational motion. In the conventional body frame it becomes

$$p\underline{H}_C^b = \underline{M}_C^b - \underline{\omega}_{nb}^b \times \underline{H}_C^b \tag{5.7-6}$$

and

$$\underline{H}_C^b = K^b \underline{\omega}_{nb}^b \tag{5.7-7}$$

Since K^b is a constant matrix,

$$p\underline{H}_C^b = p\,(K^b \underline{\omega}_{nb}^b) = K^b p\,\underline{\omega}_{nb}^b$$

$$= \begin{bmatrix} I_{xx} & 0 & -I_{xz} \\ 0 & I_{yy} & 0 \\ -I_{xz} & 0 & I_{zz} \end{bmatrix} \begin{bmatrix} \dot{P} \\ \dot{Q} \\ \dot{R} \end{bmatrix} \tag{5.7-8}$$

The cross-product is

$$\underline{\omega}_{nb}^b \times \underline{H}_C^b = \left[\underline{\omega}_{nb}^b \times\right] K^b \underline{\omega}_{nb}^b$$

$$= \begin{bmatrix} 0 & -R & Q \\ R & 0 & -P \\ -Q & P & 0 \end{bmatrix} \begin{bmatrix} I_{xx} & 0 & -I_{xz} \\ 0 & I_{yy} & 0 \\ -I_{xz} & 0 & I_{zz} \end{bmatrix} \begin{bmatrix} P \\ Q \\ R \end{bmatrix} \tag{5.7-9}$$

The components of $\underline{M}_C^b$ are designated as L, the rolling moment; M, the pitching moment; and N, the yawing moment.

$$\underline{M}_C^b = \begin{bmatrix} L \\ M \\ N \end{bmatrix} \tag{5.7-10}$$

The component equations are then

$$\dot{P} = \frac{1}{I_{xx}} [L + I_{xz} (\dot{R} + PQ) + (I_{yy} - I_{zz})QR] \tag{5.7-11}$$

$$\dot{Q} = \frac{1}{I_{yy}} [M + I_{xz} (R^2 - P^2) + (I_{zz} - I_{xx})RP] \tag{5.7-12}$$

$$\dot{R} = \frac{1}{I_{zz}} [N + I_{xz} (\dot{P} - QR) + (I_{xx} - I_{yy})PQ] \tag{5.7-13}$$

These equations are integrated to obtain the angular velocity components P, Q, R.

5.8 Attitude Determination

The attitude of an aircraft is defined in terms of its body-axis Euler angles ψ, θ, ϕ. We should like to determine these three angles by expressing their rates $\dot{\psi}$, $\dot{\theta}$, $\dot{\phi}$, in terms of body rates P, Q, R, and then integrating. A difficulty arises because the axes about which $\dot{\psi}$, $\dot{\theta}$, $\dot{\phi}$ are measured are not mutually orthogonal. $\dot{\psi}$ is

measured about the z_n axis, $\dot{\phi}$ about the x_b axis, and $\dot{\theta}$ about an axis that is obtained by rotating the y_n axis through the angle ψ or by rotating the y_b axis through the angle $-\phi$. The $\dot{\theta}$ axis is perpendicular to both the $\dot{\psi}$ and $\dot{\phi}$ axes, but the $\dot{\psi}$ and $\dot{\phi}$ axes are, in general, not perpendicular to each other. In matrix form,

$$\begin{bmatrix} P \\ Q \\ R \end{bmatrix} = \begin{bmatrix} 1 & 0 & -\sin\theta \\ 0 & \cos\phi & \cos\theta \sin\phi \\ 0 & -\sin\phi & \cos\theta \cos\phi \end{bmatrix} \begin{bmatrix} \dot{\phi} \\ \dot{\theta} \\ \dot{\psi} \end{bmatrix} \qquad (5.8\text{-}1)$$

If the matrix is not singular, it can be inverted to yield the desired relationships for the Euler angle rates in terms of the body rates.

$$\begin{bmatrix} \dot{\phi} \\ \dot{\theta} \\ \dot{\psi} \end{bmatrix} = \begin{bmatrix} 1 & \sin\phi \tan\theta & \cos\phi \tan\theta \\ 0 & \cos\phi & -\sin\phi \\ 0 & \sin\phi \sec\theta & \cos\phi \sec\theta \end{bmatrix} \begin{bmatrix} P \\ Q \\ R \end{bmatrix} \qquad (5.8\text{-}2)$$

The matrix of Equation (5.8-1) becomes singular when $\theta = \pm \frac{\pi}{2}$. When the singularity occurs, Equation (5.8-2) cannot be solved for $\dot{\phi}$ or $\dot{\psi}$, although a relation for $(\dot{\phi} \mp \dot{\psi})$ can be obtained from the first scalar equation of (5.8-1).

To avoid the problems associated with the singularity, we can employ either of two schemes which involve redundant integrations.

The first is the method of quaternions. It is a four-parameter method; there are four integrations and one constraint equation. The second alternative is the method of direction cosines, which in principle requires nine integrations and hence has six constraint equations.

The method of direction cosines has been chosen for attitude determination in our flight simulator. Although the quaternion method has the advantage of fewer integrations, its parameters are not so familiar as the direction cosines. Moreover, as we shall show, the integration of all nine cosines is not required to obtain all the cosines; some can be obtained directly from the constraint equations after the others have been obtained by integration.

A brief derivation of the mathematical formulation of the direction cosine method will now be given. Consider an arbitrary vector $\underline{u}$ and its resolution into components in two coordinate systems, the inertial, or stationary, system i and the moving system j. The two coordinate systems are related by the transformation matrix $C_i^{\ j}$.

$$\underline{u}^j = C_i^{\ j}\, \underline{u}^i \tag{5.8-3}$$

The Coriolis equation states that

$$p_i\underline{u} = p_j\underline{u} + \underline{\omega}_{ij} \times \underline{u} \tag{5.8-4}$$

In the j coordinate system this equation becomes

$$C_i^j \, (p\underline{u}^i) = p \, \underline{u}^j + \underline{\omega}_{ij}{}^j \times \underline{u}^j \tag{5.8-5}$$

We substitute (5.8-3) into (5.8-5) and expand the derivative on the right-hand side.

$$C_i^j \, (p\underline{u}^i) = p(C_i^j \underline{u}^i) + \underline{\omega}_{ij}{}^j \times C_i^j \, \underline{u}^i$$

$$= (pC_i^j) \, \underline{u}^i + C_i^j (p\underline{u}^i) + \underline{\omega}_{ij}{}^j \times C_i^j \, \underline{u}^i \tag{5.8-6}$$

Then

$$(pC_i^j) \, \underline{u}^i = - \, \underline{\omega}_{ij}{}^j \times C_i^j \, \underline{u}^i \tag{5.8-7}$$

The right-hand side of this equation may be regarded as the matrix represented by $(- \, \underline{\omega}_{ij}{}^j \times C_i^j)$ operating on the vector $\underline{u}^i$. Similarly, the left-hand side represents matrix (pC_i^j) operating on $\underline{u}^i$. Since $\underline{u}^i$ is any arbitrary vector, the two matrix operators must be equal.

$$pC_i^j = - \, \underline{\omega}_{ij}{}^j \times C_i^j \tag{5.8-8}$$

This is the matrix equation to be integrated to get the elements of C_i^j.

Usually Equation (5.8-8) is solved for the elements of C_n^b, the matrix transformation from navigation to body axes. Then Equation (5.4-8) can be used to get C_n^w, the matrix required for the gravity components along wind axes. Also, angles ψ, θ, ϕ can be obtained for display or recording purposes from C_n^b.

In our flight simulator we depart from the usual procedure by solving Equation (5.8-8) for C_n^w rather than C_n^b. This approach gives us the gravity components along wind axes directly. The matrix equation to be solved is

$$pC_n^w = - \underline{\omega}_{nw}^w \times C_n^w \tag{5.8-9}$$

The components of $\underline{\omega}_{nw}^w$, given by Equation (5.5-6), will be designated P', Q', R'. The expanded form of (5.8-9) is

$$\begin{bmatrix} \dot{c}_{11} & \dot{c}_{12} & \dot{c}_{13} \\ \dot{c}_{21} & \dot{c}_{22} & \dot{c}_{23} \\ \dot{c}_{31} & \dot{c}_{32} & \dot{c}_{33} \end{bmatrix} = \begin{bmatrix} 0 & R' & -Q' \\ -R' & 0 & P' \\ Q' & -P' & 0 \end{bmatrix} \begin{bmatrix} c_{11} & c_{12} & c_{13} \\ c_{21} & c_{22} & c_{23} \\ c_{31} & c_{32} & c_{33} \end{bmatrix}$$

$$= \begin{bmatrix} R'c_{21} - Q'c_{31} & R'c_{22} - Q'c_{32} & R'c_{23} - Q'c_{33} \\ -R'c_{11} + P'c_{31} & -R'c_{12} + P'c_{32} & -R'c_{13} + P'c_{33} \\ Q'c_{11} - P'c_{21} & Q'c_{12} - P'c_{22} & Q'c_{13} - P'c_{23} \end{bmatrix} \tag{5.8-10}$$

It may be noted that the elements of each column of C_n^w are computed independently of the elements of the other two columns. For example, the derivatives of the elements in the third column depend only on the elements of the third column and the angular velocity. This leads to the interesting conclusion that, if we are concerned only about aircraft dynamics and not about display of the Euler angles or determination of position, we need integrate only three of the direction cosine elements, those in the third column, because only those are needed to obtain the wind-axis force equations. (Of course, we should still need a constraint equation to ensure that the magnitude of the vector represented by the three elements in the third column is unity.)

If we solve for all nine direction cosines by integration, we have six constraint equations, all of which utilize properties of the three-by-three orthogonal transformation matrix. Let $\underline{c}_1$, $\underline{c}_2$, $\underline{c}_3$ be vectors representing the elements in the columns of C_n^w.

$$C_n^w = [\, \underline{c}_1 \quad \underline{c}_2 \quad \underline{c}_3 \,] \tag{5.8-11}$$

Then an independent set of six scalar constraint equations is given by

$$\underline{c}_3 \cdot \underline{c}_3 = 1 \tag{5.8-12}$$

$$\underline{c}_2 \cdot \underline{c}_2 = 1 \tag{5.8-13}$$

$$\underline{c}_2 \cdot \underline{c}_3 = 0 \tag{5.8-14}$$

$$\underline{c}_2 \times \underline{c}_3 = \underline{c}_1 \tag{5.8-15}$$

The cross-product equation represents three scalar equations.

In the implementation of the direction cosine method in the flight simulator, we adapt a procedure suggested by A.C. Robinson[1]. Only six integrations are performed. We integrate the elements of the third column, then integrate the elements of the second column, and solve for the elements of the first column algebraically. Equations (5.8-12), (5.8-13), and (5.8-14) are used as constraints, and Equation (5.8-15) is used to obtain $\underline{c}_1$. Specifically, the procedure is as follows:

1. Integrate $\dot{\underline{c}}_3$ to get the approximate components of $\underline{c}_3$, approximate because of errors inherent in integration. A tilde ($\sim$) above an element or a vector indicates an approximation to the true value of that element or vector.

$$\tilde{c}_{13} = \int(R'c_{23} - Q'c_{33})dt \tag{5.8-16}$$

$$\tilde{c}_{23} = \int(-R'c_{13} + P'c_{33})dt \tag{5.8-17}$$

$$\tilde{c}_{33} = \int (Q' c_{13} - P' c_{23}) dt \tag{5.8-18}$$

2. Correct the elements by normalizing $\underline{c}_3$. We obtain the corrected elements by dividing the approximate elements by the magnitude of the approximate vector.

$$\tilde{\underline{c}}_3 \cdot \tilde{\underline{c}}_3 = \tilde{c}_{13}^2 + \tilde{c}_{23}^2 + \tilde{c}_{33}^2 = 1 + \varepsilon \tag{5.8-19}$$

where ε is a small quantity. Let a caret ($\hat{}$) above an element indicate the corrected value of that element.

$$\hat{c}_{13} = \frac{\tilde{c}_{13}}{(\tilde{\underline{c}}_3 \cdot \tilde{\underline{c}}_3)^{1/2}} = \frac{\tilde{c}_{13}}{(1 + \varepsilon)^{1/2}} \tag{5.8-20}$$

To first order in ε,

$$\hat{c}_{13} = \tilde{c}_{13} \left(1 - \tfrac{1}{2} \varepsilon\right) = \tfrac{1}{2} \left(3 - \tilde{\underline{c}}_3 \cdot \tilde{\underline{c}}_3\right) \tilde{c}_{13} \tag{5.8-21}$$

Similarly,

$$\hat{c}_{23} = \tfrac{1}{2} \left(3 - \tilde{\underline{c}}_3 \cdot \tilde{\underline{c}}_3\right) \tilde{c}_{23} \tag{5.8-22}$$

$$\hat{c}_{33} = \tfrac{1}{2} \left(3 - \tilde{\underline{c}}_3 \cdot \tilde{\underline{c}}_3\right) \tilde{c}_{33} \tag{5.8-23}$$

3. Integrate $\dot{\underline{c}}_2$ to get the approximate components of $\underline{c}_2$.

$$\tilde{c}_{12} = \int(R'c_{22} - Q'c_{32})dt \tag{5.8-24}$$

$$\tilde{c}_{22} = \int(-R'c_{12} + P'c_{32})dt \tag{5.8-25}$$

$$\tilde{c}_{32} = \int(Q'c_{12} - P'c_{22})dt \tag{5.8-26}$$

4. Correct the approximate elements of $\underline{c}_2$ by orthogonalizing with respect to $\underline{c}_3$ and normalizing. Orthogonalization is accomplished by retaining only that portion of $\tilde{\underline{c}}_2$ that is perpendicular to $\hat{\underline{c}}_3$. The part of $\tilde{\underline{c}}_2$ parallel to $\hat{\underline{c}}_3$ is given by $(\tilde{\underline{c}}_2 \cdot \hat{\underline{c}}_3)\hat{\underline{c}}_3$; this part is to be eliminated. Normalization is accomplished as in Step 2.

$$\hat{c}_{12} = \frac{1}{2}(3 - \tilde{\underline{c}}_2 \cdot \tilde{\underline{c}}_2)[\tilde{c}_{12} - (\tilde{\underline{c}}_2 \cdot \hat{\underline{c}}_3)\hat{c}_{13}] \tag{5.8-27}$$

$$\hat{c}_{22} = \frac{1}{2}(3 - \tilde{\underline{c}}_2 \cdot \tilde{\underline{c}}_2)[\tilde{c}_{22} - (\tilde{\underline{c}}_2 \cdot \hat{\underline{c}}_3)\hat{c}_{23}] \tag{5.8-28}$$

$$\hat{c}_{32} = \frac{1}{2}(3 - \tilde{\underline{c}}_2 \cdot \tilde{\underline{c}}_2)[\tilde{c}_{32} - (\tilde{\underline{c}}_2 \cdot \hat{\underline{c}}_3)\hat{c}_{33}] \tag{5.8-29}$$

5. $\underline{c}_1$ is determined from Equation (5.8-15).

$$\hat{c}_{11} = \hat{c}_{22}\hat{c}_{33} - \hat{c}_{23}\hat{c}_{32} \tag{5.8-30}$$

$$\hat{c}_{21} = \hat{c}_{32}\,\hat{c}_{13} - \hat{c}_{12}\,\hat{c}_{33} \tag{5.8-31}$$

$$\hat{c}_{31} = \hat{c}_{12}\,\hat{c}_{23} - \hat{c}_{13}\,\hat{c}_{22} \tag{5.8-32}$$

Implementation of these equations has been carried out on the digital computer at a sample rate of fifty per second.

5.9 Position Determination

Position is determined by integrating the components of velocity in the navigation frame.

$$\underline{V}^n = C_w^{\,n}\,\underline{V}^w = (C_n^{\,w})^T\,\underline{V}^w = \begin{bmatrix} c_{11} \\ c_{12} \\ c_{13} \end{bmatrix} V \tag{5.9-1}$$

The first two integrals give distance traveled north and east of a specified starting point. The third equation gives $\dot{z}^n$, which is the negative of the rate of climb $\dot{h}$; the integral of the third equation gives decrease in altitude.

If the angle of inclination of the velocity vector to the horizontal is designated γ (positive when the airplane is climbing), then

$$\sin\gamma = \frac{\dot{h}}{V} = -\frac{\dot{z}^n}{V} = -\frac{c_{13}V}{V} = -c_{13} \tag{5.9-2}$$

5.10 Computation of Non-Gravitational Forces and Moments

The non-gravitational forces are computed in terms of non-dimensional coefficients. The coefficients are the lift coefficient C_L, the drag coefficient C_D, and the side-force coefficient C_y; they are related to the components of $\underline{F}^S$ in Equation (5.6-3) as follows:

$$\underline{F}^S = \begin{bmatrix} X^S \\ Y^S \\ Z^S \end{bmatrix} = \begin{bmatrix} -C_D \\ C_y \\ -C_L \end{bmatrix} qS \qquad (5.10\text{-}1)$$

where

$$q = \frac{1}{2} \rho V^2 \qquad (5.10\text{-}2)$$

q is the dynamic pressure, S is the wing area of the aircraft, and ρ is the air density.

In a corresponding manner the components of the external moment $\underline{M}_C{}^b$ are computed in terms of non-dimensional coefficients. The coefficients are the rolling moment coefficient C_ℓ, the pitching moment coefficient C_m, and the yawing moment coefficient C_n.

$$\underline{M}_C{}^b = \begin{bmatrix} C_\ell\ b \\ C_m\ c \\ C_n\ b \end{bmatrix} qS \qquad (5.10\text{-}3)$$

b and c are the span and the mean aerodynamic chord, respectively, of the aircraft wing.

The data for the coefficients are assumed to include the direct effects of thrust as well as all aerodynamic effects. The data are normally obtained from wind tunnel testing of powered models.

The computation of the coefficients for the aircraft simulator is nonlinear. The computation of C_L serves to illustrate the procedure that is used. First the available C_L information is preprocessed by running it through a multi-variable digital regression program which determines, on a least-squares basis, the coefficients of a series expression for $C_{L_{static}}$ as a function of angle of attack α, Mach number M, flap deflection δ_f, thrust T, stabilizer setting s, elevator deflection δ_e, sideslip β, and any other static variables for which data are available.

$$C_{L_{static}} = C_L\ (\alpha, M, \delta_f, T, s, \delta_e, \beta, \ldots) \qquad (5.10\text{-}4)$$

Based on the equation for $C_{L_{static}}$, series expressions are determined analytically for the partial derivatives $\frac{\partial C_L}{\partial \alpha}$ and $\frac{\partial C_L}{\partial \delta_e}$. Also, the regression program is used to obtain series for the dynamic derivatives $\frac{\partial C_L}{\partial\left(\frac{Qc}{2V}\right)}$ and $\frac{\partial C_L}{\partial\left(\frac{\dot{\alpha}c}{2V}\right)}$ as functions of all relevant variables.

The equations for $C_{L_{static}}$ and the four partial derivatives are stored in the digital simulator program. In a simulated flight, values of these quantities are computed digitally at some designated rate (five times per second in the present simulation) as functions

of the up-dated independent variables. Information transmitted from the digital computer to the analog computer includes the four partial derivatives and C_{L_o}, which is defined as follows:

$$C_{L_o} = C_{L_{static}} - \frac{\partial C_L}{\partial \alpha}\alpha - \frac{\partial C_L}{\partial \delta_e}\delta_e \qquad (5.10\text{-}5)$$

C_{L_o} includes the effect on C_L of such variables as flap deflection and stabilizer setting. It is the total C_L that would exist if α, δ_e, Q, and $\dot{\alpha}$ were all zero and if all the partial derivatives were "frozen" at their instantaneous values.

The actual digital-to-analog (D-A) signals, properly scaled, are the following:

(1) $\frac{\rho VS}{2m} \cdot \frac{\partial C_L}{\partial \alpha}$

(2) $\frac{\rho VS}{2m} \cdot \frac{\partial C_L}{\partial \delta_e}$

(3) $\frac{\rho S}{2m} \cdot \frac{c}{2} \cdot \frac{\partial C_L}{\partial \left(\frac{Qc}{2V}\right)}$

(4) $\frac{\rho S}{2m} \cdot \frac{c}{2} \cdot \frac{\partial C_L}{\partial \left(\frac{\dot{\alpha}c}{2V}\right)}$

(5) $\frac{\rho VS}{2m} C_{L_o}$

In the analog computer the first signal is multiplied by α, the second by δ_e, the third by Q, and the fourth by $\dot{\alpha}$. The four products are added to the fifth signal to produce a voltage that is proportional to $\frac{\rho VS}{2m} C_L$. Here C_L is the total C_L, including both static and dynamic effects. From Equations (5.10-1) and (5.10-2),

$$\frac{\rho VS}{2m} C_L = - \frac{Z^S}{mV} \tag{5.10-6}$$

This quantity is one of those used in the determination of $\dot{\alpha}$. (See Equation (5.6-39).)

The process of computing C_L digitally, separating it into several component parts, then re-assembling the parts in the analog computer, will appear, at first reading, to be unnecessarily circuitous. The procedure is used to get improved dynamic response in a nonlinear simulation. This subject is discussed in more detail in Section 5.11.

The other five non-dimensional coefficients are computed in similar fashion. The equations appear in the summary of Section 5.13.

5.11 Allocation of Computation between Analog and Digital Computers

The hybrid computer facility used for flight simulation consists of a Xerox Data Systems 9300 digital computer and two Beckman 2200 analog computers. The two types of computer complement each other, the digital being used primarily for nonlinear function generation

and the analog primarily to obtain real-time dynamic performance. The factors that were considered in determining how a specific computation should be performed are given below.

1. The digital computer has neither the speed (14 μsec. for floating point add, 12 μsec. for floating point multiply) nor the memory capacity (32,000 words) to perform all of the required real-time computation at an acceptably high sample rate (in the range of 20 to 100 samples per second).

2. To avoid excessive set-up time and special handling, the generation of arbitrary nonlinear functions is not performed on the analog computer.

3. The analog computer is preferred for the integration of the equations relating to aircraft dynamics.

4. Analog multiplication of two variables is permissible but is to be used sparingly because it is relatively inaccurate, especially when the product is at or close to zero, and because the number of analog multipliers available is limited.

5. The number of analog-to-digital (A-D) and digital-to-analog (D-A) lines is limited.

6. The sine and cosine of a variable can be generated on the analog computer, but the number of sine-cosine function generators is limited.

With these considerations in mind, it was decided to make one of the analog computer consoles a "standard" computer and the other

a "variable" computer. The standard console is designed such that no changes in the analog patching should be required in going from the simulation of one aircraft type of a given class to another aircraft type in the same class. To achieve this design objective, great care must be exercised in scaling, and a certain amount of redundancy must be provided to account for effects that may exist in one aircraft type and not another.

The integration of the force equations and the moment equations is done in the standard analog console. The class of aircraft for which the present patchboard is designed is the large subsonic transport. The original design was for the KC-135 airplane, but it has also been used recently for a simulation of the atmospheric cruise phase of the flight of the space shuttle vehicle.

The second analog console, the variable one, is used for simulation of the aircraft control systems and displays and any special effects that are desired.

The patching of the standard console can remain fixed despite the fact that the aerodynamic coefficients change from one aircraft type to another, because the coefficients are computed digitally and the scaling in the digital computer can be adjusted to maintain a fixed schedule of scale factors in the analog computer.

We shall use the C_L example of the last section to illustrate the procedure. The five signals mentioned in that section are available in the standard console on D-A lines. In addition, α,

$\dot{\alpha}$, and Q signals are generated in the standard console, and a signal representing δ_e is brought over to the standard console from the variable console. The computation that is then performed in the standard console is

$$\frac{\rho VS}{2m}\left[C_{L_o} + \frac{\partial C_L}{\partial \alpha}\alpha + \frac{\partial C_L}{\partial \delta_e}\delta_e + \frac{\partial C_L}{\partial\left(\frac{Qc}{2V}\right)}\cdot\frac{Qc}{2V} + \frac{\partial C_L}{\partial\left(\frac{\dot{\alpha}c}{2V}\right)}\cdot\frac{\dot{\alpha}c}{2V}\right]$$

$$= \frac{\rho VS}{2m}C_L = -\frac{Z^s}{mV} \qquad (5.11\text{-}1)$$

The digital signals remain fixed during a sample period (one fifth of a second), but the analog signals α, $\dot{\alpha}$, Q, and δ_e vary continuously; hence the computed C_L is varying continuously.

In effect, the hybrid computing facility is solving, during each sample period, a quasi-linear problem with fixed initial conditions and constant values of the derivatives. At the end of the sample period the initial conditions and the derivatives are up-dated, and the solution of a new quasi-linear problem is begun. Implicit in this method of computation is the assumption that the digital inputs (initial conditions and derivatives) change only slightly during a sample period, so that there will be no significant jumps in the dependent variables, such as C_L, when the up-dated digital values are introduced.

It is felt that this method of computation combines the advantages of flexibility in the nonlinear function generation and good real-time

dynamic performance. The dynamic performance is effectively independent of the digital sample rate.

Inasmuch as the integration of angular velocity to determine attitude also requires good dynamic response, it would be desirable to perform this computation on the analog computer. However, the number of analog multipliers that would be required for the implementation of the direction cosine formulation is formidable. Consequently, it was decided to use digital computation at a relatively high sample rate. A sample rate of fifty per second was chosen. This rate is at least an order of magnitude greater than any of the aircraft rates being simulated. The digital solution requires three to four milliseconds in each twenty-millisecond sample period.

Trapezoidal integration is used to solve for the elements of matrix C_n^W. To illustrate the method, consider the integration of $\dot{c}_{13}$ to obtain c_{13}. From Equation (5.8-10),

$$\dot{c}_{13} = R'c_{23} - Q'c_{33} \tag{5.11-2}$$

At the start of a sample period, we have the "old" values of c_{13}, c_{23}, c_{33} and $\dot{c}_{13}$, and from the analog computer we get up-dated ("new") values of Q' and R'. With subscripts o and n representing old and new, respectively, we have

$$\dot{c}_{13_n} = R'_n c_{23_o} - Q'_n c_{33_o} \tag{5.11-3}$$

$$\tilde{c}_{13_n} = \frac{1}{2} (\dot{c}_{13_o} + \dot{c}_{13_n}) \Delta t + \hat{c}_{13_o} \qquad (5.11\text{-}4)$$

Since the time interval Δt is 0.02 second,

$$\tilde{c}_{13_n} = 0.01 (\dot{c}_{13_o} + \dot{c}_{13_n}) + \hat{c}_{13_o} \qquad (5.11\text{-}5)$$

As in Section 5.8, the tilde denotes the approximate value, and the caret denotes the corrected value.

After all the direction cosines have been computed, the elements in the third column of the matrix are multiplied by g to get the gravity components needed for solution of the force equations. The elements in the first row of the matrix are multiplied by V and then integrated to obtain geographical position and altitude.

5.12 Signals for Recording and Display

Listed below are the signals that are made available for recording and/or display. The source of each signal is indicated.

1. V, β, and α are obtained from integration of the force equations in the standard analog console.

2. P, Q, and R are obtained from integration of the moment equations in the standard analog console.

3. ϕ, θ, and ψ are obtained from the direction cosines generated in the digital computer.

4. Control deflections are obtained from the variable analog console.

5. Simulated accelerometer readings, under the assumption that the body-mounted accelerometer package is located at the aircraft center of mass, are obtained from the digital computer.

6. Rate of climb, altitude, and geographical position are obtained from the digital computer.

The determination of Euler angles ϕ, θ, ψ from direction cosines requires explanation. The direction cosine matrix obtained by integration is $C_n^{\ w}$, but the direction cosine matrix needed to determine the angles is $C_n^{\ b}$. To get $C_n^{\ b}$ from $C_n^{\ w}$, we pre-multiply Equation (5.4-8) by $(C_b^{\ w})^T$.

$$C_n^{\ b} = (C_b^{\ w})^T \, C_n^{\ w} \tag{5.12-1}$$

$C_b^{\ w}$ depends only on α and β; signals representing both these angles are available in the digital computer on A-D lines. Therefore, the elements of $C_n^{\ b}$ can be obtained. Let $(C_n^{\ b})_{ij}$ represent the element in the i-th row and j-th column of $C_n^{\ b}$. From Equation (5.4-4),

$$\sin \theta = - (C_n^{\ b})_{13} \tag{5.12-2}$$

Since $-\frac{\pi}{2} \leq \theta \leq +\frac{\pi}{2}$, this equation can be solved for a unique value of θ. The sign of cos θ is always positive.

$$\cos\theta = + \left[(C_n^b)_{23}^2 + (C_n^b)_{33}^2 \right]^{1/2} \tag{5.12-3}$$

Then ϕ can be obtained from the elements in the second and third rows of the third column.

$$\sin\phi = \frac{(C_n^b)_{23}}{\cos\theta} \tag{5.12-4}$$

$$\cos\phi = \frac{(C_n^b)_{33}}{\cos\theta} \tag{5.12-5}$$

ψ is obtained from the elements in the first row.

$$\sin\psi = \frac{(C_n^b)_{12}}{\cos\theta} \tag{5.12-6}$$

$$\cos\psi = \frac{(C_n^b)_{11}}{\cos\theta} \tag{5.12-7}$$

Both ϕ and ψ lie in the range 0 to 2π radians. These equations can be solved for ϕ and ψ uniquely as long as $\cos\theta \neq 0$. When $\cos\theta = 0$, we have a singularity (the airplane is flying either "straight up" or "straight down"), and ϕ and ψ are indeterminate.

The body-mounted accelerometers indicate the body-frame components of the acceleration due to the non-gravitational force $\underline{F}$. Let $\underline{a}^b$ represent the vector comprised of the three accelerometer readings.

$$\underline{a}^b = \frac{1}{m}\underline{F}^b = \frac{1}{m} C_w^b \underline{F}^w = \frac{1}{m} (C_b^w)^T \underline{F}^w \tag{5.12-8}$$

From Equation (5.6-32),

$$\frac{1}{m}\underline{F}^{w} = p\,\underline{V}^{w} - C_n{}^{w}\,\underline{g}^{n} + \underline{\omega}_{nw}{}^{w} \times \underline{V}^{w} \tag{5.12-9}$$

$$\frac{1}{m}\begin{vmatrix} X^{w} \\ Y^{w} \\ Z^{w} \end{vmatrix} = \begin{vmatrix} \dot{V} - c_{13}g \\ -c_{23}g + R'V \\ -c_{33}g - Q'V \end{vmatrix} \tag{5.12-10}$$

Signals available in the digital computer on A-D lines include $\frac{1}{m}X^{w}$, V, α, β, Q', and R'. The gravity components $c_{23}g$ and $c_{33}g$ are generated digitally. Therefore, $\underline{a}^{b}$ can be computed and read out from the digital computer.

$$\underline{a}^{b} = (C_b{}^{w})^{T} \begin{bmatrix} \frac{1}{m}X^{w} \\ -c_{23}g + R'V \\ -c_{33}g - Q'V \end{bmatrix} \tag{5.12-11}$$

where the elements of $C_b{}^{w}$ are given in Equation (5.4-7)

The signals representing control deflections are computed from the autopilot control loop equations discussed in previous chapters.

If the user desires, other computed signals can be brought out and displayed in addition to, or instead of, the ones listed.

5.13 Ranges of the Major Variables

The inequalities below define the ranges of the major variables in the flight computer.

$$0 < V < 1{,}000 \text{ ft./sec.}$$
$$0 \leq |\dot{V}| < 200 \text{ ft./sec.}^2$$
$$0 \leq |\beta| < 1 \text{ radian}$$
$$0 \leq |\dot{\beta}| < 1 \text{ rad./sec.}$$
$$0 \leq |\alpha| < 1 \text{ radian}$$
$$0 \leq |\dot{\alpha}| < 1 \text{ rad./sec.}$$
$$0 \leq |P| < 1 \text{ rad./sec.}$$
$$0 \leq |\dot{P}| < 10 \text{ rad./sec.}^2$$
$$0 \leq |Q| < 1 \text{ rad./sec.}$$
$$0 \leq |\dot{Q}| < 5 \text{ rad./sec.}^2$$
$$0 \leq |R| < 1 \text{ rad./sec.}$$
$$0 \leq |\dot{R}| < 1 \text{ rad./sec.}^2$$

5.14 Summary of Equations

In this final section we present the simulator equations as they are actually formulated in the hybrid computer. In some instances the sequence of the computations differs from that which is presented in the previous sections. The reason for the differences is that the primary objective in the writing is clarity of presentation, while the primary objective in the implementation is computer efficiency and accuracy.

The force equations solved in the standard analog console are

A. Airspeed determination

$$\frac{T}{mV} - \frac{\rho VS}{2m}\left[C_{D_o} + \frac{\partial C_D}{\partial \alpha}\alpha + \frac{\partial C_D}{\partial \beta}\beta\right] = \frac{X^S}{mV} \qquad (5.14\text{-}1)$$

$$\left[\frac{X^S}{mV}\cos\beta + \frac{Y^S}{mV}\sin\beta\right] V = \frac{X^W}{m} \qquad (5.14\text{-}2)$$

$$\frac{X^W}{m} + c_{13}g = \dot{V} \qquad (5.14\text{-}3)$$

$$\int \dot{V}\, dt + V_I = V \qquad (5.14\text{-}4)$$

Subscript I denotes the initial value. Signals proportional to $\frac{X^W}{m}$ and V are transmitted to the digital computer. From the digital computer we obtain signals proportional to $\left(\frac{T}{mV} - \frac{\rho VS}{2m} C_{D_o}\right)$, $\frac{\rho VS}{2m}\frac{\partial C_D}{\partial \alpha}$, and $\frac{\rho VS}{2m}\frac{\partial C_D}{\partial \beta}$.

B. Sideslip determination

$$\frac{\rho VS}{2m}\left[C_{y_o} + \frac{\partial C_y}{\partial \beta}\beta + \frac{\partial C_y}{\partial \delta_r}\delta_r + \frac{\partial C_y}{\partial \delta_a}\delta_a\right] = \frac{Y^S}{mV} \qquad (5.14\text{-}5)$$

$$-\frac{X^S}{mV}\sin\beta + \frac{Y^S}{mV}\cos\beta + \frac{1}{V}c_{23}g = R' \qquad (5.14\text{-}6)$$

$$R' + P\sin\alpha - R\cos\alpha = \dot{\beta} \qquad (5.14\text{-}7)$$

$$\int \dot{\beta}\, dt + \beta_I = \beta \qquad (5.14\text{-}8)$$

Signals proportional to R' and β are transmitted to the digital computer. From the digital computer we obtain signals proprotional to $\frac{\rho VS}{2m} C_{y_o}$, $\frac{\rho VS}{2m} \frac{\partial C_y}{\partial \beta}$, $\frac{\rho VS}{2m} \frac{\partial C_y}{\partial \delta_r}$, and $\frac{\rho VS}{2m} \frac{\partial C_y}{\partial \delta_a}$.

C. Angle of attack determination

$$\frac{\rho VS}{2m}\left[C_{L_o} + \frac{\partial C_L}{\partial \alpha}\alpha + \frac{\partial C_L}{\partial \delta_e}\delta_e + \frac{\partial C_L}{\partial\left(\frac{Qc}{2V}\right)} \cdot \frac{Qc}{2V} + \frac{\partial C_L}{\partial\left(\frac{\dot{\alpha}c}{2V}\right)} \cdot \frac{\dot{\alpha}c}{2V}\right] - \frac{1}{V} c_{33} g = Q' \qquad (5.14\text{-}9)$$

$$\frac{1}{\cos \beta}\left[Q' + (P \cos \alpha + R \sin \alpha) \sin \beta\right] = Q - \dot{\alpha} \qquad (5.14\text{-}10)$$

$$Q - (Q - \dot{\alpha}) = \dot{\alpha} \qquad (5.14\text{-}11)$$

$$\int \dot{\alpha}\, dt + \alpha_I = \alpha \qquad (5.14\text{-}12)$$

Signals proportional to Q' and α are transmitted to the digital computer. From the digital computer we obtain signals proportional to $\frac{\rho VS}{2m} C_{L_o}$, $\frac{\rho VS}{2m} \frac{\partial C_L}{\partial \alpha}$, $\frac{\rho VS}{2m} \frac{\partial C_L}{\partial \delta_e}$, $\frac{\rho Sc}{4m} \frac{\partial C_L}{\partial\left(\frac{Qc}{2V}\right)}$, and $\frac{\rho Sc}{4m} \frac{\partial C_L}{\partial\left(\frac{\dot{\alpha}c}{2V}\right)}$.

The moment equations, which are also solved in the standard analog console, are

A. Roll rate determination

$$\frac{\rho VSb}{2I_{xx}}\left[C_{\ell_o}+\frac{\partial C_\ell}{\partial\beta}\beta+\frac{\partial C_\ell}{\partial\delta_a}\delta_a+\frac{\partial C_\ell}{\partial\delta_s}\delta_s+\frac{\partial C_\ell}{\partial\delta_r}\delta_r+\frac{\partial C_\ell}{\partial\delta_{a_{tab}}}\delta_{a_{tab}}+\frac{\partial C_\ell}{\partial\left(\frac{Pb}{2V}\right)}\cdot\frac{Pb}{2V}+\frac{\partial C_\ell}{\partial\left(\frac{Rb}{2V}\right)}\cdot\frac{Rb}{2V}\right]V=\frac{L}{I_{xx}} \tag{5.14-13}$$

$$\frac{1}{I_{xx}}\left[L+I_{xz}\dot{R}+I_{xz}PQ+(I_{yy}-I_{zz})QR\right]=\dot{P} \tag{5.14-14}$$

$$\int\dot{P}\,dt+P_I=P \tag{5.14-15}$$

δ_s is spoiler deflection, and $\delta_{a_{tab}}$ is aileron tab deflection. A signal proportional to P is transmitted to the digital computer. From the digital computer we obtain signals proportional to $\frac{\rho VSb}{2I_{xx}}C_{\ell_o}$, $\frac{\rho VSb}{2I_{xx}}\frac{\partial C_\ell}{\partial\beta}$, $\frac{\rho VSb}{2I_{xx}}\frac{\partial C_\ell}{\partial\delta_a}$, $\frac{\rho VSb}{2I_{xx}}\frac{\partial C_\ell}{\partial\delta_s}$, $\frac{\rho VSb}{2I_{xx}}\frac{\partial C_\ell}{\partial\delta_r}$, $\frac{\rho VSb}{2I_{xx}}\frac{\partial C_\ell}{\partial\delta_{a_{tab}}}$, $\frac{\rho Sb^2}{4I_{xx}}\frac{\partial C_\ell}{\partial\left(\frac{Pb}{2V}\right)}$, and $\frac{\rho Sb^2}{4I_{xx}}\frac{\partial C_\ell}{\partial\left(\frac{Rb}{2V}\right)}$.

B. Pitch rate determination

$$\frac{\rho VSc}{2I_{yy}}\left[C_{m_o}+\frac{\partial C_m}{\partial\alpha}\alpha+\frac{\partial C_m}{\partial\delta_e}\delta_e+\frac{\partial C_m}{\partial\delta_{e_{tab}}}\delta_{e_{tab}}+\frac{\partial C_m}{\partial\left(\frac{Qc}{2V}\right)}\cdot\frac{Qc}{2V}+\frac{\partial C_m}{\partial\left(\frac{\dot{\alpha}c}{2V}\right)}\cdot\frac{\dot{\alpha}c}{2V}\right]V=\frac{M}{I_{yy}} \tag{5.14-16}$$

$$\frac{1}{I_{yy}}\left[M + I_{xz}R^2 - I_{xz}P^2 + (I_{zz} - I_{xx})RP\right] = \dot{Q} \qquad (5.14\text{-}17)$$

$$\int \dot{Q}\, dt + Q_I = Q \qquad (5.14\text{-}18)$$

$\delta_{e_{tab}}$ is elevator tab deflection. A signal proportional to Q is transmitted to the digital computer. From the digital computer we obtain signals proportional to $\frac{\rho VSc}{2I_{yy}} C_{m_o}$, $\frac{\rho VSc}{2I_{yy}} \frac{\partial C_m}{\partial \alpha}$, $\frac{\rho VSc}{2I_{yy}} \frac{\partial C_m}{\partial \delta_e}$,

$\frac{\rho VSc}{2I_{yy}} \frac{\partial C_m}{\partial \delta_{e_{tab}}}$, $\frac{\rho Sc^2}{4I_{yy}} \frac{\partial C_m}{\partial \left(\frac{Qc}{2V}\right)}$, and $\frac{\rho Sc^2}{4I_{yy}} \frac{\partial C_m}{\partial \left(\frac{\dot{\alpha}c}{2V}\right)}$.

C. Yaw rate determination

$$\frac{\rho VSb}{2I_{zz}}\left[C_{n_o} + \frac{\partial C_n}{\partial \beta}\beta + \frac{\partial C_n}{\partial \delta_r}\delta_r + \frac{\partial C_n}{\partial \delta_a}\delta_a + \frac{\partial C_n}{\partial \delta_s}\delta_s + \frac{\partial C_n}{\partial \delta_{r_{tab}}}\delta_{r_{tab}} + \frac{\partial C_n}{\partial \left(\frac{Rb}{2V}\right)} \cdot \frac{Rb}{2V} + \frac{\partial C_n}{\partial \left(\frac{Pb}{2V}\right)} \cdot \frac{Pb}{2V}\right] V = \frac{N}{I_{zz}} \qquad (5.14\text{-}19)$$

$$\frac{1}{I_{zz}}\left[N + I_{xz}\dot{P} - I_{xz}QR - (I_{yy} - I_{xx})PQ\right] = \dot{R} \qquad (5.14\text{-}20)$$

$$\int \dot{R}\, dt + R_I = R \qquad (5.14\text{-}21)$$

$\delta_{r_{tab}}$ is rudder tab deflection. A signal proportional to R is transmitted to the digital computer. From the digital computer we obtain signals proportional to $\frac{\rho VSb}{2I_{zz}} C_{n_o}$, $\frac{\rho VSb}{2I_{zz}} \frac{\partial C_n}{\partial \beta}$, $\frac{\rho VSb}{2I_{zz}} \frac{\partial C_n}{\partial \delta_r}$, $\frac{\rho VSb}{2I_{zz}} \frac{\partial C_n}{\partial \delta_a}$,

$\frac{\rho VSb}{2I_{zz}} \frac{\partial C_n}{\partial \delta_s}$, $\frac{\rho VSb}{2I_{zz}} \frac{\partial C_n}{\partial \delta_{r_{tab}}}$, $\frac{\rho Sb^2}{4I_{zz}} \frac{\partial C_n}{\partial \left(\frac{Rb}{2V}\right)}$, and $\frac{\rho Sb^2}{4I_{zz}} \frac{\partial C_n}{\partial \left(\frac{Pb}{2V}\right)}$.

The non-dimensional aerodynamic coefficients C_D, C_y, C_L, C_ℓ, C_m, and C_n are computed digitally. The coefficients are, in general, non-linear functions of several variables. Either of two methods may be employed to generate the coefficients. The first method, which was mentioned in Section 5.10, involves the use of a regression analysis to pre-process the available data and obtain an analytical expression, usually in the form of a power series, for each of the coefficients. From these analytic expressions we get equations which are stored in the digital computer and are used to solve for initial conditions and derivatives as indicated in Section 10. The second method of generating the coefficients is by means of a table look-up procedure. The choice of method depends largely on the form of the available data. For the KC-135 simulation the regression analysis was used. Below we indicate the nature of the output of the regression runs, and also the equations used in the digital simulation.

Regression analysis results in the following functions:

$$C_D = C_D\ (\ \alpha,\ M,\ \delta_f,\ T,\ s,\ \delta_{SB},\ \delta_a,\ \delta_s,\ \beta,\ \ldots) \tag{5.14-22}$$

$$C_y = C_y\ (\ \beta,\ M,\ \delta_r,\ \delta_f,\ T,\ \alpha,\ \ldots\ ) \tag{5.14-23}$$

$$C_{L_{static}} = C_L\ (\ \alpha,\ M,\ \delta_f,\ T,\ s,\ \delta_e,\ \beta,\ \ldots) \tag{5.14-24}$$

$$C_{\ell_{static}} = C_\ell\ (\ \beta,\ M, \delta_f,\ T,\ \delta_a,\ \delta_s,\ \delta_r,\ \delta_{a_{tab}},\ \alpha,\ \ldots) \tag{5.14-25}$$

$$C_{m_{static}} = C_m\ (\ \alpha,\ M,\ \delta_f,\ T,\ s,\ \delta_e,\ \delta_{e_{tab}},\ \beta,\ \ldots) \tag{5.14-26}$$

$$C_{n_{static}} = C_n\ (\ \beta,\ M,\ \delta_f,\ T,\ \delta_r,\ \delta_a,\ \delta_s,\ \delta_{r_{tab}},\ \alpha,\ \ldots) \tag{5.14-27}$$

$$\frac{\partial C_L}{\partial\left[\frac{Qc}{2V}\right]} = f_1\ (\ \alpha,\ M,\ \delta_f,\ \ldots) \tag{5.14-28}$$

$$\frac{\partial C_L}{\partial\left[\frac{\dot{\alpha}c}{2V}\right]} = f_2\ (\ \alpha,\ M,\ \delta_f,\ \ldots) \tag{5.14-29}$$

$$\frac{\partial C_L}{\partial\left[\frac{Pb}{2V}\right]} = f_3\ (\alpha,\ M,\ \delta_f,\ \beta,\ \ldots) \tag{5.14-30}$$

$$\frac{\partial C_\ell}{\partial\left[\frac{Rb}{2V}\right]} = f_4\ (\ \alpha,\ M,\ \delta_f,\ \beta,\ \ldots) \tag{5.14-31}$$

$$\frac{\partial C_m}{\partial\left(\frac{Qc}{2V}\right)} = f_5 \quad (\alpha, M, \delta_f, \ldots) \tag{5.14-32}$$

$$\frac{\partial C_m}{\partial\left(\frac{\dot{\alpha}c}{2V}\right)} = f_6 \quad (\alpha, M, \delta_f, \ldots) \tag{5.14-33}$$

$$\frac{\partial C_n}{\partial\left(\frac{Rb}{2V}\right)} = f_7 \quad (\alpha, M, \delta_f, \beta, \ldots) \tag{5.14-34}$$

$$\frac{\partial C_n}{\partial\left(\frac{Pb}{2V}\right)} = f_8 \quad (\alpha, M, \delta_f, \beta, \ldots) \tag{5.14-35}$$

In Equation 5.14-22), δ_{SB} is speed brake deflection. $f_1,\ldots\ldots,f_8$ in Equations (5.14-28) to (5.14-35) refer to functions of the designated independent variables.

From these functions we get analytic expressions for the initial condition functions that are stored as part of the digital simulator program.

$$C_{D_o} = C_D - \frac{\partial C_D}{\partial \alpha}\alpha - \frac{\partial C_D}{\partial \beta}\beta \tag{5.14-36}$$

$$C_{y_o} = C_y - \frac{\partial C_y}{\partial \beta}\beta - \frac{\partial C_y}{\partial \delta_r}\delta_r - \frac{\partial C_y}{\partial \delta_a}\delta_a \tag{5.14-37}$$

$$C_{L_o} = C_{L_{static}} - \frac{\partial C_L}{\partial \alpha}\alpha - \frac{\partial C_L}{\partial \delta_e}\delta_e \tag{5.14-38}$$

$$C_{\ell_o} = C_{\ell_{static}} - \frac{\partial C_\ell}{\partial \beta}\beta - \frac{\partial C_\ell}{\partial \delta_a}\delta_a - \frac{\partial C_\ell}{\partial \delta_s}\delta_s - \frac{\partial C_\ell}{\partial \delta_r}\delta_r - \frac{\partial C_\ell}{\partial \delta_{a_{tab}}}\delta_{a_{tab}} \tag{5.14-39}$$

$$C_{m_o} = C_{m_{static}} - \frac{\partial C_m}{\partial \alpha}\alpha - \frac{\partial C_m}{\partial \delta_e}\delta_e - \frac{\partial C_m}{\partial \delta_{e_{tab}}}\delta_{e_{tab}} \qquad (5.14\text{-}40)$$

$$C_{n_o} = C_{n_{static}} - \frac{\partial C_n}{\partial \beta}\beta - \frac{\partial C_n}{\partial \delta_r}\delta_r - \frac{\partial C_n}{\partial \delta_a}\delta_a - \frac{\partial C_n}{\partial \delta_s}\delta_s - \frac{\partial C_n}{\partial \delta_{r_{tab}}}\delta_{r_{tab}} \qquad (5.14\text{-}41)$$

We also obtain analytic expressions for all of the partial derivatives in the above equations. The partial derivatives are stored along with the initial condition functions in the digital simulator program.

At the beginning of each sample period, up-dated values of all the variables on the right-hand sides of Equations (5.14-22) to (5.14-35) are made available in the digital computer. The initial condition functions and derivatives are evaluated digitally, and the results are transmitted to the standard analog console in the form described in the discussion of the force equations and the moment equations at the beginning of this section.

Next we turn to the determination of attitude. The signals needed in the digital computer from the analog computer are those proportional to the angular velocity components P', Q', R'. Q' is computed from Equation (5.14-9), R' from Equation (5.14-6). P' is obtained from the following equation:

$$(P \cos\alpha + R \sin\alpha)\cos\beta + (Q - \dot{\alpha})\sin\beta = P' \qquad (5.14\text{-}42)$$

The first digital computation is that of the new rates of change of six of the nine direction cosines comprising the transformation

matrix C_n^W. With subscripts o and n now being used to designate "old" and "new" data,

$$\dot{c}_{13_n} = R_n' \hat{c}_{23_o} - Q_n' \hat{c}_{33_o} \tag{5.14-43}$$

$$\dot{c}_{23_n} = P_n' \hat{c}_{33_o} - R_n' \hat{c}_{13_o} \tag{5.14-44}$$

$$\dot{c}_{33_n} = Q_n' \hat{c}_{13_o} - P_n' \hat{c}_{23_o} \tag{5.14-45}$$

$$\dot{c}_{12_n} = R_n' \hat{c}_{22_o} - Q_n' \hat{c}_{32_o} \tag{5.14-46}$$

$$\dot{c}_{22_n} = P_n' \hat{c}_{32_o} - R_n' \hat{c}_{12_o} \tag{5.14-47}$$

$$\dot{c}_{32_n} = Q_n' \hat{c}_{12_o} - P_n' \hat{c}_{22_o} \tag{5.14-48}$$

Using the new rates, we integrate digitally to get the "approximate" values of the direction cosines.

$$\tilde{c}_{13_n} = 0.01 \left(\dot{c}_{13_o} + \dot{c}_{13_n}\right) + \hat{c}_{13_o} \tag{5.14-49}$$

$$\tilde{c}_{23_n} = 0.01 \left(\dot{c}_{23_o} + \dot{c}_{23_n}\right) + \hat{c}_{23_o} \tag{5.14-50}$$

$$\tilde{c}_{33_n} = 0.01 \left(\dot{c}_{33_o} + \dot{c}_{33_n}\right) + \hat{c}_{33_o} \tag{5.14-51}$$

$$\tilde{c}_{12_n} = 0.01\ (\dot{c}_{12_o} + \dot{c}_{12_n}) + \hat{c}_{12_o} \tag{5.14-52}$$

$$\tilde{c}_{22_n} = 0.01\ (\dot{c}_{22_o} + \dot{c}_{22_n}) + \hat{c}_{22_o} \tag{5.14-53}$$

$$\tilde{c}_{32_n} = 0.01\ (\dot{c}_{32_o} + \dot{c}_{32_n}) + \hat{c}_{32_o} \tag{5.14-54}$$

The correction factor for the elements in the third column is

$$k_3 = \frac{1}{2}\ (3 - \tilde{c}_{13_n}{}^2 - \tilde{c}_{23_n}{}^2 - \tilde{c}_{33_n}{}^2) \tag{5.14-55}$$

The corrected elements are

$$\hat{c}_{13_n} = k_3\ \tilde{c}_{13_n} \tag{5.14-56}$$

$$\hat{c}_{23_n} = k_3\ \tilde{c}_{23_n} \tag{5.14-57}$$

$$\hat{c}_{33_n} = k_3\ \tilde{c}_{33_n} \tag{5.14-58}$$

To correct the elements in the second column, we need two factors:

$$k_2 = \frac{1}{2}\ (3 - \tilde{c}_{12_n}{}^2 - \tilde{c}_{22_n}{}^2 - \tilde{c}_{32_n}{}^2) \tag{5.14-59}$$

$$d_{23} = \hat{c}_{13_n}\ \tilde{c}_{12_n} + \hat{c}_{23_n}\ \tilde{c}_{22_n} + \hat{c}_{33_n}\ \tilde{c}_{23_n} \tag{5.14-60}$$

Then the corrected elements are

$$\hat{c}_{12_n} = k_2 \left(\tilde{c}_{12_n} - d_{23}\, \hat{c}_{13_n}\right) \tag{5.14-61}$$

$$\hat{c}_{22_n} = k_2 \left(\tilde{c}_{22_n} - d_{23}\, \hat{c}_{23_n}\right) \tag{5.14-62}$$

$$\hat{c}_{32_n} = k_2 \left(\tilde{c}_{32_n} - d_{23}\, \hat{c}_{33_n}\right) \tag{5.14-63}$$

The elements of the first column are obtained from those in the second and third columns.

$$c_{11_n} = \hat{c}_{22_n}\, \hat{c}_{33_n} - \hat{c}_{23_n}\, \hat{c}_{32_n} \tag{5.14-64}$$

$$c_{21_n} = \hat{c}_{32_n}\, \hat{c}_{13_n} - \hat{c}_{12_n}\, \hat{c}_{33_n} \tag{5.14-65}$$

$$c_{31_n} = \hat{c}_{12_n}\, \hat{c}_{23_n} - \hat{c}_{13_n}\, \hat{c}_{22_n} \tag{5.14-66}$$

This completes the direction cosine computation.

The wind-frame gravity components are then determined digitally and transmitted to the standard analog console.

$$g_x^{\,w} = c_{13}\, g \tag{5.14-67}$$

$$g_y^{\,w} = c_{23}\, g \tag{5.14-68}$$

$$g_z^w = c_{33}\, g \tag{5.14-69}$$

Since there is no longer any ambiguity, we have eliminated the caret and the subscript n from the matrix elements.

The elements of C_n^w are also needed to determine position. The components of velocity in the navigation frame are computed and then integrated in the digital computer.

$$V_x^n = c_{11}\, V \tag{5.14-70}$$

$$V_y^n = c_{12}\, V \tag{5.14-71}$$

$$V_z^n = c_{13}\, V \tag{5.14-72}$$

With x and y denoting position north and east, respectively, of some earth-fixed reference point, and with h denoting altitude above that point,

$$x_n = 0.02\, V_x^n + x_o \tag{5.14-73}$$

$$y_n = 0.02\, V_y^n + y_o \tag{5.14-74}$$

$$h_n = -0.02\, V_z^n + h_o \tag{5.14-75}$$

The Euler angles are determined digitally from the elements of C_n^b. These elements are computed from C_b^w and C_n^w. First we solve for the elements of C_b^w as functions of α and β.

$$(C_b^w)_{11} = \cos\beta \cos\alpha \tag{5.14-76}$$

$$(C_b^w)_{12} = \sin\beta \tag{5.14-77}$$

$$(C_b^w)_{13} = \cos\beta \sin\alpha \tag{5.14-78}$$

$$(C_b^w)_{21} = -\sin\beta \cos\alpha \tag{5.14-79}$$

$$(C_b^w)_{22} = \cos\beta \tag{5.14-80}$$

$$(C_b^w)_{23} = -\sin\beta \sin\alpha \tag{5.14-81}$$

$$(C_b^w)_{31} = -\sin\alpha \tag{5.14-82}$$

$$(C_b^w)_{32} = 0 \tag{5.14-83}$$

$$(C_b^w)_{33} = \cos\alpha \tag{5.14-84}$$

We use Equation (5.12-1) to get the elements of C_n^b.

$$(C_n^b)_{11} = (C_b^w)_{11}\, c_{11} + (C_b^w)_{21}\, c_{21} + (C_b^w)_{31}\, c_{31} \qquad (5.14\text{-}85)$$

$$(C_n^b)_{12} = (C_b^w)_{11}\, c_{12} + (C_b^w)_{21}\, c_{22} + (C_b^w)_{31}\, c_{32} \qquad (5.14\text{-}86)$$

$$(C_n^b)_{13} = (C_b^w)_{11}\, c_{13} + (C_b^w)_{21}\, c_{23} + (C_b^w)_{31}\, c_{33} \qquad (5.14\text{-}87)$$

$$(C_n^b)_{21} = (C_b^w)_{12}\, c_{11} + (C_b^w)_{22}\, c_{21} + (C_b^w)_{32}\, c_{31} \qquad (5.14\text{-}88)$$

$$(C_n^b)_{22} = (C_b^w)_{12}\, c_{12} + (C_b^w)_{22}\, c_{22} + (C_b^2)_{32}\, c_{32} \qquad (5.14\text{-}89)$$

$$(C_n^b)_{23} = (C_b^w)_{12}\, c_{13} + (C_b^w)_{22}\, c_{23} + (C_b^w)_{32}\, c_{33} \qquad (5.14\text{-}90)$$

$$(C_n^b)_{31} = (C_b^w)_{13}\, c_{11} + (C_b^w)_{23}\, c_{21} + (C_b^w)_{33}\, c_{31} \qquad (5.14\text{-}91)$$

$$(C_n^b)_{32} = (C_b^w)_{13}\, c_{12} + (C_n^b)_{23}\, c_{22} + (C_n^b)_{33}\, c_{32} \qquad (5.14\text{-}92)$$

$$(C_n^b)_{33} = (C_b^w)_{13}\, c_{13} + (C_n^b)_{23}\, c_{23} + (C_n^b)_{33}\, c_{33} \qquad (5.14\text{-}93)$$

Although only five of the elements of C_n^b are needed for the Euler angle computation, all nine are computed for the sake of completeness. Pitch angle θ is now determined from

$$\theta = -\sin^{-1} (C_n^b)_{13} \qquad (5.14\text{-}94)$$

Since the magnitude of θ cannot exceed $\frac{\pi}{2}$ radians, there is no ambiguity in the angle determination.

$$\cos \theta = [(C_n^b)_{23}^2 + (C_n^b)_{33}^2]^{1/2} \tag{5.14-95}$$

If $\cos \theta \neq 0$, ϕ and ψ are found from the following two pairs of equations:

$$\sin \phi = \frac{(C_n^b)_{23}}{\cos \theta} \tag{5.14-96}$$

$$\cos \phi = \frac{(C_n^b)_{33}}{\cos \theta} \tag{5.14-97}$$

$$\sin \psi = \frac{(C_n^b)_{12}}{\cos \theta} \tag{5.14-98}$$

$$\cos \psi = \frac{(C_n^b)_{11}}{\cos \theta} \tag{5.14-99}$$

If $\cos \theta = 0$, no computation of ϕ and ψ is made.

The flight path angle γ is obtaining digitally from

$$\gamma = -\sin^{-1} c_{13} \tag{5.14-100}$$

Since γ, like θ, is limited to the range $\pm \frac{\pi}{2}$ radians, there is no ambiguity in the determination of γ from this equation.

The body-frame components of the non-gravitational acceleration

of the center of mass are computed from the wind-frame components by use of the transformation matrix $(C_b{}^w)^T$. The equations are

$$a_x{}^w = \frac{1}{m} X^w \tag{5.14-101}$$

$$a_y{}^w = -c_{23}\, g + R'V \tag{5.14-102}$$

$$a_z{}^w = -c_{33}\, g - Q'V \tag{5.14-103}$$

$$a_x{}^b = (C_b{}^w)_{11}\, a_x{}^w + (C_b{}^w)_{21}\, a_y{}^w + (C_b{}^w)_{31}\, a_z{}^w \tag{5.14-104}$$

$$a_y{}^b = (C_b{}^w)_{12}\, a_x{}^w + (C_b{}^w)_{22}\, a_y{}^w + (C_b{}^w)_{32}\, a_z{}^w \tag{5.14-105}$$

$$a_z{}^b = (C_b{}^w)_{13}\, a_x{}^w + (C_b{}^w)_{23}\, a_y{}^w + (C_b{}^w)_{33}\, a_z{}^w \tag{5.14-106}$$

Reference

1. Robinson, A.C., On the Use of Quaternions in Simulation of Rigid-Body Motion, WADC Technical Report 58-17, December 1958.

CHAPTER VI

CONCLUSIONS

The research work described in this report consisted of the following activities. An extensive hybrid simulation was set up to allow for the simulation of an aircraft equipped with a digital flight control system. Digital control algorithms were designed for a KC-135 aircraft and tested on the hybrid simulation. The design of an attitude reference system for use in a digital flight control system was studied. The question of how to take advantage of the computational power of a digital computer to reduce attitude sensor complexity and provide high reliability by tolerating sensor failures was addressed and several sensor configurations were suggested. The problem of obtaining high computational reliability in a system employing presently available flight rated computers was studied and a computer configuration was proposed.

The following conclusions result from this work.

(1) Digital stabilization and control of a transport aircraft such as the KC-135 is not difficult. Since the control computations which must be carried out iteratively for this class of aircraft involve only a small amount of arithmetic, a high iteration rate is possible and the effect of sampling on aircraft response may be reduced to the point where it is not perceptible.

(2) The added computational power of a digital flight control computer relative to an analog computer allows simpler sensors to be employed in the flight control system. The report describes how the directional gyro and vertical gyro could be eliminated in a digital flight control system if accurate rate gyros were employed. Presently available rate gyros suitable for this application are expensive and the cost saving obtained by eliminating the directional and vertical gyros would not be dramatic. However, eliminating these gyros would increase system reliability and maintainability and decrease the number of backup sensors needed for a high reliability system.

(3) For flight control tasks, such as automatic landing, where extremely high reliability is required, a single presently available flight rated digital computer would not provide sufficient reliability, and some form of backup computation capability would have to be provided. The same conclusion evidently holds for analog computers since analog autoland systems normally employ backup computers. A computer configuration employing three digital computers is recommended for these applications as the minimum cost configuration which provides provable tolerance to all single computer failures. An alternative approach would be to design a single fault tolerant computer.

☆ U.S. GOVERNMENT PRINTING OFFICE: 1974—635-042/5

NATIONAL AERONAUTICS AND SPACE ADMINISTRATION
WASHINGTON, D.C. 20546

OFFICIAL BUSINESS
PENALTY FOR PRIVATE USE $300

SPECIAL FOURTH-CLASS RATE BOOK

POSTAGE AND FEES PAID
NATIONAL AERONAUTICS AND SPACE ADMINISTRATION
451

U.S.MAIL

POSTMASTER : If Undeliverable (Section 158 Postal Manual) Do Not Return

"The aeronautical and space activities of the United States shall be conducted so as to contribute . . . to the expansion of human knowledge of phenomena in the atmosphere and space. The Administration shall provide for the widest practicable and appropriate dissemination of information concerning its activities and the results thereof."

—NATIONAL AERONAUTICS AND SPACE ACT OF 1958

NASA SCIENTIFIC AND TECHNICAL PUBLICATIONS

TECHNICAL REPORTS: Scientific and technical information considered important, complete, and a lasting contribution to existing knowledge.

TECHNICAL NOTES: Information less broad in scope but nevertheless of importance as a contribution to existing knowledge.

TECHNICAL MEMORANDUMS: Information receiving limited distribution because of preliminary data, security classification, or other reasons. Also includes conference proceedings with either limited or unlimited distribution.

CONTRACTOR REPORTS: Scientific and technical information generated under a NASA contract or grant and considered an important contribution to existing knowledge.

TECHNICAL TRANSLATIONS: Information published in a foreign language considered to merit NASA distribution in English.

SPECIAL PUBLICATIONS: Information derived from or of value to NASA activities. Publications include final reports of major projects, monographs, data compilations, handbooks, sourcebooks, and special bibliographies.

TECHNOLOGY UTILIZATION PUBLICATIONS: Information on technology used by NASA that may be of particular interest in commercial and other non-aerospace applications. Publications include Tech Briefs, Technology Utilization Reports and Technology Surveys.

Details on the availability of these publications may be obtained from:

SCIENTIFIC AND TECHNICAL INFORMATION OFFICE

NATIONAL AERONAUTICS AND SPACE ADMINISTRATION

Washington, D.C. 20546